NEW OBSERVATIONS OF RELATIVE SEA LEVEL FROM THE NORTHERN CASCADIA SUBDUCTION ZONE: CORDILLERAN ICE SHEET HISTORY AND MANTLE RHEOLOGY

by

Kevin Karl Belanger
B.Sc., University of Toronto, 1996

A Thesis Submitted in Partial Fulfillment of the
Requirements for the Degree of

MASTERS OF SCIENCE

in the School of Earth and Ocean Sciences

Supervisory Committee

NEW OBSERVATIONS OF RELATIVE SEA LEVEL FROM THE NORTHERN CASCADIA SUBDUCTION ZONE: CORDILLERAN ICE SHEET HISTORY AND MANTLE RHEOLOGY

by

Kevin Karl Belanger
B.Sc., University of Toronto, 1996

Supervisory Committee

Dr. Thomas S. James, Co-supervisor
(School of Earth and Ocean Sciences, Geological Survey of Canada)

Dr. George D. Spence, Co-supervisor
(School of Earth and Ocean Sciences)

Dr. Kelin Wang, Departmental Member
(School of Earth and Ocean Sciences, Geological Survey of Canada)

Dr. Roy D. Hyndman, Departmental Member
(School of Earth and Ocean Sciences, Geological Survey of Canada)

Abstract

Supervisory Committee
Dr. Thomas S. James, Co-supervisor
(School of Earth and Ocean Sciences, Geological Survey of Canada)

Dr. George D. Spence, Co-supervisor
(School of Earth and Ocean Sciences)

Dr. Kelin Wang, Departmental Member
(School of Earth and Ocean Sciences, Geological Survey of Canada)

Dr. Roy D. Hyndman, Departmental Member
(School of Earth and Ocean Sciences, Geological Survey of Canada)

New relative sea-level (RSL) observations dating from the late Pleistocene and early Holocene, during and after the collapse of the Cordilleran ice-sheet (CIS), are provided for two regions in southern coastal British Columbia. They record the glacial isostatic adjustment (GIA) response of the Earth to the changing surface load of the waning CIS. The data provide a new RSL curve for Sechelt, on the mainland coast north of Vancouver, and extend and revise a previously constructed curve for Barkley Sound on the west coast of Vancouver Island. The observations create a new profile of RSL curves oriented southwest-northeast across Vancouver Island and the Strait of Georgia. A previously-defined profile of RSL curves is oriented northwest-southeast profile along the east coast of Vancouver Island. The two profiles intersect in the central Strait of Georgia.

The new RSL curves sample different parts of the Cascadia Subduction Zone (CSZ) and provide constraints on the history of the CIS. The Juan de Fuca plate subducts beneath the North American plate in roughly the same southwest to northeast direction as

the RSL profile. GIA modelling of the RSL observations along this profile may indicate spatial variations related to the structure of the Cascadia Subduction Zone (CSZ). The CIS flowed roughly from northeast to southwest over the regions of interest. RSL observations along this path indicate how sea-level change differed with distance from the edge of the ice-sheet towards its centre.

The CIS model of James *et al.* (2009b) is refined to fit observed sea levels while applying glacial geological constraints to regional ice sheet advance and retreat. Sea level in Barkley Sound dropped from greater than 27 m elevation before 15 cal kyr BP to -46 m below present around 12 cal kyr BP. At Sechelt, sea level closely follows the same trend as in the central Strait of Georgia, dropping from over 150 m before 14 cal kyr BP and falling past present levels after 12.4 cal kyr BP to a poorly constrained lowstand between 12 and 9 cal kyr BP.

The initial crustal uplift rate near Sechelt was at least 85 mm/yr, comparable to that of the central Strait of Georgia. The sea-level observations are best fit with predictions employing an Earth model with a 60-km effective lithosphere thickness and asthenospheric viscosity and thickness of 4×10^{19} Pa s and 380 km, respectively. The transition zone and lower mantle viscosities are based on the VM2 Earth model (Peltier 2002). Sea level in Barkley Sound fell quickly (15-30 mm/yr), and observed sea level is best fit with the same asthenospheric viscosity, but with a thinner 30-km thick lithosphere, consistent with the regional tectonic structure. Revisions to the ice model are consistent with radiocarbon constraints on ice sheet history and provide good agreement with the observed sea-level history for the study regions as well as RSL histories previously described for the Strait of Georgia and southern Vancouver Island.

Table of Contents

List of Abbreviations

BC	(the Province of) British Columbia, Canada
^{14}C yr BP	radiocarbon* years before present
^{14}C kyr BP	thousands of radiocarbon* years before present
cal yr BP	calendar* years Before Present
cal kyr BP	thousands of calendar* years before present
CIS	Cordilleran Ice Sheet
CSZ	Cascadia Subduction Zone
GIA	glacial isostatic adjustment
GSC	Geological Survey of Canada
gyttja	bulk organic, freshwater, lacustrine sediment
LGM	Last Glacial Maximum
LIM	Last Isotope Maximum
myr	millions of years ago
OIS	Oxygen Isotope Stage
PDF	probability density function
PGC	Pacific Geoscience Centre, Sidney, BC
RSL	Relative Sea Level

*Section 2.3.2 describes detailed radiocarbon date calibration methods.

List of Tables

List of Figures

Acknowledgments

First and foremost, I thank Thomas James, my supervisor, for providing the opportunity to work on this project. Without his diligent professionalism and patient support, this work would not have been possible. Thanks to the other members of my supervisory committee: George Spence, Kelin Wang, and Roy Hyndman. Their expert advice and kind suggestions vastly improved my thesis. Thanks also to the external reviewer, Dan Smith. Randy Enkin and Audrey Dallimore both helped me resolve issues concerning reservoir corrections and gave advice on interpreting depositional environments.

Sediment cores central to this thesis were collected in 2001 and 2002. Field work was led by Ian Hutchinson, John Clague and Thomas James, all of whom collaborated to interpret the cores and other samples. Thanks to all field assistants, including: Kim Conway, Bill Hill, Charlotte Bowman, Vaughn Barrie, Karen Simon, Jessica Jorna, Paul Ferguson, Michelle Watson and Mike Sanborn, Lucinda Leonard. Thanks to Bea and Harold Swanson of Sechelt, BC.

Special thanks to Evan Gowan, M.Sc. for his excellent thesis work on sea-level in Victoria, BC. His scripts, methods and advice were indispensible to this study. This work benefitted from discussions with my fellow students at the School of Earth and Ocean Sciences, including Karen Simon, Fabian Lienert, Sheri Molnar, Yan Hu, Lucinda Leonard, Sabine Hippchen, Angela Schlesinger and Ikuko Wada.

Thanks to the staff at the School of Earth and Ocean Sciences, in particular to the graduate secretaries, Allison Rose and Kathleen Chrétien, and the departmental secretary,

Kimberly Smith-Jones, who solved all administrative issues. Staff, students and visitors too many to name—particularly in the geodynamics group at the Pacific Geoscience Center—assisted with technical issues and provided useful comments. I couldn't have asked for a more supportive, inspiring place to do research.

Finally, I would like to thank my wife Jindra, my children Tereza and Nikolai, and the rest of my family & friends for their loving & patient support during my studies.

Dedication

To my teacher-parents: Cathy, Karl, & Terry, who taught me to do right and love learning. Thanks for the fine examples you set and the love you give.

Chapter 1 – Introduction

The Cascadia Subduction Zone (CSZ) is a linear tectonic feature—associated with significant risk from earthquakes—that parallels the west coast of North America from Vancouver Island to northern California. Several oceanic plates (Explorer, Juan de Fuca, Gorda) converge with and subduct beneath the North American plate, which was covered by two large ice sheets during the last glacial cycle. We can learn about the history of the ice sheet and the physical properties of the subduction zone by studying and modeling sea-level change. Evidence of rapid sea-level change along the coastline of southwestern British Columbia (BC) is also interesting to anthropologists because it occurred at the same time as the peopling of the Americas (Fedje and Christensen 1999, Ward *et al.* 2003). New observations described in this thesis precisely constrain the history of sea-level change around Vancouver Island. The observations are then compared against the predictions of a computer model to improve our understanding of the history of the ice sheet that covered British Columbia and the structure and tectonic processes of the CSZ.

1.1 Thesis Outline

Chapter 1 introduces the study area, describes the history of the Cordilleran Ice Sheet (CIS) and sea level in southwestern BC during the last glacial cycle and summarizes published regional studies. *Chapter 2* explains the methods used to collect and analyze the data that determine a detailed sea-level curve. *Chapter 3* and *Chapter 4*

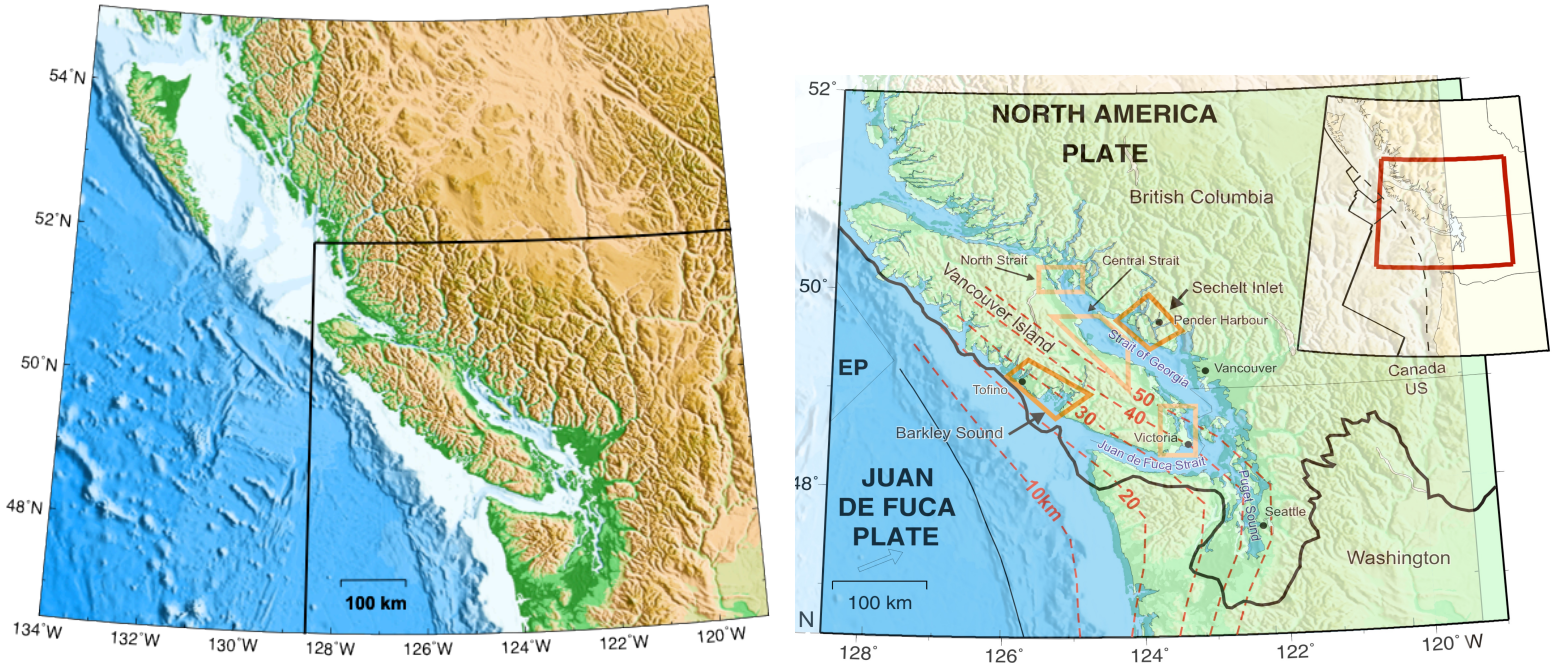

Figure 1.1. (left) Physiography of the west coast of British Columbia and northwestern Washington State. Outline shows region depicted in the right panel. (right) New relative sea-level observations are described and interpreted for two study regions of Sechelt and Barkley Sound (dark orange) overlying the Cascadia Subduction Zone. Three previously published curves (faded orange) are located in the Straits of Georgia and Juan de Fuca (after James *et al.* 2009a). Dashed red lines show depth to the top of the subducting slab. Solid black line shows the extent of the CIS at the Last Glacial Maximum (~18 cal kyr BP). EP is Explorer Plate.

present new observations of sea level in the two study regions of Sechelt, on the mainland coast north of Vancouver, BC, and Barkley Sound, on the west coast of Vancouver Island (Figure 1.1). *Chapter 5* presents models of ice load and earth response and explains how new information on the timing and amplitudes of sea-level change during CIS deglaciation described in chapters 3 and 4 are used to refine existing models of ice-sheet history and earth response. *Chapter 6* presents the conclusions drawn from observations and modeling.

1.2 Brief review of CIS history

During the last glacial cycle, polar ice caps expanded and created continental-scale ice sheets several kilometres thick in Europe and North America. One of these, the Cordilleran Ice Sheet (CIS), covered most of BC and northern Washington (Fig 1.2).

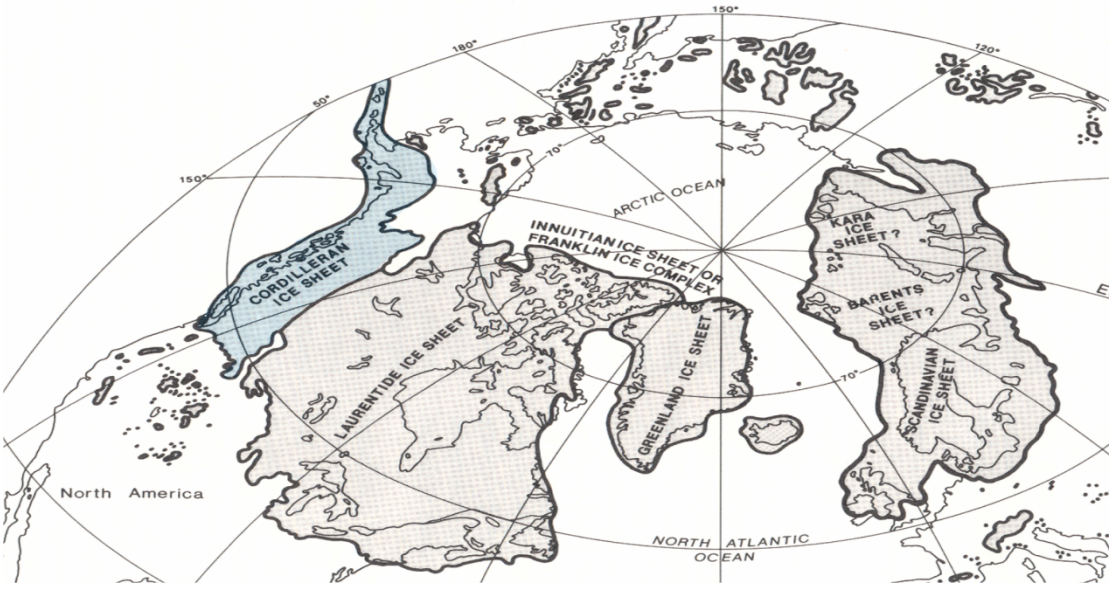

Figure 1.2. Maximum extent of northern hemisphere ice sheets during the last ice age (after Denton and Hughes 1981).

The timing of the last global glacial cycle varied regionally. Studies in Southwestern BC (Clague 1981; Clague and James 2002) set the Last Glacial Maximum (LGM) several thousand years later for the CIS than for other ice sheets in the Northern Hemisphere. The CIS formed when regional valley glaciers thickened and coalesced so that even steep local relief no longer controlled ice flow direction (Roberts and Rood 1984). Clague *et al.* (2005) set the inception of the CIS around 35 cal kyr BP, though an even earlier LGM may have occurred on the Olympic Peninsula (Thackray 2001). Growing to 1 km thick over Vancouver, BC by 28 cal kyr BP, the CIS reached its maximum extent around 18 cal kyr BP, about 10 kyr later than the Laurentide Ice Sheet (LIS). Ice flowed southwestward from its source in the Coast Mountains, achieving a maximum thickness of about 3 km in the Georgia Basin, overtopping all but the highest peaks of Vancouver Island and the Olympic Peninsula, and forming the vast Puget Sound and Juan de Fuca lobes. End moraines around Olympia, Washington and fanning troughs on the continental shelf mark the furthest extent of the CIS, where it remained for only a few hundred years before the onset of rapid deglaciation (~17 cal kyr BP). In contrast, the LIS persisted near its maximum extent for over 10 kyr. Deglaciation of the coastal CIS occurred primarily by down-wasting and stagnation rather than retreat, except in the Queen Charlotte Basin, where extensive iceberg scour is observed (Alley and Chatwin 1979; Barrie and Conway 2002). Several local re-advances have been correlated to the Younger Dryas climatic event (Osborn *et al.* 1995; Friele and Clague 2002). Glacial extent by ~10 cal kyr BP was similar to modern alpine conditions.

1.3 Brief summary of published work on regional sea level

Mathews *et al.* (1970) presented the first detailed sea-level histories of the Strait of Georgia and the Fraser Lowland, establishing a sea-level highstand co-incident with deglaciation at 13 ^{14}C kyr BP followed by rapid sea-level fall around 12 ^{14}C kyr BP until 8 ^{14}C kyr BP. After this time, eustatic sea-level rise dominated the residual GIA uplift. Clague (1975) and Clague *et al.* (1982) contrast 'inner-coast' relative sea level (RSL) change around the Strait of Georgia with 'outer-coast' emergence of Haida Gwaii and the west coast of Vancouver Island, recognizing a difference compatible with decreasing ice thickness toward the periphery of the CIS. Howe Sound deglaciation and RSL change is discussed by Friele and Clague (2002). To the author's knowledge, no previous study has reconstructed a detailed sea-level history for the nearby Sechelt region.

Hutchinson *et al.* (2004a) described sea-level in the central Strait of Georgia as falling rapidly from a high-stand position of about 150 m to below present sea level in 1.5 to 2 cal kyr (Hutchinson *et al.* 2004a). After reaching an uncertain low-stand position, sea level returned to near present levels by 8 or 9 cal kyr BP. Sea level in the northern Strait of Georgia fell from a high-stand position of about 175 m to around present levels in about 2 to 3 cal kyr (James *et al.* 2005).

A recent study by James *et al.* (2009a) of relative sea level near Victoria, BC and in the Strait of Juan de Fuca established a sea-level high-stand of 75 m at 14 cal kyr BP and a drop below the present level by 13.2 cal kyr BP. Direct observations loosely constrain the low stand below -11 m and above -40 m, somewhat shallower than in an earlier study by Mosher and Hewitt (2004).

Dallimore *et al.* (2009) constructed a Holocene RSL history for Barkley Sound by combining new data from a marine core in Effingham Inlet on Vancouver Island with samples from Hutchinson's (1992) catalogue of radiocarbon dates near Tofino, BC. The study presents a well-constrained low-stand at 13.8 cal kyr BP and a Holocene high-stand around 5.5 cal kyr BP. Previous studies of Holocene RSL near Tofino (Clague *et al.* 1982; Friele and Hutchinson 1993; Gutsell *et al.* 2004) indicate a drop in sea level from over 30 m elevation sometime before 15 cal kyr BP to below the present level around 14.5 cal kyr BP. The earlier portions of the curve during the late Pleistocene emergence of the west coast of Vancouver Island are poorly constrained.

Shaw and Forbes (1992) described LIS deglaciation around Newfoundland as following a radial trend of ice-sheet retreat and down-wasting. The same radial trend in CIS deglaciation resulted in relatively early and deep low-stands on the periphery of the ice-sheet and later and shallower low-stands towards the interior of BC. The Victoria area emerged 1 kyr earlier than the central Strait of Georgia. The northern Strait emerged 1 kyr later still. This study's first objective is to place RSL histories for Sechelt and Barkley Sound within the regional pattern of emergence.

1.4 Tectonic setting of the study area

The southwestern British Columbia margin is an active subduction zone (Fig. 1.3). The North American Plate overrides the subducting Juan de Fuca plate, which is produced at a mid-ocean ridge that forms a triple-junction with the Nootka and Sovanco Faults about 250 km west of Tofino, BC on the west coast of Vancouver Island. The plate is young (6 million yrs) and hot. It subducts long before thermal

equilibrium is reached at 65 million yrs or more (Stein and Stein 1992). Corresponding regions of high heat flow occur north and west of Vancouver Island, in the Queen Charlotte and Tofino Basins (Flück *et al.* 2003).

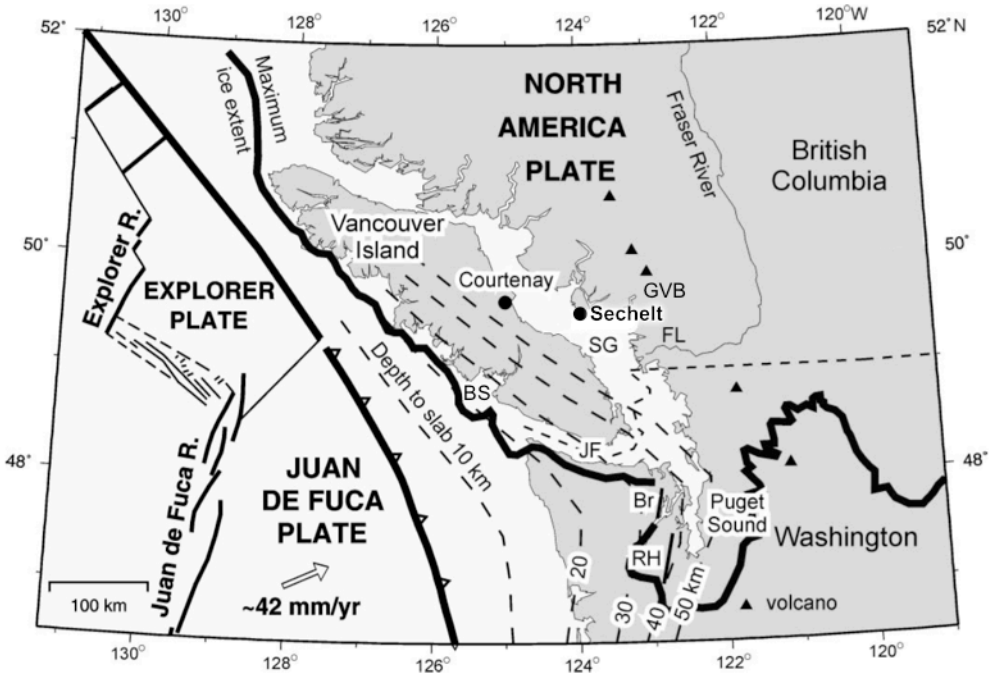

Figure 1.3. Geometry of the Cascadia subduction zone below Sechelt and Barkley Sound (BS). Contours indicate depth to the top of the Juan de Fuca plate as it subducts under the North American Plate. Triangles indicate arc volcanoes, e.g. Garibaldi Volcanic Belt (GVB). Fraser Lowlands (FL), Strait of Georgia (SG) and Juan de Fuca (JF) are indicated (after Balfour *et al.* 2008 and Flück *et al.* 1997).

Hyndman *et al.* 1990 described the tectonic setting and crustal structure of the Cascadia Subduction Zone (CSZ) at Vancouver Island, integrating seismic and other geophysical studies. Two main geological belts: the Insular and Coast Belts trend roughly northwest to southeast between the edge of the continental shelf and the Garibaldi Volcanic Belt (Figure 1.3, Hyndman and Lewis (1995), Figure 2). The Insular Belt is a lower heat flow zone consisting of the newest terranes of the North American Plate. It forms the west coast of Canada from Haida Gwaii to Vancouver

Island, including the Strait of Georgia. About 100 million years ago, the Wrangellia terrane was first to collide with the southern Canadian Cordillera, followed around 40 to 50 million years ago by the Pacific Rim and Crescent terranes. Though it is among the newest terranes of the Cordilleran crust, Wrangellia—including Vancouver Island—has been a strong, relatively cool block of lithosphere since at least the Cretaceous. This study considers RSL along a transect from Barkley Sound to Sechelt that corresponds closely to the southern Canadian Cordillera Lithoprobe corridor presented in Hyndman and Lewis 1995 and updated in Hyndman 2010 (Figure 4). GIA modeling of RSL observations along this transect may indicate spatial variations related to the structure of the Cascadia Subduction Zone (CSZ).

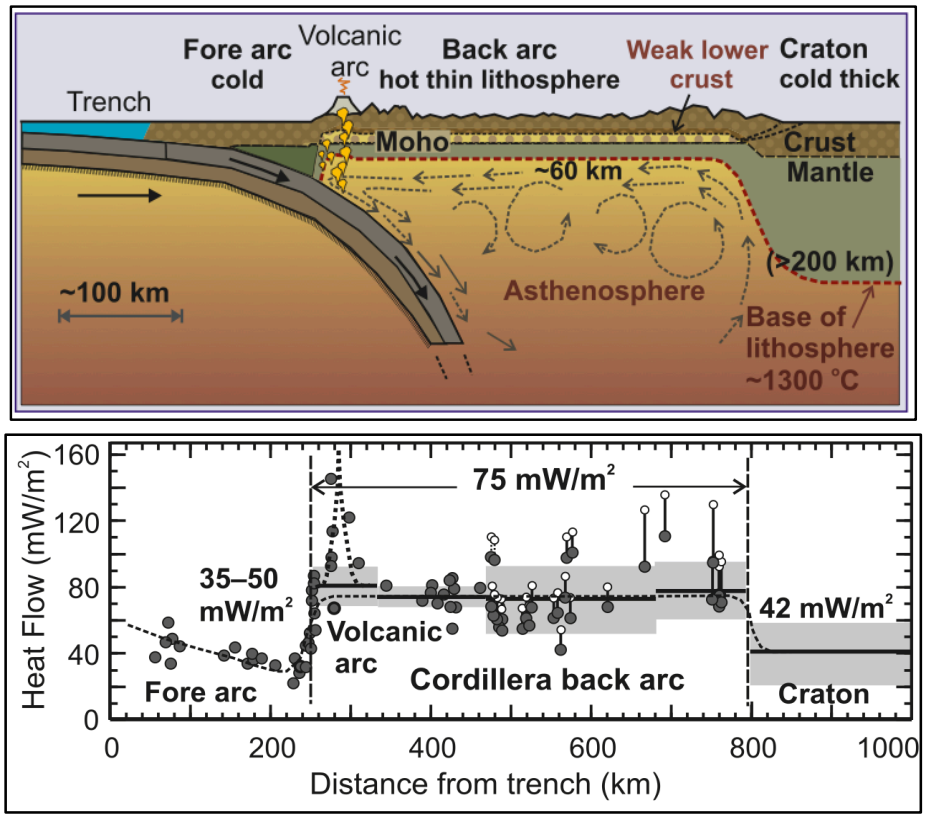

Figure 1.4. Schematic cross-sections illustrating uniform high temperatures and thin, weak lithosphere across the southern Canadian Cordillera. Heat flow data show values as both uncorrected (open circles) and corrected (filled circles) to account for upper crustal heat generation of 1.3 mW/m^2 (Figures 1 and 2 in Hyndman 2010).

A thermal cross-section along the same transect illustrates the gradually decreasing heat flow to the northeast and the steep geothermal gradient at the Garibaldi Volcanic Belt northeast of Sechelt, BC, ~50 km beyond the study region (Figure 1.3). The west coast of Vancouver Island and the eastern arm of Sechelt Inlet both lie on the 50 mW $\cdot$ m^{-2} heat flow contour. Heat flow data from Vancouver Island and the Strait of Georgia range from 25-45 mW m^{-2}, about half the value in the active backarc region (Lewis *et al.* 1988). Heat flow through Vancouver Island is reduced by a relatively cool mantle wedge beneath the continental crust and above the subducting Juan de Fuca Plate. The mantle wedge exists at depths of up to 80 km (James *et al.* 2009b). A 60-km thick elastic layer is considered representative of the lithospheric thickness for Sechelt, BC, as well as southern Vancouver Island and the Strait of Georgia (Figure 1.4; Gowan 2007; James *et al.* 2009b; Hyndman 2010).

1.5 Brief summary of published work on GIA modeling

Computer models of earth response to ice load are used to explore the characteristics of the crust and mantle, the reconstruction of glacial history, and their interaction in the context of non-glacial forces like tectonic uplift.

James *et al.* (2000) examined glacial lake tilts around Puget Sound and compared RSL observations from the central Strait of Georgia to derive estimates of regional effective mantle viscosity. The tectonic component of vertical crustal motion was found to be negligible during initial emergence after CIS deglaciation, which was sufficiently rapid that less than 0.1 mm/yr residual GIA-induced uplift remains. Present crustal motion depends almost completely on tectonic forces (Mazzotti *et al.*

2003). Upper mantle viscosity below southwestern British Columbia was estimated at 5×10^{18} to 5×10^{19} Pa s for an effective lithospheric thickness of 35 km.

Clague and James (2002) confirmed that an upper mantle viscosity less than 10^{20} Pa s best fits observed RSL patterns and shoreline tilts in the region. A lithospheric thickness of 60 km was inferred from heat flow and seismic data to best represent the combined flexural rigidity of the continental crust and oceanic slab. Fitting observed RSL data with a 60-km model lithosphere required a 20% thicker ice model than a thinner 35-km lithosphere.

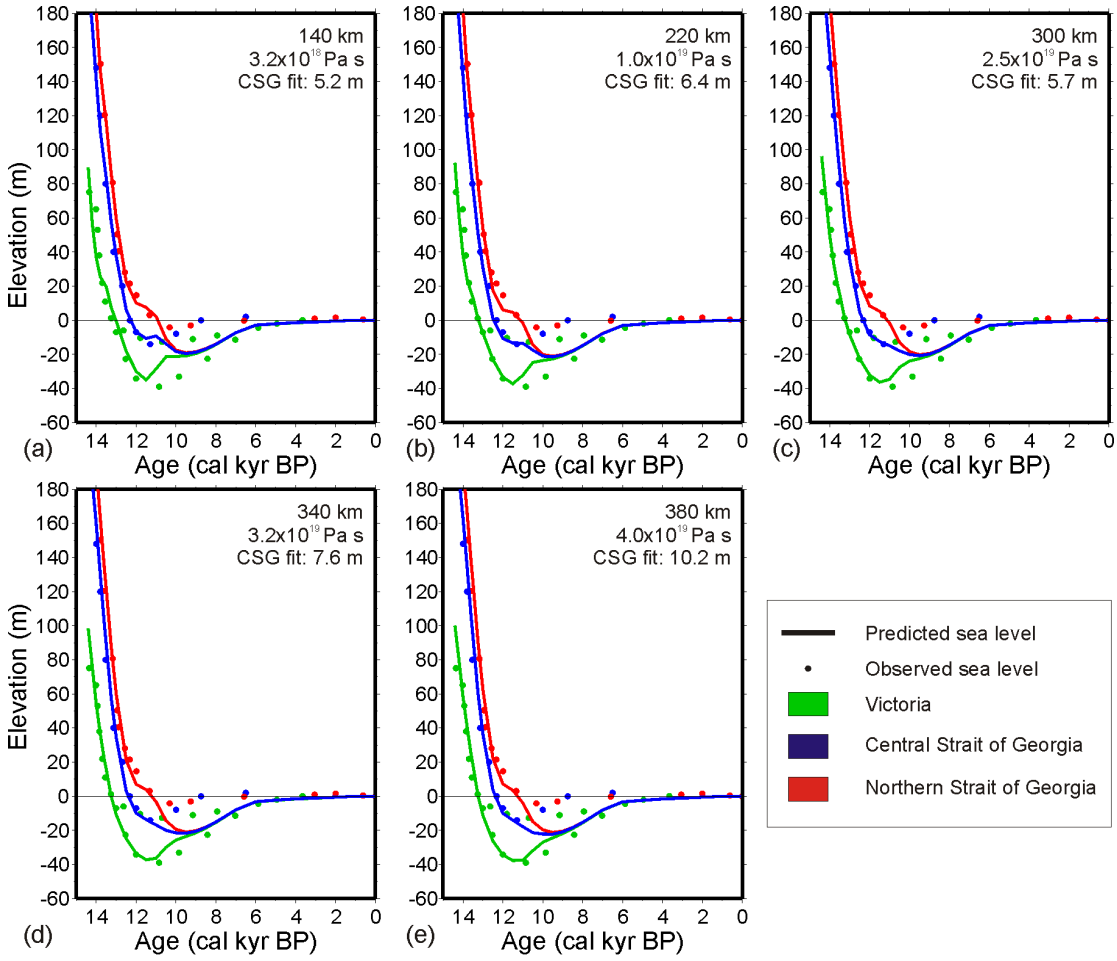

Figure 1.5. Predictions of a previous GIA model are in good agreement with previously published sea-level observations for a range of asthenospheric thicknesses (km) and viscosities (Pa s). CSG: Central Strait of Georgia. Diffusive channel flow theory predicts lower viscosity with a thinner asthenosphere (James *et al.* 2009b).

Gowan (2007) and James *et al.* (2009b) updated these findings and used a revised ice-model to compare sea level in Victoria to that in the central and northern Strait of Georgia (Fig 1.5). Good agreement was observed for a 60-km thick lithosphere at a range of asthenospheric thicknesses and low viscosity values. Diffusive channel flow theory predicts lower viscosity with a thinner asthenosphere (James *et al.* 2009b).

1.6 Objectives

This study's main goal is to synthesize post-LGM sea-level observations for Barkley Sound and Sechelt and use them to improve a GIA model of CIS ice history and CSZ earth response. This goal is divided into the following four tasks: (1) establish a new RSL curve at Sechelt, (2) extend an existing RSL curve at Barkley Sound, (3) model the ice load of the CIS, and (4) model the crustal response at each study location.

1.6.1 Establish Sechelt RSL curve and extend existing Barkley Sound data

New data collected around Sechelt (Fig 1.1) allow the region's sea-level history to be reconstructed during and after the collapse of the CIS. Since the observed sea-level curve is similar to that of the central Strait of Georgia, the first objective was to use the existing GIA model of ice history and earth response to predict and compare modeled RSL to the observed sea-level history for Sechelt.

New RSL data for Barkley Sound widen the range of existing records to earlier times. Late Pleistocene dates provide observations of sea level during the collapse of the CIS and allow sea-level histories to be compared to other regions, including Sechelt (this study) and the central Strait of Georgia (Hutchinson *et al.*

(2004a). Previous observations lie on a northwest-southeast profile along the east coast of Vancouver Island.

The new early emergence data from Barkley Sound and Sechelt delimit a new profile oriented southwest-northeast across Vancouver Island and the Strait of Georgia: perpendicular to that of previously published observations. The two profiles intersect in the central Strait of Georgia.

Adding this second spatial dimension to regional sea-level modeling provides two important opportunities to improve understanding of sea-level change. Firstly, the new data will refine the CIS model to fit observations on the west coast of Vancouver Island; secondly, we can compare predictions to observations along a NE-SW profile oriented perpendicular to the strike of the CSZ.

1.6.2 GIA modeling: ice load and earth response

The CIS flowed roughly from northeast to southwest over the regions of interest. Measurements along this path should indicate how sea-level change differed with distance from the edge to the centre of the ice-sheet. Relative timing and amplitudes of sea-level change will refine existing models of ice-sheet history during the rapid CIS deglaciation. This required modifications to models of ice sheet history and Earth rheology, because: (i) the ice-sheet model had not previously been tuned for this region, and (ii) Barkley Sound is located further westward, where the subducting oceanic plate is closer to the surface.

Tectonic forces subduct the Juan de Fuca plate below the North American plate in roughly the same southwest to northeast direction. Spatial variations related

to the structure of the CSZ along this profile may be explored by modeling the Earth's response to the CIS.

The present study does not model the detailed structure within the crust or upper mantle of the CSZ. Instead, earth modeling considers regional variations in mantle viscosity and lithospheric flexural rigidity across the Insular Belt from the southwest in Barkley Sound to the northeast in Sechelt.

Chapter 2 - Methods

This chapter outlines evidence of late Pleistocene and Holocene sea-level change in coastal BC. It explains the isolation basin coring methods employed by this study to constrain the time of onset and the rate of sea-level fall, both of which are crucial to GIA modeling of ice history and earth response in the study regions.

2.1 Measuring Quaternary Sea-level Change

In the Quaternary period, sea-level change has been driven by the glacial-interglacial cycle of ice-sheet growth and retreat that has changed the amount and distribution of water in the ocean basins (Figure 2.1).

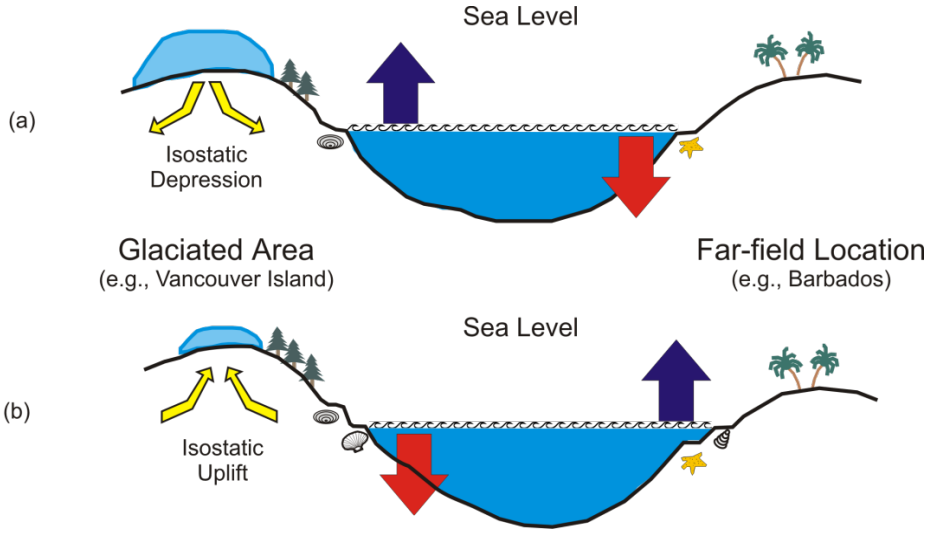

Figure 2.1. (a) The onset of glaciation depresses the crust, raising relative sea level near the ice sheets. Far from the ice, eustatic sea level falls as water accumulates in large ice sheets. (b) Deglaciation allows the crust to rebound, creating raised beaches and allowing marine features to emerge above relative sea level. Far from the ice, eustatic sea level rises and inundates terrestrial features (figure after Gowan 2007).

Ice sheets several km thick loaded the Earth's crust, forcing it downward. When the ice melted, the denser, viscous mantle pushed the buoyant crust back upward, restoring isostatic equilibrium via postglacial rebound (PGR), more generally referred to as glacial isostatic adjustment.

Global sea level fell when the glacial cycle began, as land-based ice sheets accumulated vast amounts of water from the oceans. When the land-based ice melted back into the oceans, sea level rose. Eustatic sea level changes are represented by the globally averaged amount of water added to or removed from the oceans. Eustatic sea level fell from about -60 m (relative to present) at the end of oxygen isotope stage 3 (OIS-3, about 35 kyr BP) to an LGM minimum of about -120 m (Lambeck and Chappell 2001; Bassett *et al.* 2005). It has risen by more than 120 m since the LGM to its present value. Present sea-level is the highest since the beginning of OIS-5 (about 120 kyr BP).

To first order, changes in relative sea-level *(ΔRSL*) are determined from the difference in changes to eustatic sea level *(ΔESL*) and changes in the crustal response *(ΔCR*):

$$\Delta RSL = \Delta ESL - \Delta CR \qquad (1)$$

where the crustal response is measured positive upwards. As an example, if the crust locally rises by 50 m, and eustatic sea-level change is nil, then relative sea-level is -50 m (drops 50 m). If eustatic sea-level rises by 50 m, and there is no crustal response, then local relative sea-level also rises by 50 m.

Equatorial regions are far enough from the large Quaternary ice sheets that the isostatic crustal motion directly related to continental-scale ice loads is minimal. Thus, in the tropics, relative and eustatic sea level are approximately equal, excepting other crustal motions, such as that arising from tectonics. Tectonically-corrected relative sea level records from raised corral terraces in Barbados (Bassett *et al.* 2005) are used in this study as a proxy for eustatic sea level.

A second-order effect of melting ice is the hydrostatic load of rising sea-level, which is pronounced in shallow marine basins (e.g., Huon Peninsula, Papua New Guinea; Lambeck and Chappell (2001)). However, for coastal BC, a 'steep-shoreline approximation' is considered adequate to meet the objectives of the current study (section 4.2.3 of this paper; cf. Mitrovica and Milne 2003, Fig. 8).

In southwestern BC, shorelines shifted dramatically during the last glacial cycle. Eustatic sea level was globally about 120 m lower than at present, yet the enormous weight of the CIS (up to 3 km thick) depressed the crust by over 300 m in some parts of southwestern BC. The net effect is that observed or relative sea level (RSL) was over 200 m higher than at present in a large region around Vancouver Island. After deglaciation, rapid crustal uplift dropped relative sea level to nearly 50 m below present level in the study area (Dallimore *et al.* 2009), and to about 150 m in Juan Perez Sound, Haida Gwaii (Josenhans *et al.* 1997).

2.1.1 Raised beaches

Sea-level change is most vividly recorded by raised relict beaches. Such features are definitive records of the retreat of a body of water during uplift of land that was loaded by an ice sheet. Raised beaches stretch for tens and hundreds of kilometres around Hudson Bay (Figure 2.2), stranded by the crustal uplift response to Laurentide Ice Sheet (LIS) retreat.

Figure 2.2. Raised shorelines record crustal emergence at Fort Severn, Hudson's Bay, Ontario, Canada.
(http://geoinfo.amu.edu.pl/wpk/geos/GEO_6/GEO_PLATE_C-24.HTML)

In densely vegetated regions of greater relief like BC, however, such features are less evident and are typically found in much smaller, isolated exposures. Reconstruction of regional sea level histories in BC typically requires a collection of evidence, including material collected from raised beaches, perched deltas, and marine deposits. Samples are often collected by isolation basin coring, the primary method of this study.

2.1.2 Isolation basin coring

Isolation basin coring studies reconstruct sea level histories by collecting samples for radiocarbon dating from sediments that preserve transitions between marine and freshwater depositional environments. The radiocarbon ages of samples at a range of core depths are assembled to construct an age-depth model for the core.

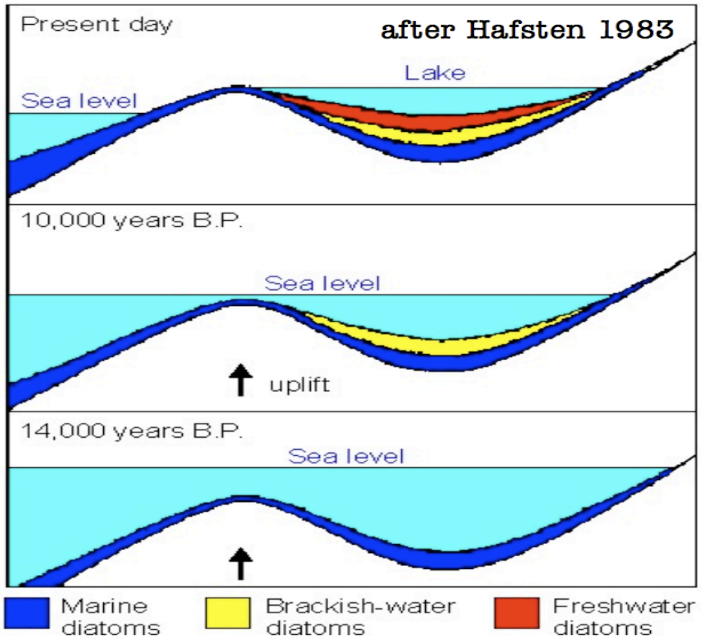

Figure 2.3. Isolation basin emergence, after Hafsten (1983) (http://www.maine.gov/doc/nrimc/mgs/explore/surficial/facts/dec00-1sm.jpg).

Isolation basins are bodies of water such as lakes, bogs or submarine basins that record transitions of emergence from marine to brackish to freshwater or submergence from fresh to brackish to marine. Ideally, a sampled basin is isolated by a bedrock sill that has experienced little erosion since the Pleistocene and thus represents a constant-elevation barrier separating the reservoir from marine waters. All samples from a given core are later plotted on an age-elevation figure at the elevation of the basin's sill, regardless of sampled core depth, since it is the sill height that determines whether the basin is freshwater, brackish, or marine, and hence determines the nature of deposited materials. Thus, to plot a relative sea-level curve using age-elevation data, the depositional environment of each stratigraphic unit must be accurately interpreted.

Basins are sampled in a target region at a range of elevations as complete as possible. Typically, samples range from above the local marine limit, which is the

mapped maximum elevation of marine deposits at a locality or in a region, to below the marine low-stand, which is the mapped minimum elevation of terrestrial deposits. Sites above the high-stand should contain only freshwater sediments, since they were not inundated by the sea. Sites below the lowest marine limit should contain only marine sediments, since no emergence has occurred. Between these end members, both marine and freshwater sediments occur. The sediments often preserve micro-fossils such as diatoms, radiolaria and foraminifera, and sometimes contain macro-fossils such as shells and wood.

2.1.3 Late Pleistocene Emergence: date of onset and rate of uplift

During initial emergence caused by CIS retreat and thinning, sites immediately below the marine limit can record rapidly falling sea levels. If sea-level fall is rapid, a core may feature a sharp transition from a marine to a freshwater environment. Such sites are central to this study, as they closely constrain both the initial date of onset of sea-level fall. A number of sites at varying elevations are needed to obtain constraints on the rate of crustal uplift after deglaciation. This information is crucial to GIA modeling of ice history and earth response.

2.1.4 Early Holocene Submergence

Sea level reached its minimum when crustal uplift slowed and before eustatic sea level rose to near-modern levels. At the end of the Pleistocene and during the early Holocene, the ocean inundated sites at elevations between the lower marine limit and slightly above the present datum. Sediments often preserve transitions from terrestrial to brackish to marine deposition, and some sites exhibit a transition back to terrestrial deposition when they re-emerged after a second, mid-Holocene high-stand.

Constraints on the timing and rate of early Holocene marine inundation improve the resolution of the nonlinear decay of crustal uplift rate from the continued rise of eustatic sea level. Submergence records also help correlate new data to existing regional trends by connecting the relatively sparse late Pleistocene records of emergence to better documented mid and late Holocene sea-level histories.

2.2 Data Collection

For this study, ten cores were recovered from sites near Sechelt and Pender Harbour, BC, in 2002. Sixteen organic samples were extracted from the cores and radiocarbon dated. The coring methods employed were percussion coring and vibra-coring.

For the west coast of Vancouver Island (Barkley Sound and Tofino), previously collected and new cores were sampled. Seventeen new radiocarbon ages were obtained. In October, 1998, two cores were recovered north-east of Tofino, BC at Darville Lake and Quait Bay, as part of an earlier study (López 2002). In April 2002, nine cores were recovered around Bamfield, BC. In June, 2004, shell fragments were collected (Brent Ward, pers. communication, 2004) from a creek-bed near Radar Hill, just south of Tofino, BC.

The new data for the west coast of Vancouver Island (Bamfield to Tofino) and for the BC mainland coast (Sechelt and Pender Harbour area) are presented in Chapters 3 and 4. Using new and previously published constraints on sea-level history, a new sea-level curve is presented for the mainland coast and a revised sea-level curve is developed for the west coast of Vancouver Island.

Most cores were logged and sampled in the field and several were re-logged and re-sampled by Thomas James and the author in the sediment laboratory at the Pacific Geoscience Centre (PGC) of the Geological Survey of Canada (GSC). Core diagrams were developed from field notes to represent depositional units by composition, grain size, colour, water content, and other notable characteristics. Chapters 3 and 4 present core sample detail for the study locations.

Samples of organic matter were selected from above, within, and below the depositional units believed to represent transitions between marine and freshwater deposition. Radiocarbon ages of samples at a range of core depths were assembled to construct a rudimentary age-depth model for each core. In several cases, the initial interpretation of the transitional sequences was not confirmed by the radiocarbon ages, and cores were re-sampled at broader depth ranges.

To avoid sampling errors due to the coring process (e.g., drag-down, slumping, contamination) samples were taken near core centres. The samples were washed in distilled water and oven-dried overnight. Labeled samples were wrapped in aluminum foil and transported in sealed beakers for offsite marine shell species determination (when required) and to radiocarbon laboratories for dating (see section 2.2.1 below).

Macroscopic materials such as intact shells and wood fragments were preferred to bulk organic samples, since bulk samples can incorporate material with variable provenance and age. Bulk samples may also introduce larger errors due to carbon reservoir effects (section 2.3.1). Similarly, twigs, bark, seeds, and cones are preferred to other wood fragments, since the oldest parts of a tree could be hundreds

of years older than its newest growth. Large samples may also allow for a second attempt to date a problematic material, and species identification of a shell or pine-cone can also help determine the paleoecological conditions.

2.2.1 Radiocarbon dating

Radiocarbon dates provide the primary age constraint on sea level and ice history. Radiogenic carbon (^{14}C) is a product of cosmic-ray radiation of atmospheric and terrestrial nitrogen and oxygen (Libby 1946; Dickin 2004). Living organic tissues take up radiocarbon proportional to its concentration in the environment. When an organism dies, it can no longer incorporate 'fresh' carbon. If some of its tissues are preserved, the amount of radiocarbon remaining at present can be used to derive the age of the sample.

Carbon-14 (^{14}C) decays to carbon -12 (^{12}C) with a half-life of 5730 ± 40 yrs, providing relatively accurate dating of Late Quaternary (< 50 kyr) organic matter (Guilderson *et al.* 2005). Radiocarbon dating was performed by the IsoTrace Laboratory of the University of Toronto, except for one sample dated at Beta Analytic and six other samples dated at the Keck Carbon Cycle AMS Facility.

2.2.2 Uncertainty in radiocarbon dates

Even when an ideal sample—such as a submerged tree-stump—is found in growth position and sampled without contamination or other experimental error, there are practical limits to the precision and accuracy of radiocarbon dating. Laboratory precision is expressed as a component of the total raw sample error, which also includes uncertainties in the secular variation of atmospheric C^{14} isotope levels. Further error is introduced by radiocarbon calibration (see section 2.3.3 below).

Minimum sample sizes are required for reliable age determination. Tables of raw, corrected and calibrated radiocarbon dates, including laboratory and calibration uncertainties are presented in Chapters 3 and 4.

2.3. Data Analysis

Raw radiocarbon ages provide the basis for the construction of preliminary age-depth models for each isolation basin core. While it is possible and sometimes useful to describe a relative sea-level curve in raw (uncorrected) radiocarbon years, corrections must be applied to raw radiocarbon dates before terrestrial and marine samples can be applied to establish a sea-level curve expressed in corrected radiocarbon years. In the study area, published values for marine reservoir correction during the late Pleistocene (> 10 ^{14}C kyr BP) range from 600 to 1200 years. Corrected radiocarbon dates are then calibrated so they can be expressed in calibrated (or calendar) years before present (cal yr BP).

2.3.1 Marine carbon reservoir correction

Marine and terrestrial organic matter of the same calendar age will display two different radiocarbon ages (Bard 1988). For example, if a marine shell and a twig of wood are emplaced in the same sediment, the shell will contain a lower concentration of ^{14}C than the twig, appearing depleted. Thus, a shell will appear older than coeval terrestrial plant matter, even when sampled at the same depth in a given core. Marine dates must, therefore, be corrected for a lag between ocean and atmospheric reservoir concentrations of ^{14}C before they may be accurately compared with terrestrial dates.

The concentration of ^{14}C in a living terrestrial plant reflects that of the atmosphere it breathed. Similarly, the concentration of ^{14}C in a living marine shell is in equilibrium with local ocean water. However, the amount of ^{14}C in the ocean is determined not only by the amount of ^{14}C in the atmosphere, but also by rates and patterns of oceanic circulation. On average, radiocarbon in ocean waters is 410 years old because of the long residence time that much ocean water spends in the abyssal depths. Thus, the ocean is a reservoir of carbon (Stuiver and Suess 1966). Corrected radiocarbon dates are presented as ^{14}C kyr BP (thousands of years before present, where conventional present time is 01 January 1950).

The marine reservoir correction varies with geographic location and water depth. Slower mixing at depth and at the poles causes deep water and polar oceans to be relatively depleted: their ^{14}C age appears 1200 years 'older' than the atmosphere. In southwestern British Columbia, marine samples from the late Pleistocene (older than 10 kyr BP) appear to be ~ 950 ± 50 years older than coeval terrestrial dates; Holocene samples (younger than 10 kyr BP) appear ~ 720 ± 90 years older than their terrestrial equivalent (Hutchinson *et al.* 2004b).

Coastal exposure may alter the marine reservoir effect: seasonal ice and glacial meltwater also interfere with patterns of oceanic circulation. Samples often represent reworked material from older sources, but a larger correction may reflect an amplified marine reservoir effect at a relatively sheltered locality (Hutchinson *et al.* 2005). For example, a reservoir value of ~1200 ± 130 years occurs at the relatively sheltered heads of some fjords, and a study by Kovanen and Easterbrook (2002a) determined a correction of 1250 years for dates older than 11.5 ^{14}C kyr BP in the

Fraser Lowland. Published marine reservoir correction values in the region range from 600 to 1200 years during the late Pleistocene (> 10 ^{14}C kyr BP).

2.3.2 Freshwater bulk organic (gyttja) carbon reservoir correction

Freshwater (limnic) sediment composed of bulk organic detritus is called *gyttja*. Gyttja yields radiocarbon dates that can be influenced by both the composite source material of bulk organics and by the transport of carbon within a catchment, thus rendering interpretation of gyttja radiocarbon ages uncertain. To avoid such dating issues, plant macro-fossils are selected unless only gyttja is present. Basal gyttja ages—defined as those collected from immediately above the marine-freshwater transition—require additional correction, since organisms growing in recently isolated freshwater basins can incorporate old, depleted carbon from the regional catchment (Hutchinson *et al.* 2004b). Old carbon can be leached from sources such as carbonate rocks (e.g., limestone, coal-beds, and their metamorphic products) or unconsolidated organics such as dissolved marine shells or decaying plant matter that lived before the last glaciation. During the first millennia after deglaciation, terrestrial plant growth and further groundwater leaching typically deplete sources of old carbon so that gyttja correction is no longer necessary. This study corrects basal gyttja and peat ages by 625 ± 60 yrs, the average reservoir correction for southwestern BC as determined by Hutchinson *et al.* (2004b).

2.3.3 Calibration of radiocarbon dates

Calendar ages (cal kyr BP) were obtained from laboratory radiocarbon ages using the computer program *Calib 5.0* (Stuiver and Reimer 1993) with the marine reservoir corrections mentioned above; marine samples reference the *Marine04* data-

set (Hughen *et al.* 2004) and terrestrial samples the *Intcal04* data-set (Reimer *et al.* 2004). The calendar ages were plotted as probability density functions (PDFs).

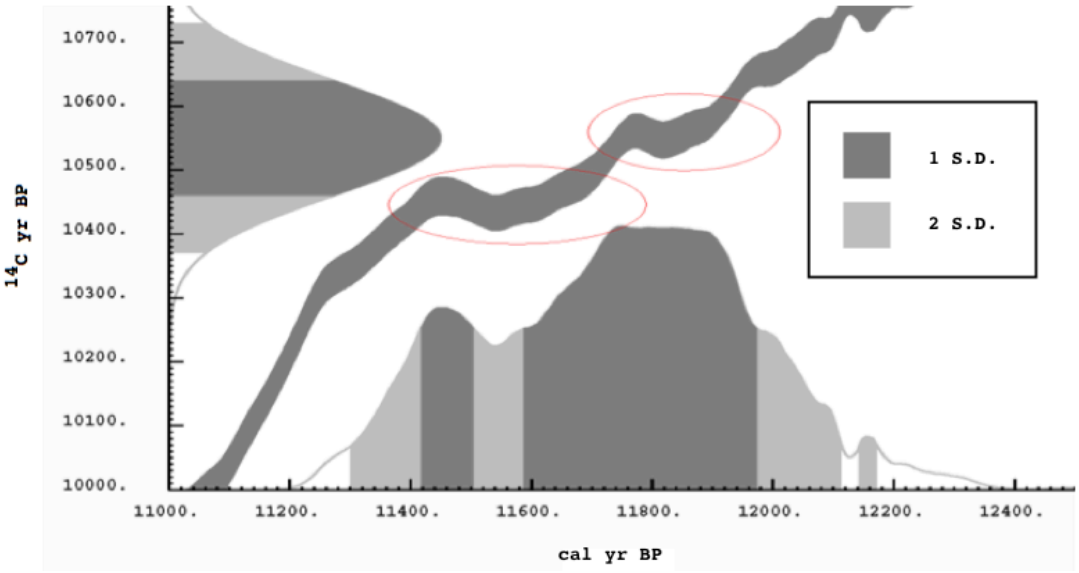

Fig 2.3. Calibrated (cal BP) probability density function (PDF) for lab no. TO-10844 (Table 4.1) plotted against radiocarbon age (^{14}C yr BP) by the computer program *Calib 5.0*. Variations in radiocarbon production result in the envelope trending as (cal yr BP ≈ ^{14}C yr BP) with plateaus (circled red) between 11.5-11.7 and 11.8-11.9 cal kyr BP. Dark grey shades one standard deviation (1 S.D.), light shades 2 S.D.

For basal gyttja ages, the laboratory radiocarbon age was corrected before being entered into CALIB 5.0 and calibrated with the *Intcal04* dataset. Correct calibration can introduce significant error even for dates with relatively low laboratory error, since late Pleistocene variations in the production of radiocarbon produce plateaus in the calibration curve (see Fig 2.3).

2.4 Describing Relative Sea Level history

To determine a relative sea level curve, radiocarbon ages of samples having a defined relationship to sea-level are plotted on an age-elevation figure. Ideally, ages from several locations are incorporated, representing different elevations from above the marine limit to below the marine low-stand. For each radiocarbon

age, the calibrated probability density function (PDF) is plotted on the figure at the sill elevation and is identified as lying above, near, or below sea-level. Where no true sill exists, lake surface elevation or lowest-low tide bathymetry is quoted. A curve (or in some cases, a maximal and minimal curve defining an envelope of solutions) is then drawn through marginal (transitional) points to satisfy as many upper and lower bounding constraints as possible. Thus, to plot a relative sea-level curve using age-elevation data, the depositional environment of each stratigraphic unit must first be interpreted as marine, brackish, or freshwater. Detailed descriptions of core samples and their interpretation are presented in Chapters 3 and 4.

2.4.1 Depositional environment

Isolation basin cores preserve transitions between marine and freshwater depositional environments (as described above in section 2.1.2). A piece of wood may be deposited in terrestrial, brackish, or marine sediments; marine shell species can indicate paleoclimatic zones and depth ranges. In the study area, transitions between marine and freshwater units are typically sharp and distinct during rapid late Pleistocene emergence and tended to be gradational during slower Holocene submergence and sequences recording late Holocene reemergence.

High-energy depositional environments (e.g., locations near fluvial sources of sediment or exposed to offshore winds and waves) may contain significant amounts of reworked material; lower-energy environments (e.g., protected embayments and fjords) often record fine laminae or varves. The varied coastline of the study region complicates the interpretation of both late Pleistocene emergence and Holocene submergence, even at neighbouring sites. Energy levels at a single location can

fluctuate from low to high-energy patterns of deposition. For example, extremely steep, bedrock-dominated fjord-head terrain periodically blankets isolation basins with colluvial mass-flows (landslides and turbidites); tsunami run-up deposits over lowland beaches can affect isolation basins at up to ten metres elevation.

Along with the aforementioned radiocarbon dating, correction, and calibration techniques, an accurate interpretation of depositional environment—consistently applied to all samples—is crucial to correctly constraining a relative sea-level curve.

2.4.2 Regional Sea-Level Trends

A relative sea-level curve indicates the sea-level history over a restricted area with dimensions ideally no more than a few tens of kilometres. The timing and magnitude of sea-level change can be related to the nearby ice-sheet history. A comparison of relative sea-level curves in a region then provides regional trends, or variations, in how sea-level has changed that can also be linked to the regional history of ice-sheet advance, retreat, and down-wasting.

The leading edge of the CIS overtopped Vancouver Island shortly after 21 kyr BP and coalesced with a large independent glacier in Barkley Sound, advancing to the edge of the continental shelf by around 19.8 cal kyr BP (Herzer and Bornhold 1982, Hendy 2009). Ice-cover on the south-west of Vancouver Island down-wasted first as it was cut off from the distant ice-centres of the CIS in the Coast Mountains northwest of Whistler, BC (Alley and Chatwin 1979). Ice-rafted debris deposition indicates that the CIS experienced rapid break-up by 17 cal kyr BP (Hendy and Cosma 2008). The Victoria area emerged about 1000 years later (James *et al.* 2009a), followed by the central Strait of Georgia after another millennium (Hutchinson *et al.*

2004a). The northern Strait of Georgia emerged about 1000 years later again (James *et al*. 2005).

The data presented here seek to establish a sea-level curve for the mainland coast of British Columbia and to revise a curve for the west coast of Vancouver Island. These curves complement the existing sea-level record for Victoria, the mid-Strait of Georgia, and the northern Strait of Georgia. The new sea-level curves allow a transect to be drawn that is oriented across the strike of the Cascadia Subduction Zone (CSZ), complementing the existing sea-level curves along the strike of the CSZ.

Chapter 3 – Observations and Inferred Sea-level Curve for Sechelt, Mainland British Columbia

This chapter presents constraints on sea-level history during and after the collapse of the CIS in the region of Sechelt on the mainland coast north of Vancouver, BC (Figure 3.1). As summarized by James *et al.* (2009a), prior investigations have described detailed sea-level constraints for three regions on a profile running northwest-southeast along the east coast of Vancouver Island and western Strait of Georgia.

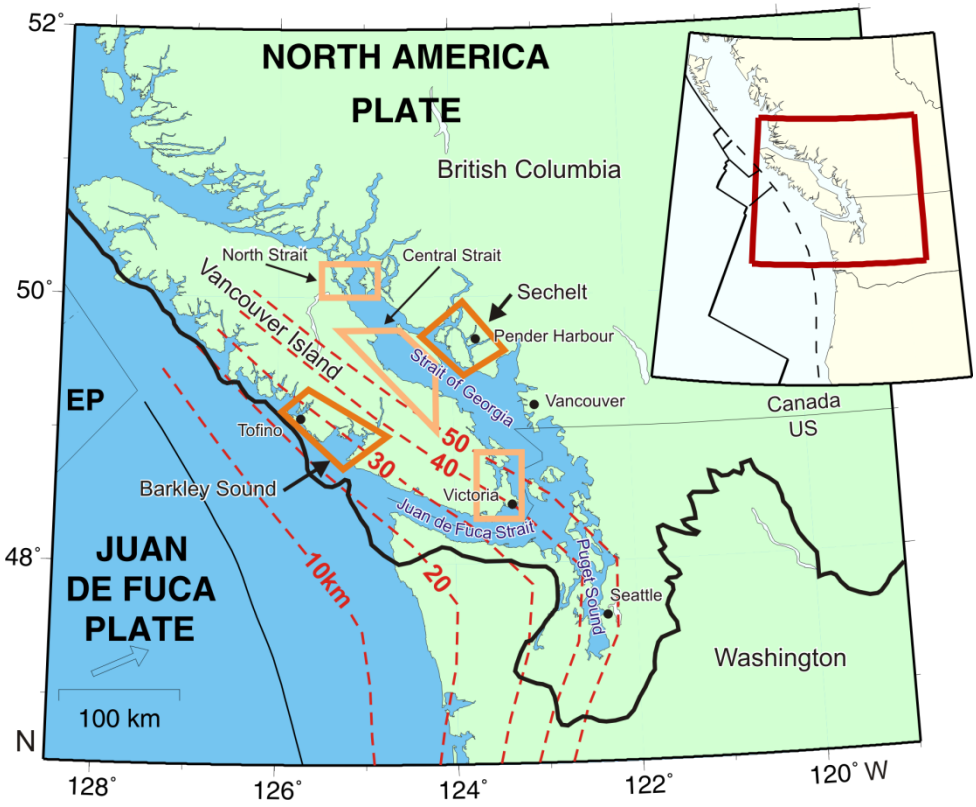

Figure 3.1. Location map showing regions for which relative sea-level curves are newly defined (Sechelt) or extended (Barkley Sound) (dark orange quadrilaterals) in this study. Three previously published curves (pale orange) for Victoria (James *et al.* 2009a), central Strait of Georgia (Hutchinson *et al.* 2004a), and northern Strait of Georgia (James *et al.* 2005) are also located over the northern Cascadia subduction zone in the Straits of Georgia and Juan de Fuca (figure after James *et al.* 2009a).

New data presented here and in Chapter 4 for Barkley Sound on the west coast of Vancouver Island define a second profile that is approximately perpendicular to the existing profile. The new profile is oriented southwest-northeast across Vancouver Island and the Strait of Georgia. The two profiles intersect in the central Strait of Georgia, where Hutchinson *et al.* (2004a) described the sea-level history.

The CIS had a source region in the Coast Mountains and spilled over onto coastal lowlands. It flowed south along the Strait of Georgia and overtopped Vancouver Island, extending offshore onto the continental shelf (Clague and James 2002). Sea-level observations over this region indicate how sea-level change differed with distance from the edge of the ice-sheet.

3.1 Summary of prior sea-level investigations in SW British Columbia

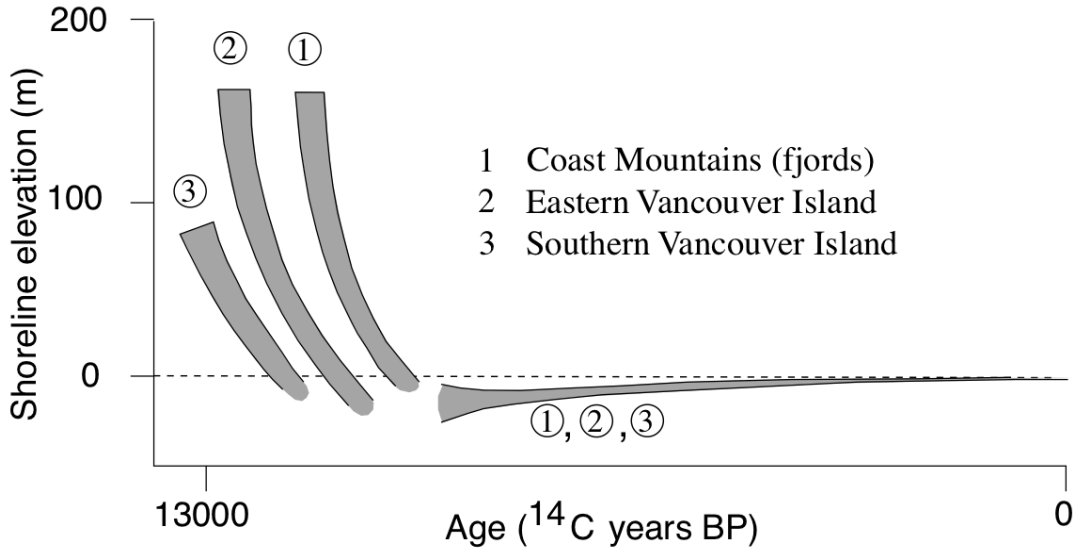

Figure 3.2. Generalized patterns of sea-level change on the BC coast since the end of the last glaciation (in Clague and James 2002, modified from Muhs *et al.* 1987, Fig. 10). Deglaciation and isostatic rebound occurred later in the Coast Mountains than on Vancouver Island.

Mathews *et al.* (1970) reviewed relative sea-level history near Courtenay, BC, on eastern Vancouver Island, noting more than a 170 m drop over a few hundred years around 12 ^{14}C kyr BP from a well constrained maximum of 150 m to a weakly constrained minimum 21 m below sea-level. Clague (1983) described the progression of isostatic depression of southern BC at the onset of the Fraser Glaciation from Coast Mountain glaciers onto plateaus and lowlands. During late Pleistocene deglaciation, marine limit elevation varied inversely with distance from the ice centres: the marine limit was highest (150-200 m) near the centres and lowest (< 50 m) at the leading edge of the CIS on the west coast of Vancouver Island (Clague *et al.* 1982, Clague and James 2002). Depth and timing of relative sea-level lowstands varied in a diachronous, radial trend; a similar pattern was observed in Newfoundland by Shaw and Forbes (1992). On the west coast of Vancouver Island—at the periphery of the

CIS—lowstands were relatively deep and early. Towards the interior of the CIS in the Coast Mountains, lowstands were shallower and occurred later.

Friele and Clague (2002) reconstructed the final stages of CIS deglaciation to establish a sea level history at the head of Howe Sound around Squamish, BC. Hutchinson (1992) and Friele and Hutchinson (1993) presented new data and proposed a new Holocene relative-sea-level (RSL) curve for the central west coast of Vancouver Island.

Clague and James (2002) presented general patterns of sea-level change around Vancouver Island. Relative sea-level dropped dramatically in the entire region during the rapid isostatic uplift from 14 to 10 ^{14}C kyr BP. The Victoria area emerged a thousand years earlier than the central Strait of Georgia. Emergence occurred another thousand years later in the northern Strait of Georgia.

Most of the isostatic uplift at each site occurred within about 2000 years and possibly faster. Data analysis yielded a 'relaxation time' of about 1 kyr (Clague and James 2002), when about 63% of total uplift occurs (1-1/*e*, as defined by Heiskanen and Vening Meinesz 1958). The rate of isostatic uplift in southwestern British Columbia decreased exponentially during the late Pleistocene and early Holocene: relative uplift continued but at a much slower rate, leading to a period of relative sea-level stability in the early Holocene, when residual glacial isostatic rebound was balanced by eustatic sea-level rise. Once isostatic uplift was effectively complete, eustatic sea level rise became dominant, leading to re-submersion of land below present sea level. This marine transgression began by 8 ^{14}C kyr BP, transgressing Vancouver to 5 m below present by 7 ^{14}C kyr BP and Victoria to 4 m of present by 6

^{14}C kyr BP (Clague and James 2002). The timing and geographic pattern of isostatic uplift differ over short distances around Vancouver Island and along the mainland coast. Isostatic uplift in upper Howe Sound postdates that of the Vancouver area. Similarly, Sechelt and the eastern Fraser Lowland likely experienced delayed or restrained isostatic uplift since they were deglaciated later than areas further south and west. While Victoria and Vancouver were ice free by 13 ^{14}C kyr BP, outlet glaciers of the CIS remained in the eastern Fraser Lowland until about 11 ^{14}C kyr BP and at inlet fjord heads like Howe Sound until nearly 10 ^{14}C kyr BP (Clague and James 2002).

3.1.1 Victoria

A recent study by James *et al.* (2009a) of relative sea level near Victoria, BC and in the Strait of Juan de Fuca established a sea-level high-stand of 75 m at 12.5 ^{14}C kyr BP that dropped below the present level by 11.5 ^{14}C kyr BP. A lowstand around 10 ^{14}C kyr BP is loosely constrained by observations to below -11 m and above -40 m; geophysical analysis suggests the lowstand is near -30 ± 5 m, significantly shallower than an earlier study by Mosher and Hewitt (2004).

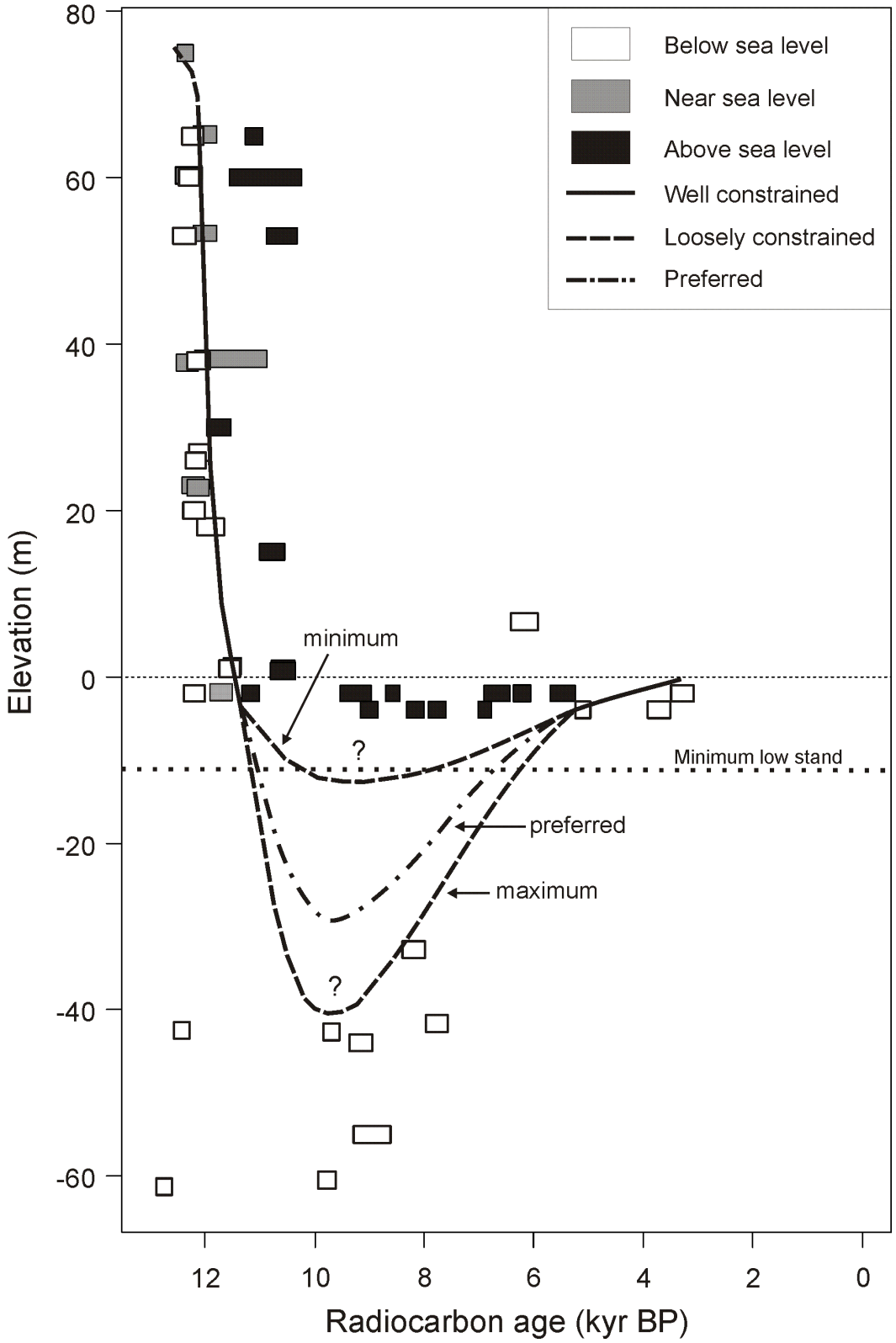

Figure 3.3. Previously published sea-level curve for Victoria, BC and southern Vancouver Island (after James *et al.* 2009a).

3.1.2 Mid-Strait of Georgia

Hutchinson *et al.* (2004a) describe sea-level in the central Strait of Georgia as falling rapidly from a high-stand of about 150 m around 11.8 ^{14}C kyr BP to below present sea level in 1.5 to 2 kyr (I(GSC)-10, Table 1, Hutchinson *et al.* 2004a). After reaching a poorly constrained lowstand of less than -20 m, sea level returned to near present levels by 7.3 ^{14}C kyr BP (TO-9902, Table 1., Hutchinson *et al.* 2004a). The lowstand in the central Strait of Georgia was reached at about the same time as Victoria (10 ^{14}C kyr BP) but was likely about 15 m shallower than in Victoria; the lowstand in the central strait occurred about 1 kyr earlier than in the northern strait of Georgia. Seismic studies and stratigraphic analysis of shallow marine cores (24-28 m depth) taken in the central Strait of Georgia suggest a lowstand between -10 to -20 m (Barrie & Conway 2002).

3.1.3 Northern Strait of Georgia

Sea level in the northern Strait of Georgia fell from a high-stand position of about 175 m to around present levels in about 2 to 3 kyr (James *et al.* 2005). After reaching an uncertain lowstand position no deeper than -20 m, sea level returned to near present levels by 6 or 7 ^{14}C kyr BP. The lowstand in the northern Strait of Georgia was reached around 9 ^{14}C kyr BP, about 1 kyr later than in the mid-strait and Victoria. The lowstand was likely shallower in the northern strait than in the mid-strait, but neither curve is well constrained during the early Holocene transgression.

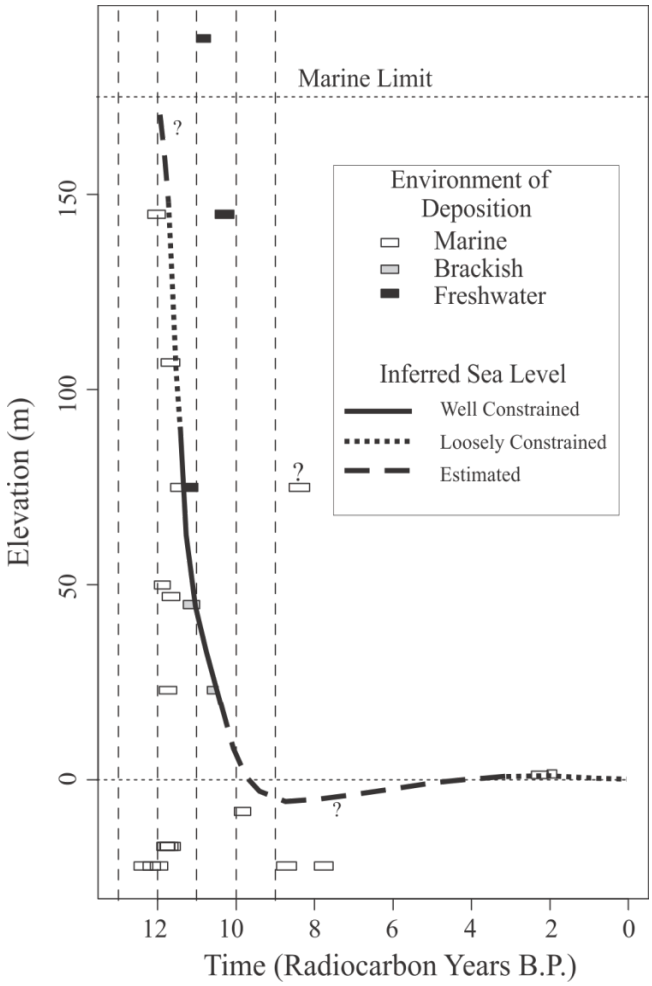

Figure 3.4. Postglacial relative sea-level change in the northern Strait of Georgia (James *et al.* 2005).

3.2 Sechelt

For this study, 13 cores were recovered at eight locations: one marine basin (Hospital Bay), one bog (Mercer Road Bog), and six lakes (Randall, Trout, Klein, Little Klein, Hotel, and Katherine Lakes). Eight cores, one from each of the locations mentioned above, yielded samples of plants, shells, and other organic matter (seeds, gyttja, etc.) that were radiocarbon dated. Ideally, radiocarbon ages were sampled to bracket the transition from marine to freshwater conditions, but frequently the underlying clastic sediments were barren of shell material. In some instances transitional units were logged that may record brackish conditions.

Two additional marine shells were obtained through enquiries with local residents. A marine shell and information on its provenance was provided by a local resident (Swanson's Well). A local resident provided guidance to a spoil heap where a second shell was recovered (John Burt's Well).

Samples were collected by Thomas James, Ian Hutchinson, Bill Hill, Lucinda Leonard, and Peter Locher. Sedimentology was described by Thomas James and Ian Hutchinson. Study locations are numbered and presented in order of decreasing elevation from 220 m elevation (1-Randall Lake) to -8 m (10-Hospital Bay). A total of 16 samples were radiocarbon-dated (Table 1). Lake elevations were calculated by barometric altimeter readings calibrated to the high-tide mark as the 0 m datum. The marine sill depth at Hospital Bay was obtained from a Canadian Hydrographic Survey chart and adjusted to the local high tide level.

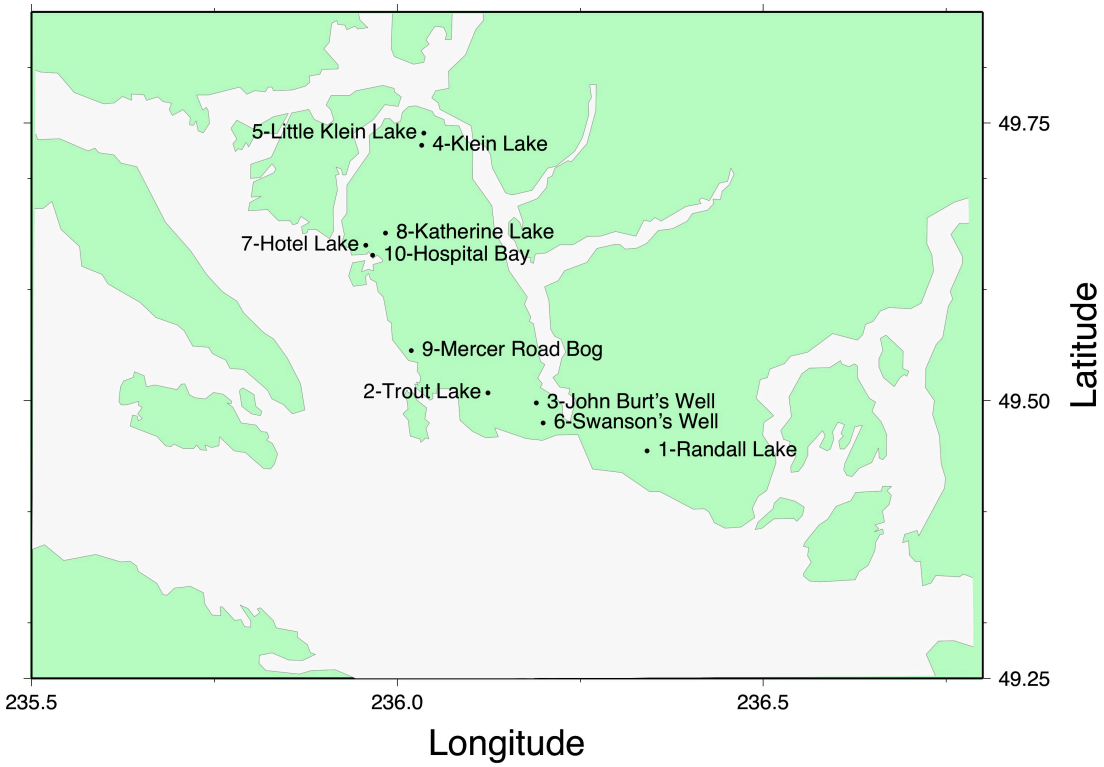

Figure 3.5. Location map of sample sites in the Sechelt region.

Radiocarbon ages are presented as corrected years or kyr (thousands of years) BP (before present: defined as 01 January 1950). Marine sample ages are corrected by -950 ± 50 years for the late Pleistocene and -720 ± 90 years for the Holocene. Basal gyttja and peat ages are corrected by -625 ± 60 yrs to account for old carbon effects (Hutchinson *et al.* 2004b).

The Sechelt region lies at the southern end of the Coast Plutonic Belt, where two major Jurassic intrusions are dominant (Ray and Kilby 1996). The Creston Lake pluton includes pyritic mafic rocks, gabbro, and quartz diorite. The Snake Bay pluton contains quartz diorite to granodiorite with minor mafics. Intrusions include granodiorite, basalt, and gabbro-andesite dikes and sills. The Jurassic Bowen Island Group includes argillite, greywacke and conglomerates, and the Triassic Quatsino

Formation includes marble. Such carbonate-bearing rocks can influence radiocarbon corrections for the marine-reservoir effect, since old carbon may have been leached and transported by groundwater into organic sediments in a catchment with carbon-rich components.

Table 3.1. Summary of radiocarbon ages of samples used for constraining postglacial sea level around Sechelt, BC.

Location	Site (Fig. 2)	Latitude (ºN)	Longitude (ºW)	Elevation (m)	Material dated	Sample id	Lab no.	Radiocarbon age	Corrected age	Calibrated age (1 S.D.)	Sea-level position
Randall Lake	1	49.455	123.659	220	gyttja	CIA-02-20-360/362	TO-10835	12650 ± 100	12025 ± 117	13770-14002	above
Trout Lake	2	49.507	123.876	154	gyttja	CIA-02-15-288/291	TO-10833	12080 ± 100	11455 ± 117	13208-13417	above
John Burt's Well	3	49.498	123.810	141	*Panomya ampla*	CIA-02-23	TO-10832	12920 ± 90	11970 ± 103	13730-13942	below
Klein Lake	4	49.730	123.967	135	gyttja	CIA-02-13-95/98	TO-10830	12590 ± 100	11965 ± 117	13719-13960	above
Klein Lake	4	49.730	123.967	135	*Mya truncata*	CIA-02-13-103/105	TO-10831	12690 ± 100	11740 ± 112	12784-12863	below
Little Klein Lake	5	49.741	123.964	113	plant fragments; rootlet	CIA-02-18-551/561	TO-10827	11070 ± 90	11070 ± 90	12916-13068	above
Little Klein Lake	5	49.741	123.964	113	gyttja	CIA-02-18-567/569	TO-10828	11960 ± 100	11335 ± 117	13106-13302	above
Little Klein Lake	5	49.741	123.964	113	twigs	CIA-02-18-572/574	TO-10829	12100 ± 90	12100 ± 90	13843-14043	below
Swanson's Well	6	49.480	123.801	107	*Clinocardium nutalli*	CIA-02-21	TO-10826	12400 ± 150	11450 ± 158	13146-13447	below
Hotel Lake	7	49.640	124.043	50	gyttja	CIA-02-22-362/364	TO-10824	11100 ± 80	10475 ± 100	12191-12653	above
Hotel Lake	7	49.640	124.043	50	wood fragment (knot)	CIA-02-22-374	TO-10825	11270 ± 90	11270 ± 90	13578-13767	below
Katherine Lake	8	49.651	124.016	18	gyttja	CIA-02-11-190/193	TO-10823	6080 ± 60	5455 ± 85	6028-6398	above
Mercer Road Bog	9	49.545	123.981	5	*Potamogeton sp*	CIA-02-10-248/250	TO-10821	9350 ± 70	9350 ± 70	10442-10676	above
Mercer Road Bog	9	49.545	123.981	5	shell fragments	CIA-02-10-275/288	TO-10822	11620 ± 80	10670 ± 94	12419-12826	below
Hospital Bay	10	49.631	124.034	-8	wood fragments	CIA-02-24-90/95	TO-10819	5440 ± 60	5440 ± 60	6190-6296	below
Hospital Bay	10	49.631	124.034	-8	shell fragments	CIA-02-24-102/107	TO-10820	8390 ± 70	7440 ± 86	8394-8678	below

3.2.1 Randall Lake

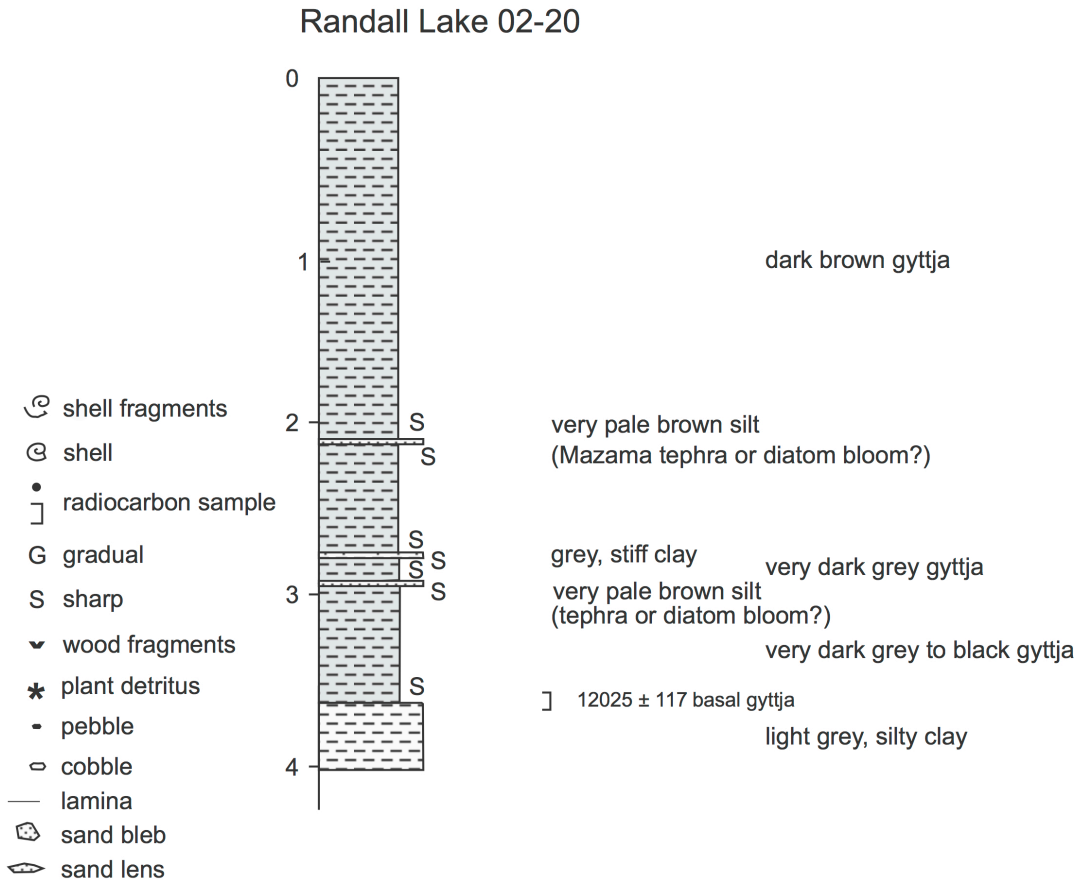

Figure 3.6. Stratigraphy (m) and radiocarbon age (yr) for core taken at Randall Lake.

A 402 cm core (CIA-02-20) penetrated 757 cm in 4 m water depth. The lake is at 220 m elevation. A 211 cm layer of dark brown gyttja darkens with depth to a sharply defined, 0.5 cm thin layer of pale brown very fine sand at 211 cm with blebs < 1 cm. A massive 65.5 cm layer of very dark grey gyttja topped a sharp transition to a 0.5 cm thin layer of stiff grey clay, again with a sharp transition over a 26 cm layer of very dark grey gyttja. A 0.3 cm thin, layer of pale brown very fine sand was contorted (perhaps by the corer), with 1 mm thick laminae at 293.5 cm atop a 69.2 cm massive layer of very dark grey to black gyttja. A sharp transition topped a 39 cm

layer of light grey (10YR 6/1) silty clay (that liquefied during transport), with clay clasts and granules at 181 and 189 cm (Figure 3.6).

A single basal gyttja sample (CIA-02-20-360/362) dated to 12025 ± 117 BP and was deposited when relative sea-level had dropped just below 220 m elevation.

3.2.2 Trout Lake

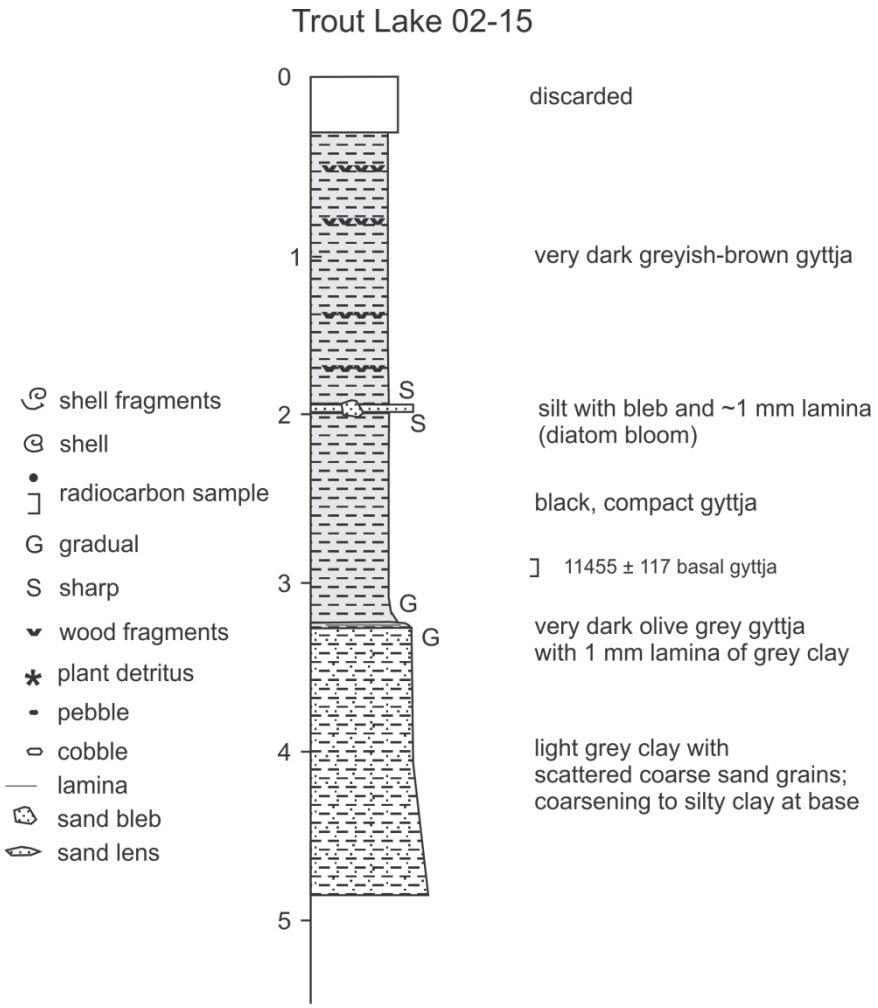

Figure 3.7. Stratigraphy (m) and radiocarbon age (yr) for core taken at Trout Lake.

Lake elevation was 154 m. A 473 cm core (CIA-02-15) penetrated 710 cm in water depth of 9.5 m. The top layer of watery gyttja was discarded. A 164 cm layer of very dark greyish-brown gyttja contained occasional twigs and other plant detritus. A

sand bleb and ~1 mm lamina of very fine sand occurred at 164 cm with a gradual transition to a 127 cm layer of black, compact gyttja. This graded to a 2.5 cm thin, very dark olive grey gyttja, with a 1 mm grey clay layer at 293 cm and again graded to a 158.5 cm layer of light grey, wet clay with scattered coarse sand grains and silty clay at its base. A single gyttja sample (CIA-02-15-288/291, Figure 3.7) dated to 11455 ± 117 corrected ^{14}C yr BP indicates the onset of freshwater conditions.

3.2.3 John Burt's Well

Around 1990, a well was dug by a local resident near Sechelt, BC at about 141 m elevation. The spoil heap contained the valve of a *Panomya ampla* (CIA-02-21). Sea level remained above 141 m elevation until at least 11970 ± 103 ^{14}C kyr BP.

3.2.4 Klein Lake

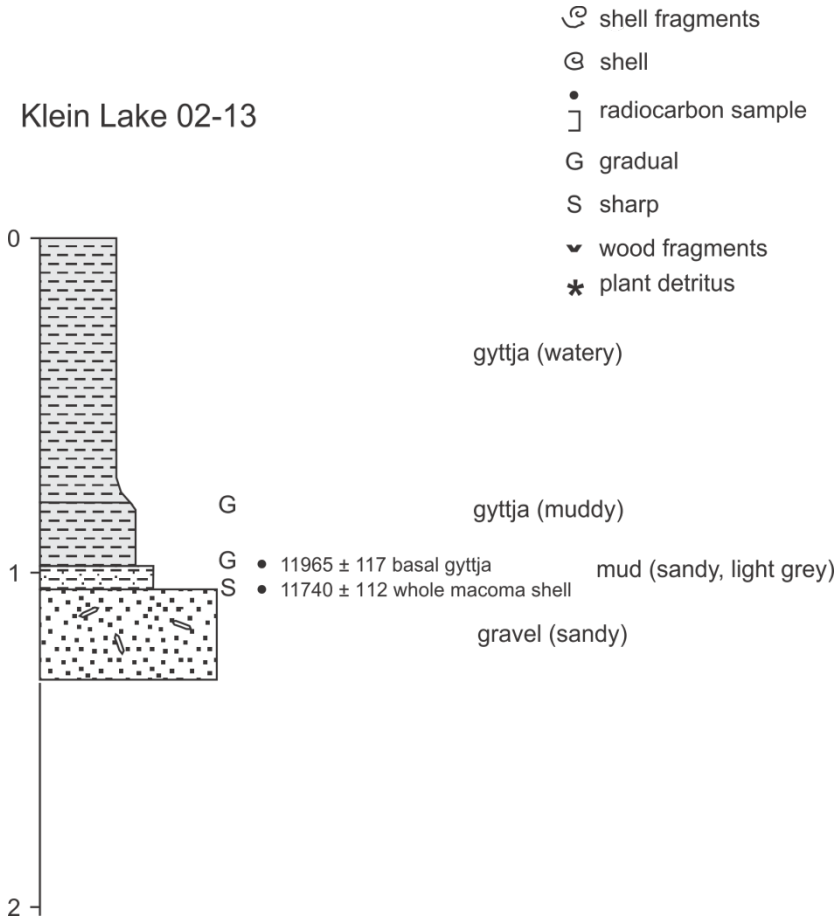

Figure 3.8. Stratigraphy (m) and radiocarbon ages (yr) for core taken at Klein Lake.

A core (CIA-02-13) was taken from the NE part of the lake at 135 m elevation and 7 m water depth. It penetrated 2.05 m and 1.50 m of core was recovered. Angular gravel was found in the core catcher and initially interpreted as landslide alluvium from a steep slope; when split, the core contained a shell above the gravel.

A watery 79 cm layer of gyttja graded to 19 cm of muddy gyttja with mud laminae at 93 and 94 cm and occasional wood fragments, which in turn graded to a 7 cm layer of light grey sandy mud with a whole Macoma shell. An abrupt boundary separated this from a 27 cm layer of coarse sandy gravel with sub-angular pebbles and cobbles (< 7 cm length).

The Macoma shell (CIA-02-13-103/105, Figure 3.8) and basal gyttja (CIA-02-13-95/98, Figure 3.8) date to the late Pleistocene. A shell in grey mud indicates that sea-level remained over 135 m higher than present until about 11740 ± 112 corrected ^{14}C yr BP. Sea-level must have then fallen below 135 m before 11965 ± 117 corrected ^{14}C yr BP, when the basal gyttja was deposited. The small age inversion (225 radiocarbon years) is within the uncertainties of the ages and indicates that sea-level must have dropped below the elevation of the sill around 11850 BP.

3.2.5 Little Klein Lake

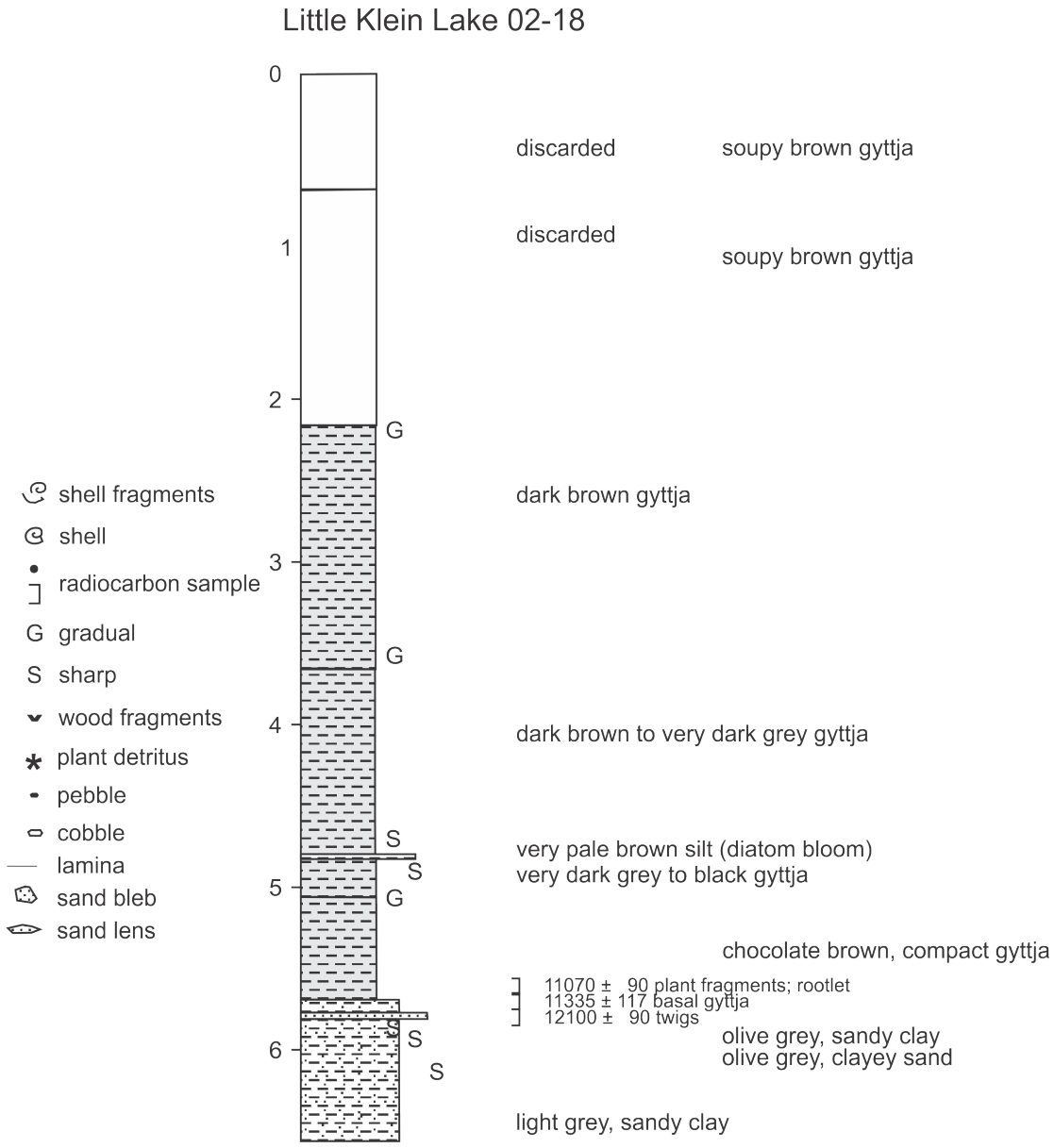

Figure 3.9. Stratigraphy (m) and radiocarbon ages (yr) for core taken at Little Klein Lake.

A core (CIA-02-19) was taken at 113 m elevation in 5.8 m water depth and 11.2 m penetration. A 150 cm thick layer of dark brown gyttja was very watery at the top and graded to a 115 cm layer of dark brown to very dark grey gyttja. A very thin 0.2 cm layer of very pale brown very fine sand topped a 24.8 cm layer of very dark

grey to black gyttja, which graded to a 63 cm layer of chocolate-brown, compact gyttja with a thin clay stringer at 567.5 cm and plant fragments including a rootlet at 551-561 cm.

An abrupt transition led to an 8 cm layer of olive-grey sandy clay over 4 cm of olive-grey clayey sand. An abrupt transition topped a 75 cm layer of light grey clay with granules, a sandy layer at 589 cm, and a sand lens at 618 cm. No shells were found, but urchin spines and a twig were recovered from the clay at 570-574 cm and 572-574 cm (respectively, Figure 3.9). The sea urchin spines were not dated (insufficient sample mass for reliable radiocarbon dating).

A twig in grey mud next to sea urchin spines indicates that sea-level remained over 113 m higher than present until about 12100 ± 90 corrected ^{14}C yr BP. An age on basal gyttja indicates that sea-level must have then fallen below 113 m before 11335 ± 117 corrected ^{14}C yr BP. Plant fragments from the same horizon give a slightly younger age of 11070 ± 90 ^{14}C yr BP.

3.2.6 Swanson's Well

Sometime around 1972, a local resident dug a well near Sechelt, BC at 107 m elevation. A single, complete valve of a *Clinocardium Nutalli* (CIA-02-21) was obtained from the excavation. The age of the shell indicates that sea-level fell below 107 m elevation some time after 11450 ± 158 BP.

3.2.7 Hotel Lake

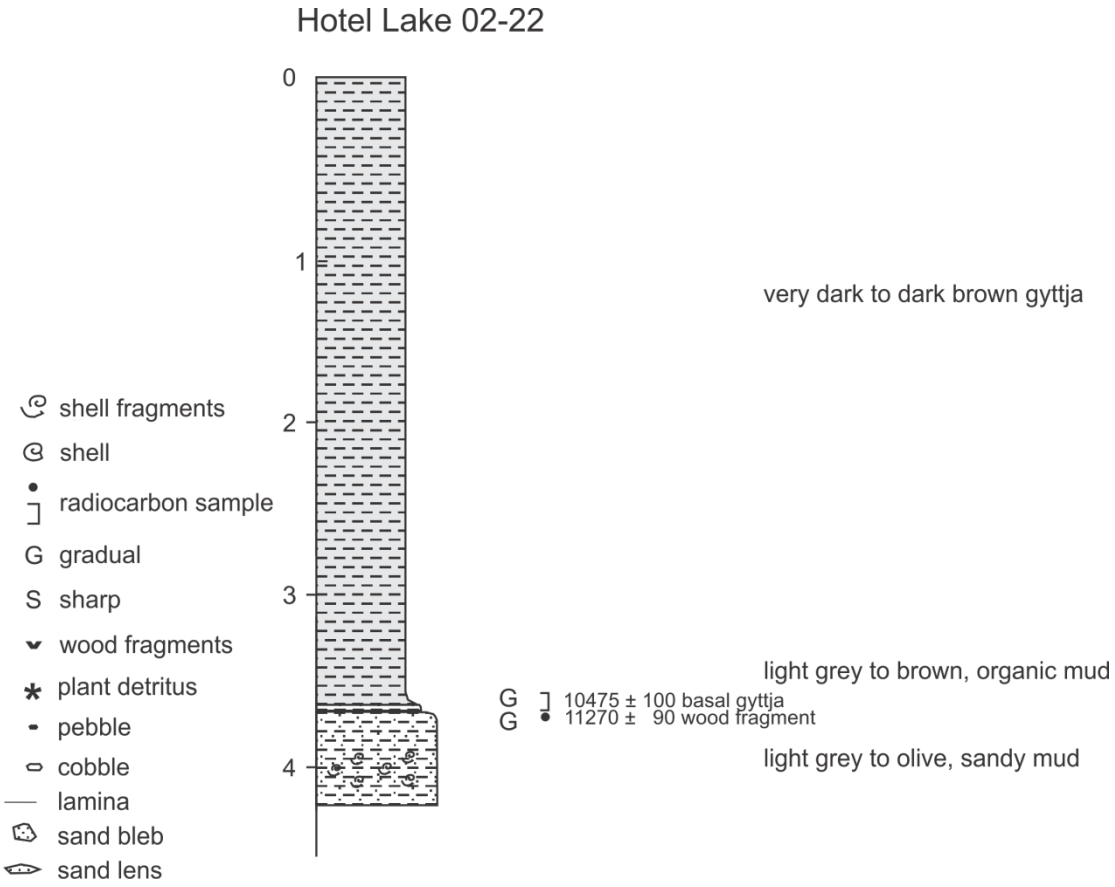

Figure 3.10. Stratigraphy (m) and radiocarbon age (yr) for core taken at Hotel Lake.

Three cores (CIA-02-16, CIA-02-17 and CIA-02-22) were taken at 50 m elevation. The first core recovered only gyttja; the second was taken too close to shore and recovered a single section that did not sample the transition from marine to freshwater sedimentation. A third core (CIA-02-22) was successfully taken midway between the first two and penetrated 7.5 m at 10.25 m water depth.

The third core was topped with 364 cm layer of dark brown gyttja, which was watery near the surface. Within this top unit, muddy gyttja lay below a gradational boundary at 350 cm. The gyttja graded to a 3 cm thin layer of laminated, organic-rich, light grey mud with yellowish brown laminae ~2-4 mm thick. This mud graded to a

55 cm layer of very fine, light grey sandy mud with a large (~5 cm) clast at 397-402 cm and abundant shell hash from 390 - 407 cm.

A wood fragment (CIA-02-22-374, Figure 3.10) and basal gyttja (CIA-02-22-362/364, Figure 3.10) both date to the late Pleistocene. A wood fragment in grey mud indicates that sea-level remained over 50 m higher than present until about 11270 ± 90 ^{14}C yr BP. Sea-level must then have fallen below 50 m before 10475 ± 100 corrected ^{14}C yr BP, when the basal gyttja was deposited.

3.2.8 Katherine Lake

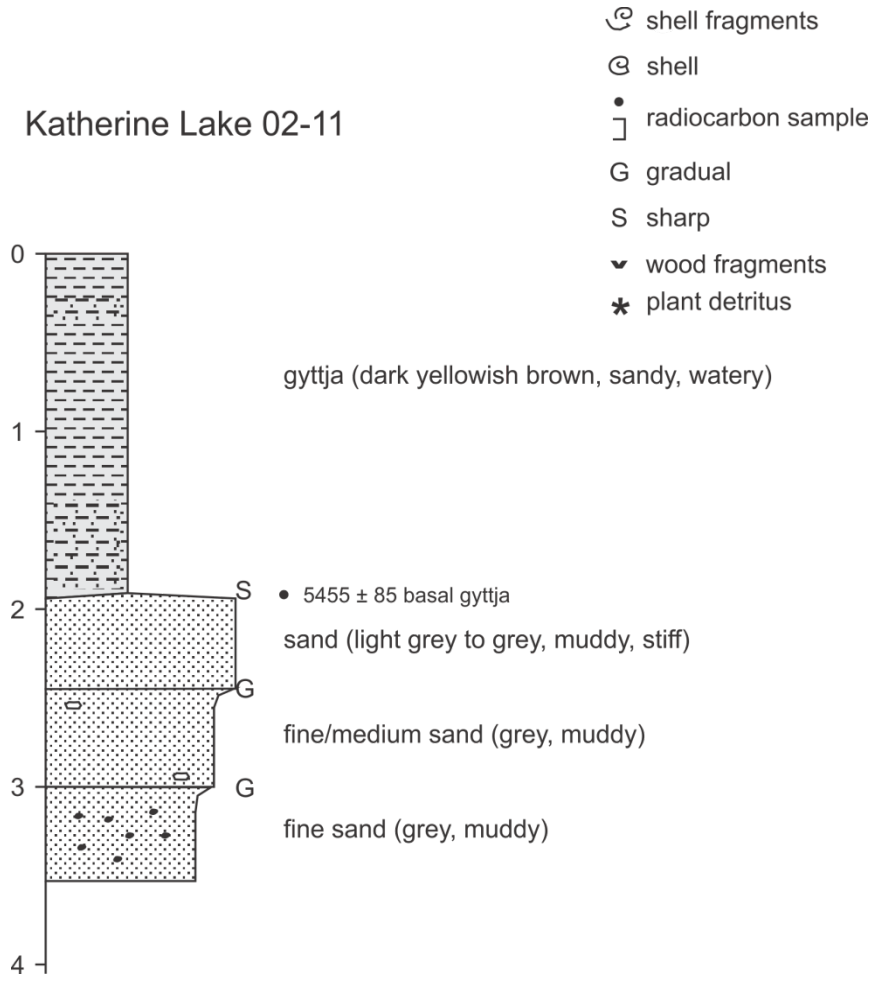

Figure 3.11. Stratigraphy (m) and radiocarbon age (yr) for core taken at Katherine Lake.

A 352 cm core (CIA-02-11) was taken at 18 m elevation (water depth not recorded) and contained a 194-cm layer of dark yellowish brown to dark brown gyttja with scattered medium sand grains and granules, increasing in frequency to its base. A very sharp, angular boundary separated the gyttja from a 50 cm layer of stiff, grey muddy sand with occasional granules. The blue-grey clay contained no obvious shells and graded to 45 cm layer of grey muddy to fine-medium sand, which contained large

sub-angular clasts (3-4 cm) at 253 cm and 298 cm. The muddy to fine-medium sand graded to a 53 cm layer of grey, muddy, fine sand with scattered sub-angular pebbles.

The core yielded a single basal gyttja sample (CIA-02-11-190/193, Figure 3.11) that dated to the mid-Holocene. Sea level dropped below 18 m elevation before 5455 ± 85 corrected ^{14}C yr BP. This basal gyttja age is anomalously young. Perhaps the sand was deposited in the early to mid-Holocene, displacing or overlying gyttja that had already been deposited. Alternatively, erosional processes may have removed older organic sediments.

3.2.9 Mercer Road Bog

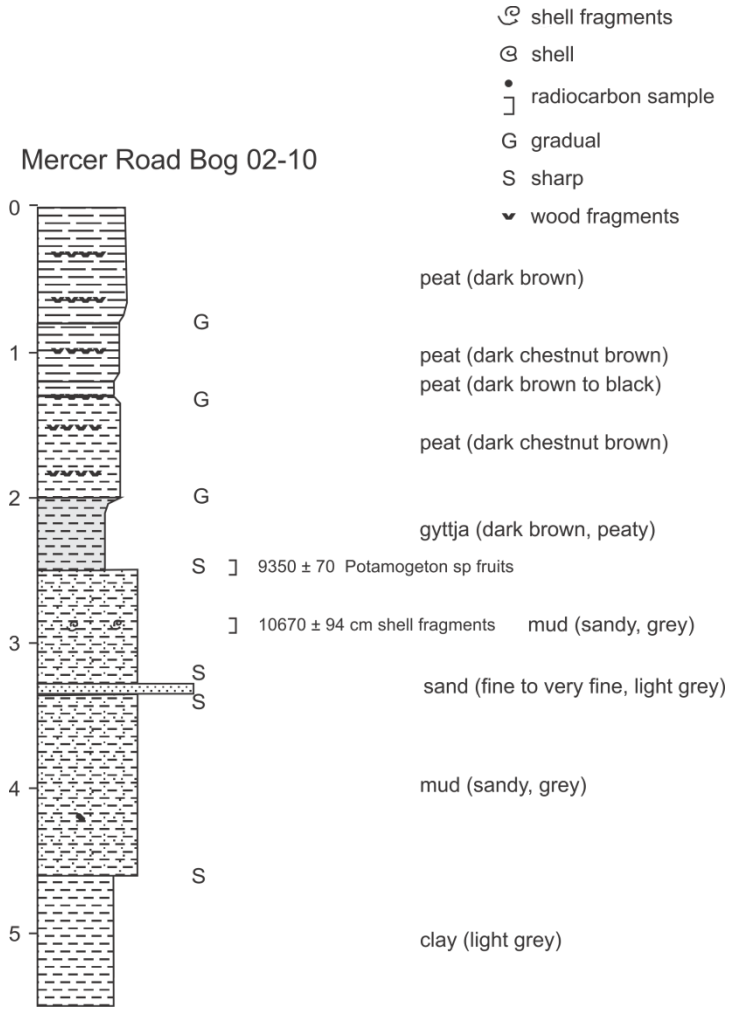

Figure 3.12. Stratigraphy (m) and radiocarbon age (yr) for core taken at Mercer Road Bog.

Mercer Road Bog is at 5 m elevation above the high tide mark. A 5.5 m Vibra-core (CIA-02-10) was taken in an 80 cm deep dug pit. A total of 18 seeds were collected from two peat samples above an abrupt boundary between a 50 cm layer of dark brown, well-humified peat/gyttja with occasional rhizomes and a 78 cm layer of grey mud with small admixture of very fine sand and occasional shell fragments. Small quantities of sea urchin spines and vegetation among shell fragments were insufficient to radiocarbon date.

Shell fragments (CIA-02-10-275/288, Figure 3.12) and *Potamogeton sp* fruit seeds (CIA-02-10-248/250, Figure 3.12) date to the late Pleistocene. The age of marine shells from grey mud indicate that sea-level remained more than 5 m higher than present until 10670 ± 94 corrected ^{14}C yr BP. Sea-level must have then fallen below 5 m before 9350 ± 70 corrected ^{14}C yr BP, when seeds were deposited in gyttja.

3.2.10 Hospital Bay

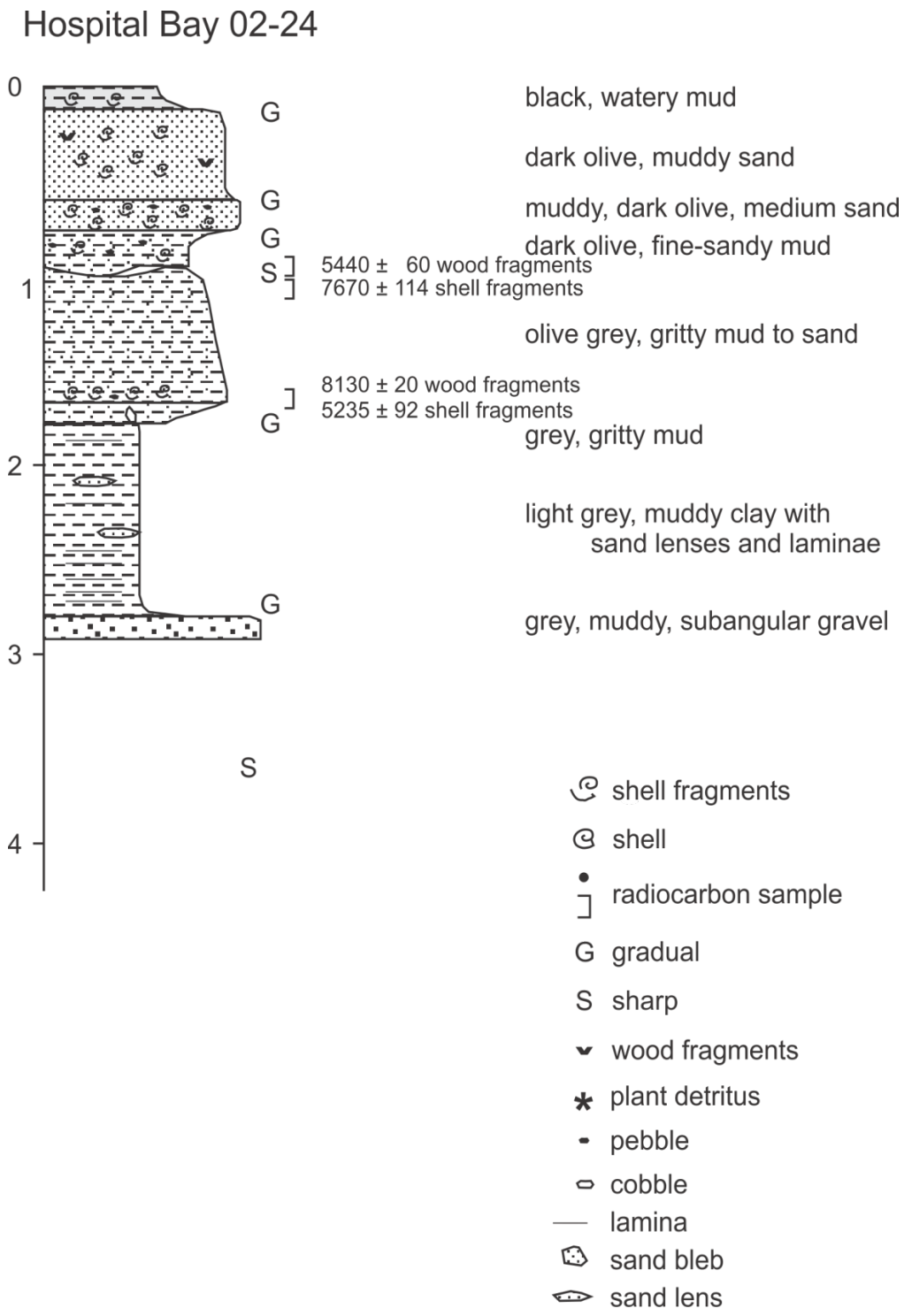

Figure 3.13. Stratigraphy and radiocarbon age (yr) for core taken at Hospital Bay.

A single 292 cm long percussion core (CIA-02-24) was taken from the docks of John Henry's Marina. Core penetration was 385 cm. Sill depth is estimated at -8 m. Twelve cm of watery black mud with fine shell fragments graded to 48 cm of dark olive muddy sand, fining to mud with abundant shell fragments and a few plant macro-fossils. This mud overlaid 16 cm of dark olive muddy medium sand with granules and pebbles and abundant shell fragments, grading to another 16-20 cm of olive grey fine sandy mud to muddy sand with pebbles and occasional shell fragments with an abrupt wavy boundary at 92/96 cm to about 73 cm of grey fine sandy mud fining to clayey mud. The lower part of this unit contained occasional granules and very fine shell hash and a 4 cm sub-angular pebble at 164-166 cm. The unit transitioned to 11 cm of grey gritty mud containing a large sub-angular/semi-rounded cobble at 173-178 cm, and significantly less sand and silt than the overlying unit. This mud graded to 102 cm of light grey muddy very fine sand, with sand lenses at 214-217 cm and 252-255 cm above 12 cm of muddy grey sub-angular gravel in the core catcher (Figure 3.13).

Shell fragments (CIA-02-24-90/95) and wood fragments at 1 m core depth both (CIA-02-24-102/107) returned mid-Holocene dates of 7670 ± 115 corrected ^{14}C yr BP and 5440 ± 60 corrected ^{14}C yr BP, respectively. The sharp boundary at 1 m core depth was thought to represent the transition between Holocene marine and Pleistocene glaciomarine sediments, but the ages clearly indicate that this is a Holocene boundary.

A second pair of samples at a gradational boundary near 165 cm core depth also returned Holocene ages: shell fragments (CIA-02-24-159/165-w) dated to 5235 ±

92 corrected ^{14}C yr BP; wood fragments (CIA-02-24-159/165-s) dated to 8130 ± 20 corrected ^{14}C yr BP. Thus, further sampling did not clarify the stratigraphic record and suggests substantial reworking of sediments in this basin. This core indicates that marine conditions have probably persisted in the basin since about 8000 ^{14}C yr BP.

3.3 Relative Sea-Level Curve

At Sechelt, BC, data from the present study indicates that sea level dropped from at least 150 m before 12 ^{14}C kyr BP. Previous studies of marine deposits and deltas in the region indicate that sea level during the late Pleistocene was at least 180 m above present (McCammon 1977). Between 12 and 11 ^{14}C kyr BP, sea level fell past the present level to a poorly constrained lowstand between about 10.5 and 8.5 ^{14}C kyr BP. The absolute depth and precise timing of the lowstand position at Sechelt, BC are not directly constrained by the observations. Sea level returned to near present levels around 6.0 ^{14}C kyr BP (Figure 3.14).

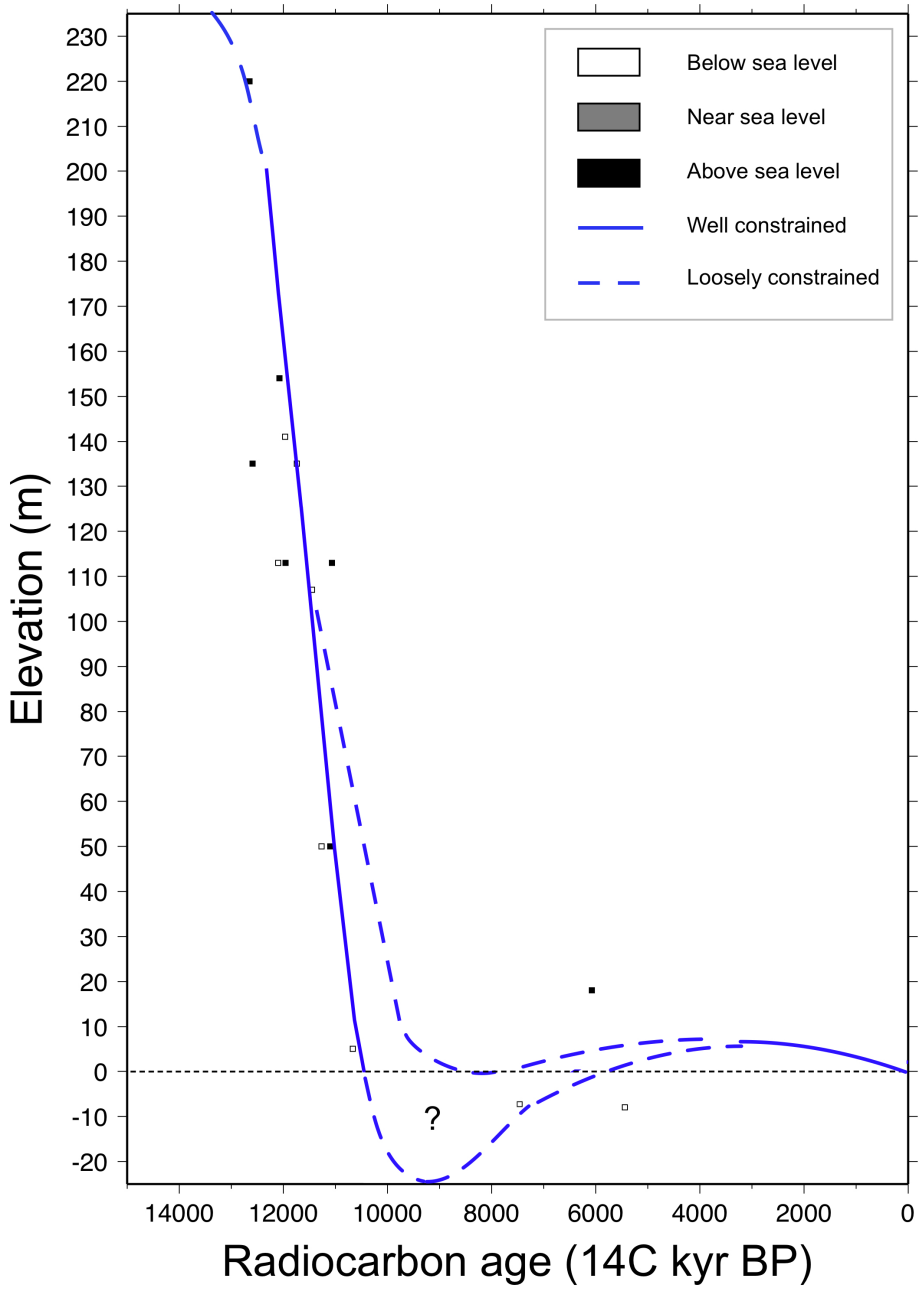

Figure 3.14. Postglacial relative sea-level change at Sechelt, BC, in radiocarbon years.

Corrected radiocarbon dates were calibrated and plotted as probability density functions (PDFs) using the computer program Calib 5.0 (Stuiver and Reimer 1993);

marine samples reference the Marine04 data-set (Hughen *et al.* 2004) and terrestrial samples the Intcal04 data-set (Reimer *et al.* 2004).

Figure 3.15 plots relative sea-level in calendar years as derived from the calibrated PDFs of corrected radiocarbon ages. Dotted lines represent the envelope or range of values as constrained by the study data.

Sea level dropped from at least 150 m before 14 cal kyr BP to near present levels by about 12 cal kyr BP. Sea level continued to fall below present level to a poorly constrained lowstand between 12 and 9 cal kyr BP. The observations do not directly constrain the absolute depth and precise timing of the lowstand position at Sechelt, BC. (Specifically, cores from marine basins such as Hospital Bay and deeper basins, sampling late Pleistocene and early Holocene sediments, are needed to constrain the low stand.) Sea level returned to near present levels around 6.0 cal kyr BP (Figure 3.15).

A regional comparison of sea-level curves shows relative sea-level at Sechelt to have closely followed the same trend as in the central and northern Strait of Georgia. Relative sea-level at all three locations dropped from at least 150 m before 14 cal kyr BP (Hutchinson *et al.* 2004a: Fig. 5; James *et al.* 2005: Fig. 6 and 7). Sea level at all three locations returned to near present levels around 6 cal kyr BP.

At Sechelt, sea level fell past the present level sometime after 12.4 cal kyr BP (CIA-02-10-275/288). In the central Strait of Georgia, sea level most likely fell below

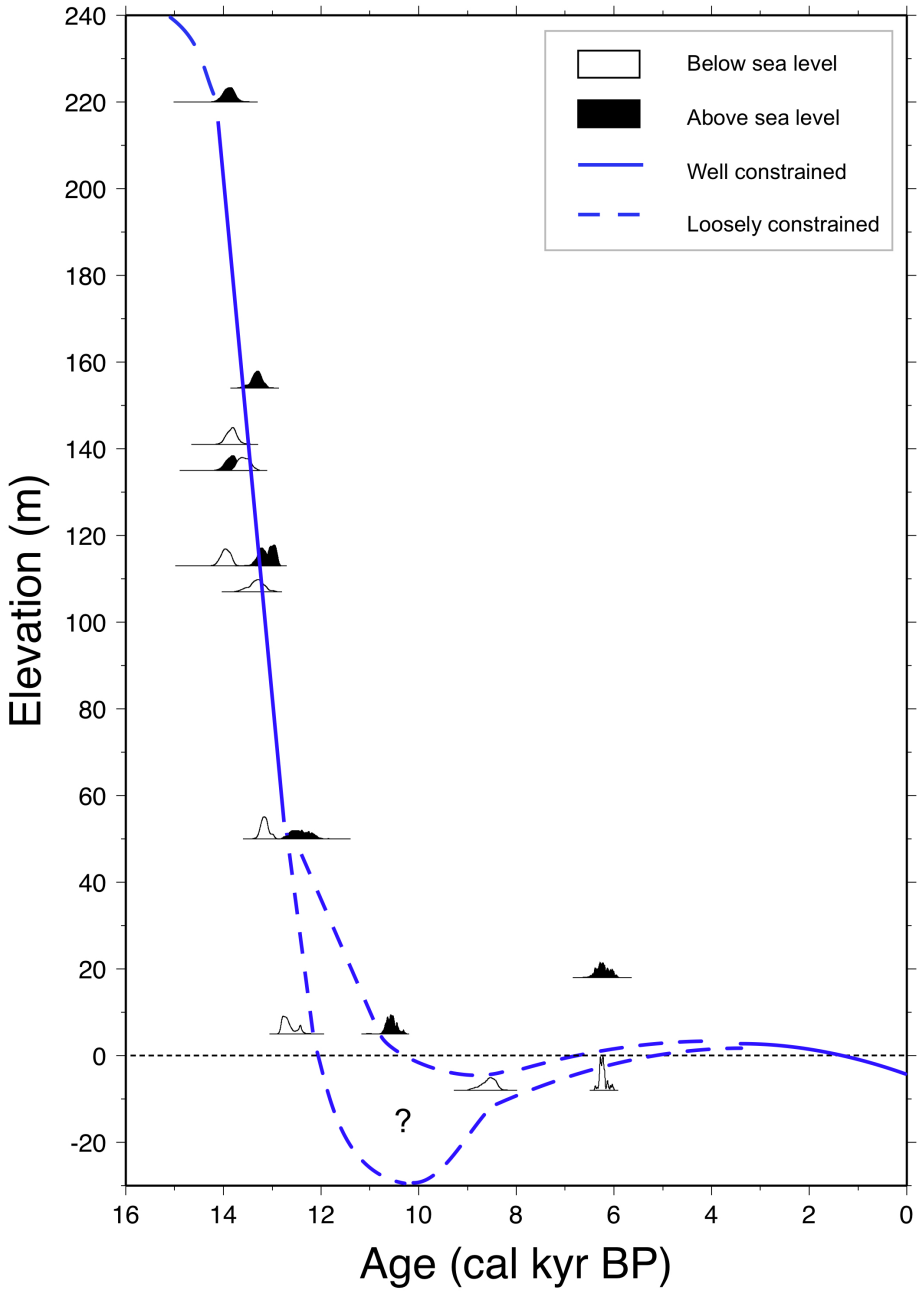

Figure 3.15. Postglacial relative sea-level change at Sechelt, BC, in calendar years. Dashed lines plot the envelope or range of values as constrained by the study data.

present at approximately the same time as in Sechelt but may have fallen below present levels as early as 13.0 cal kyr BP (TO-9905/9906, James *et al.* 2005). In the

north Strait of Georgia, sea level fell past present levels sometime after 13.5 cal kyr BP but possibly as late as 11.1 cal kyr BP (TO-9896/9909, Hutchinson *et al.* 2004a). The maximal ages for the time that sea level dropped below present are: northern Strait: 13.5 kyr, central Strait: 13.0 kyr, and Sechelt: 12.4 cal kyr BP. They are consistent with a noted trend of relatively early and deep lowstands toward the (south-west) periphery of the CIS and later and shallower lowstands towards its (north-east) interior (Fig. 3.2, after Fig. 10. Muhs *et al.* 1987, in Clague and James, 2002). However, sea level may have fallen past present levels well after the maximal age sampled at each location; maximal ages may not represent the actual sequence of emergence. Thus, determining a regional trend must wait on the establishment of further constraints.

At Sechelt, BC, the absolute depth and precise timing of the lowstand position are not directly constrained by observations. However, an analysis of crustal response and decay rate can be used to infer the lowstand depth and timing that is most likely or 'preferred' by the available data. Section 3.2.3 below calculates constraints on relative sea level provided by inferred isostatic depression and eustatic sea level rise. A regional comparison of the timing and amplitude of the low stand is then presented in the context of the isostatic depression analysis.

3.4 Crustal response and decay rate

The crustal response due to isostatic depression can be derived by subtracting assumed eustatic sea-level change from observed relative sea-level. Equatorial regions are distant enough from large Quaternary ice sheets that the isostatic crustal motion directly related to continental-scale ice load is muted. Thus, in the tropics,

relative and eustatic sea level approximate each other, excepting crustal motions arising from other processes, such as tectonics. Here, tectonically-corrected relative sea level records from raised corral terraces in Barbados (Basset, 2005) are used as a proxy for eustatic sea level. Figure 3.16 below plots the isostatic depression at Sechelt, BC, obtained by subtracting eustatic sea-level from observed relative sea-level.

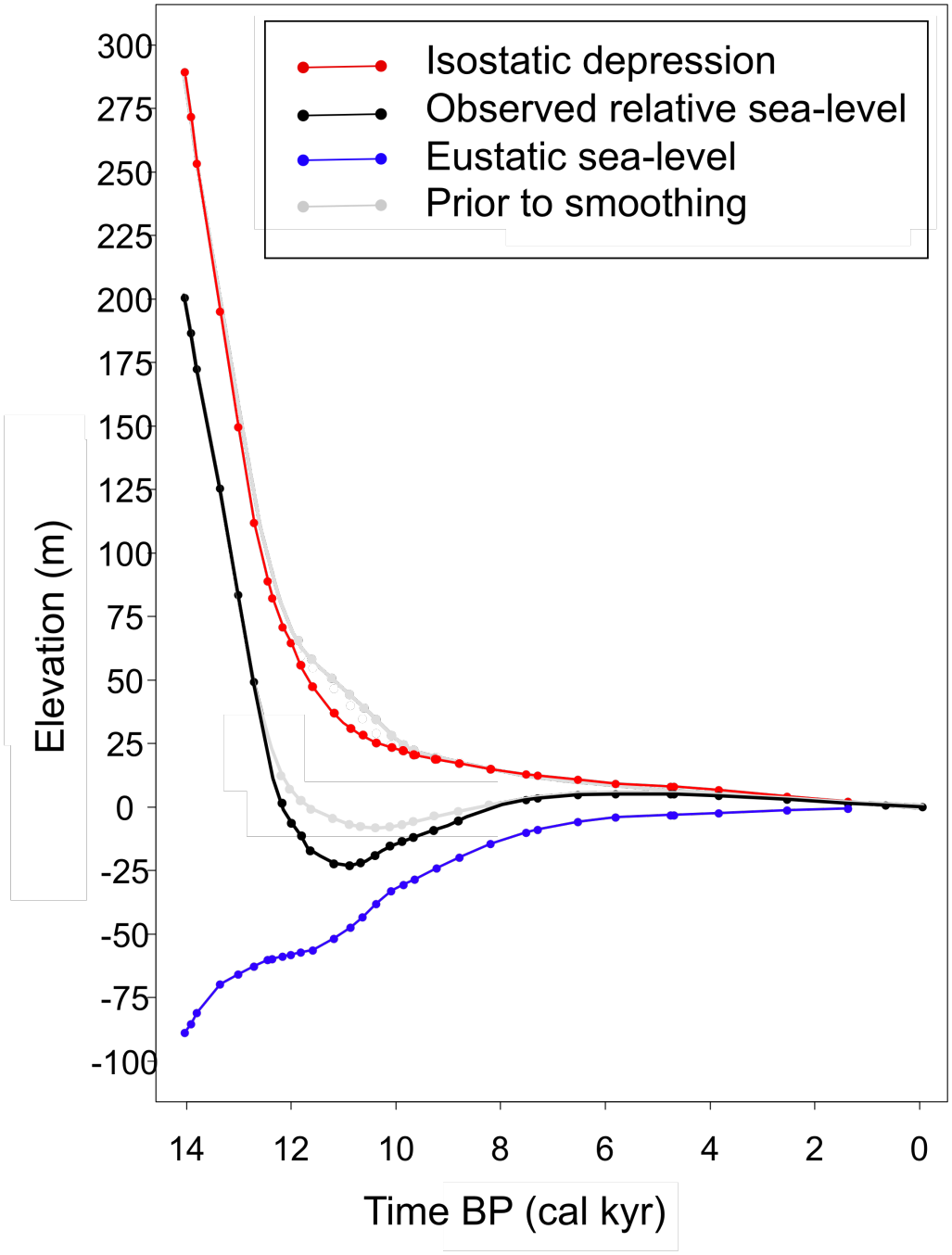

Figure 3.16. Isostatic depression at Sechelt, BC derived by subtracting eustatic sea-level from observed relative sea-level. Greyed portions of the curves represent derived crustal response and observed sea level before smoothing.

Figure 3.16 shows the isostatic depression derived from the initial assumed relative sea-level curve (grey curves). The isostatic depression features a sudden change in the rate of decay commencing about 12 cal kyr. This slowing of the Earth's isostatic response arises from the choice made for the amplitude of the poorly-constrained lowstand. The final phases of the retreat of the Cordilleran ice sheet do not feature a marked stillstand or resurgence, which would be required to generate the significant slowing of crustal uplift.

Instead, because the relative sea-level low stand is poorly constrained, the isostatic depression can be adjusted to give a smoother rate of decay. The smoothed isostatic depression curve was then used to generate a new relative sea-level curve by adding the assumed eustatic sea-level change to the smoothed isostatic depression curve. Smoothing the isostatic depression leads to a deeper lowstand of the relative sea-level curve. Isostatic depression analysis serves as a geophysical constraint on relative sea-level. Figure 3.17 plots this preferred relative sea-level curve (dotted, dashed blue line) within the same envelope of values (dashed black lines) for relative sea-level as first presented in Figure 3.15.

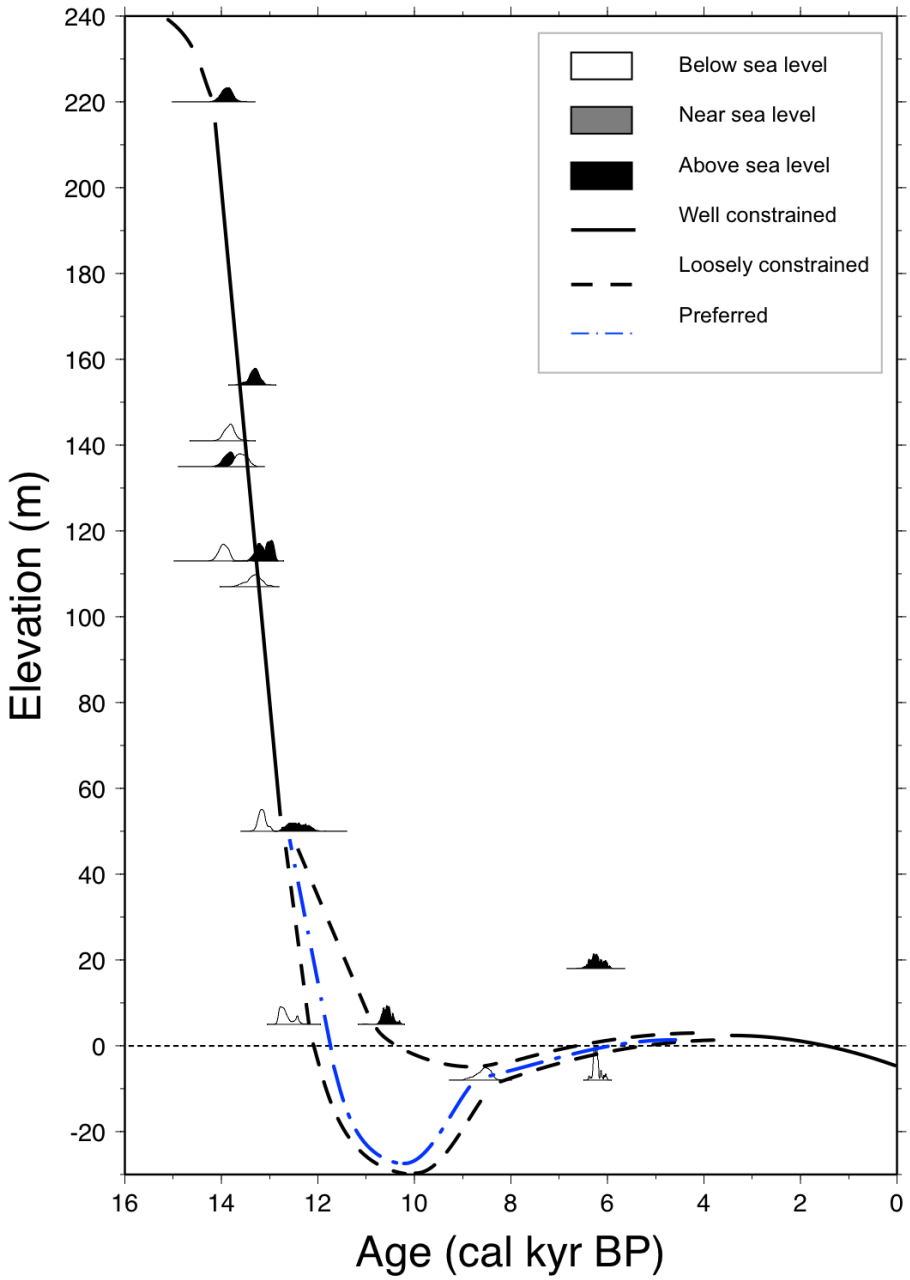

Figure 3.17. Postglacial relative sea-level change at Sechelt, BC, in calendar years. The dotted, dashed blue line is the preferred relative sea-level curve derived from an analysis of the combined effect of isostatic depression and eustatic sea-level rise. Dashed black lines plot the envelope or range of values as constrained by the study data. White PDF (probability distributions) are expected to plot below the RSL curve. Black PDFs are expected to plot above the RSL curve.

A lowstand magnitude of about -25 m at 10.5 cal kyr BP is preferred by isostatic depression analysis for Sechelt, BC. A similar analysis of the central Strait of Georgia (Hutchinson *et al.* 2004a) established a preferred lowstand magnitude of approximately -10 m at about 11.5 cal kyr BP. In the northern Strait of Georgia the preferred lowstand is about -5 m at 10 cal kyr BP (James *et al.* 2005). Sea level at all three locations returned to near present levels around 9 cal kyr BP.

GIA theory models the Earth's response to glacial mass changes as the sum of exponential decay terms (Peltier 1985; Turcotte and Schubert, 2002). The equation $D = D_0 \exp(-t/\tau)$ expresses the special case where a single term describes isostatic depression decreasing with time; D_0 is the initial isostatic depression after deglaciation, t is the decay time, and τ is the exponential decay constant and is dependent on the model viscosity of the Earth's asthenosphere and mantle.

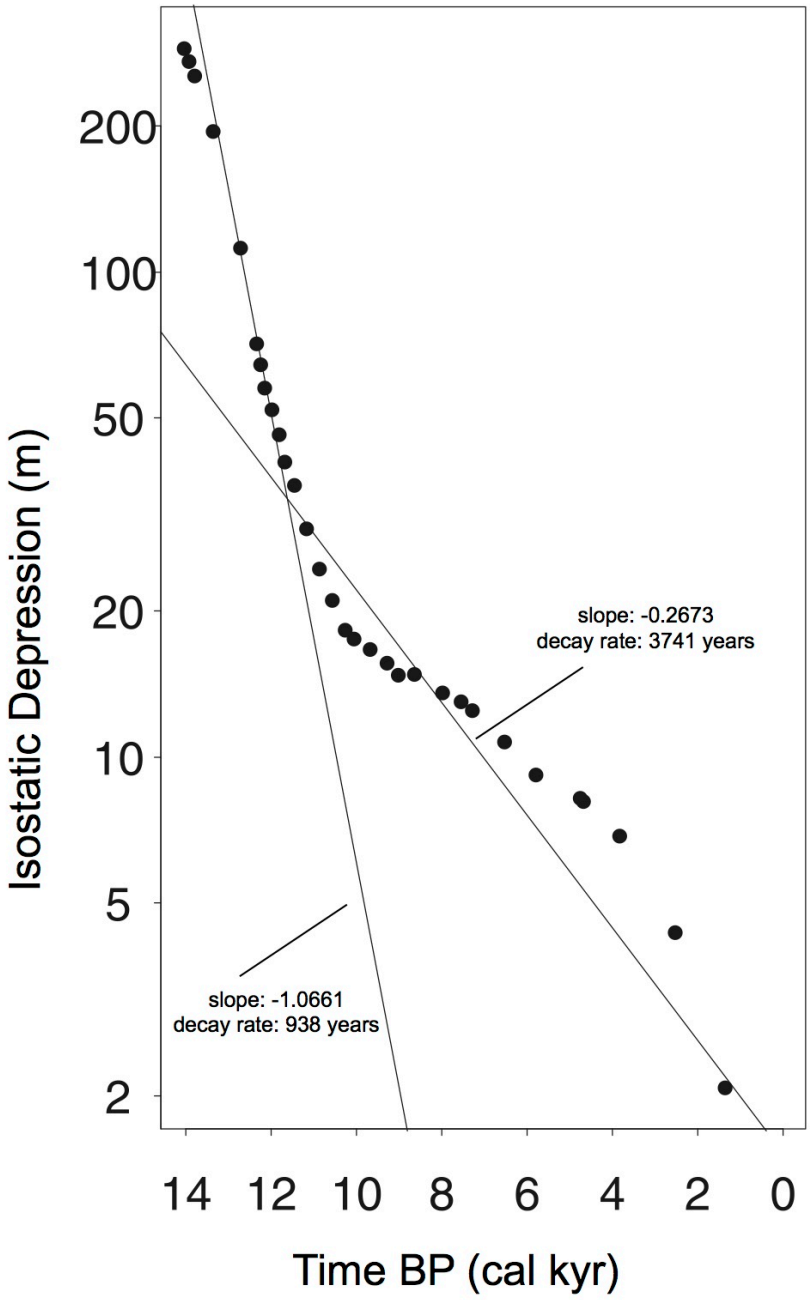

Figure 3.18. Characteristic decay times of the derived isostatic depression curve at Sechelt, BC.

Figure 3.18 presents the isostatic crustal depression on a semi-logarithmic plot. The slope of a straight line through the points is the negative inverse of the decay time, $-1/\tau$. The slopes of the two lines of the semi-logarithmic plot (Figure

3.18) were determined using linear regression. The isostatic depression features a steep decay rate of 938 years (slope = -1.0661) immediately following deglaciation from 14 to 12 cal kyr BP, followed by a slower response fit of 3741 years (slope = -0.2673) with a shallower slope from 12 to 10 cal kyr BP.

The isostatic depression was fit by assuming two decaying exponential terms, fixing the decay time of one term to 3700 years, and varying the decay time of the second term until the best fit to the observed isostatic depression was obtained. A faster 800-year decay time combined with a slower 3700-year term fits the entire time series well. During initial GIA response, the 800-year and 3700-year decay times combined to produce an apparent decay time of 938 years (Figure 3.19).

The mean decay rate in Sechelt, BC during initial late Pleistocene deglaciation (from 14 to 12 cal kyr BP) was at least 85 mm/yr, dominated by the quicker GIA component driven by the less-viscous asthenosphere (τ = 800 years). The mean decay rate then decreased to about 49 mm/yr from 12 to 10 cal kyr BP, when the fast GIA component had decayed sufficiently that the dominant force shifted to the slower, visco-elastic response of the more-viscous deeper mantle (τ = 3700 years). By 10 cal kyr BP, remnant effects of GIA were less than 0.1 mm/yr, whereafter sea-level change was dominated by eustatic sea-level rise until the late Holocene. Current sea level change is determined by regional tectonics (Mazzotti *et al.* 2003).

In the northern Strait of Georgia, the rate of crustal uplift in the first millennium following deglaciation was estimated to be at least 100 mm/yr and may have exceeded 200 mm/yr during early emergence (James *et al.* 2005). In the central Strait of Georgia, the rate of crustal uplift in the first millennium following

deglaciation was estimated to be at 110 mm/yr and may have exceeded 200 mm/yr during early emergence (Hutchinson *et al.* 2004a). Thus, initial sea-level fall at Sechelt appears to have occurred at a somewhat slower rate than in the central and north Strait of Georgia.

Present-day relative sea-level around Vancouver Island is predominantly controlled by regional tectonics of the CSZ (James *et al.* 2009a). Holocene segments of sea-level curves around Vancouver Island are also thought to include a significant tectonic component (Hutchinson 1992). Residual GIA effects due to the unloading of the CIS have been estimated to affect the present-day rate of crustal uplift as follows: a) less than 0.10 mm/yr in the central Strait of Georgia (James *et al.* 2005), b) about 0.12 mm/yr at Victoria (James *et al.* 2009b) and c) about 0.25 mm/yr at the northern Strait of Georgia (James *et al.* 2005). This question of vertical velocity due to GIA is discussed further in this thesis following the presentation of the computer modeling.

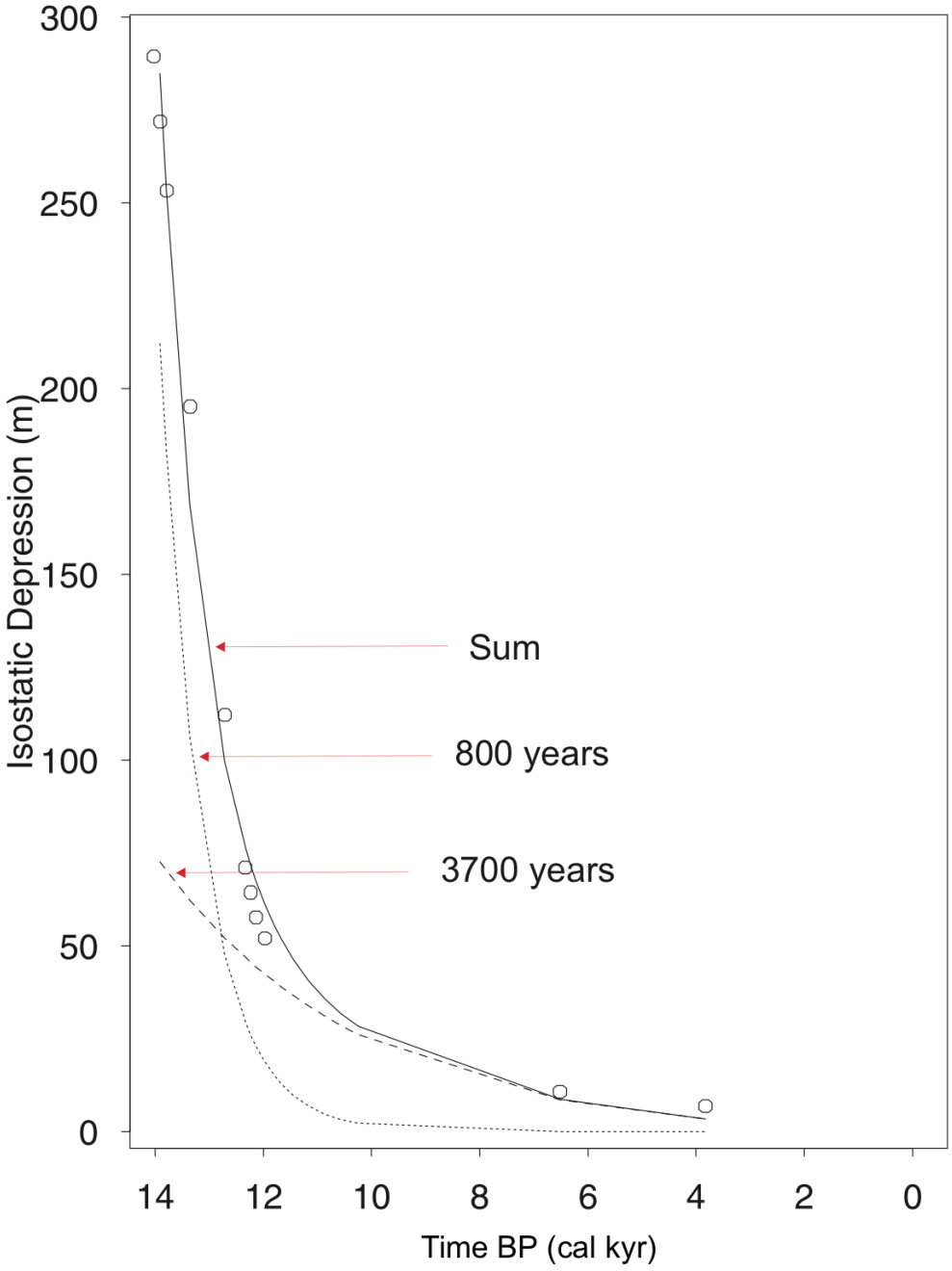

Figure 3.19. Two exponentially-decaying components of the crustal response at Sechelt, BC.

Chapter 4 - Observations and Inferred Sea-level Curve for Barkley Sound, Vancouver Island, British Columbia

This chapter presents constraints on sea-level history during and after the collapse of the Cordilleran Ice Sheet (CIS) for the Barkley Sound region on the west coast of Vancouver Island, BC (Figure 4.1). As summarized by James *et al.* (2009a), prior investigations have described detailed sea-level constraints for three regions on a profile running northwest-southeast along the east coast of Vancouver Island and western Strait of Georgia.

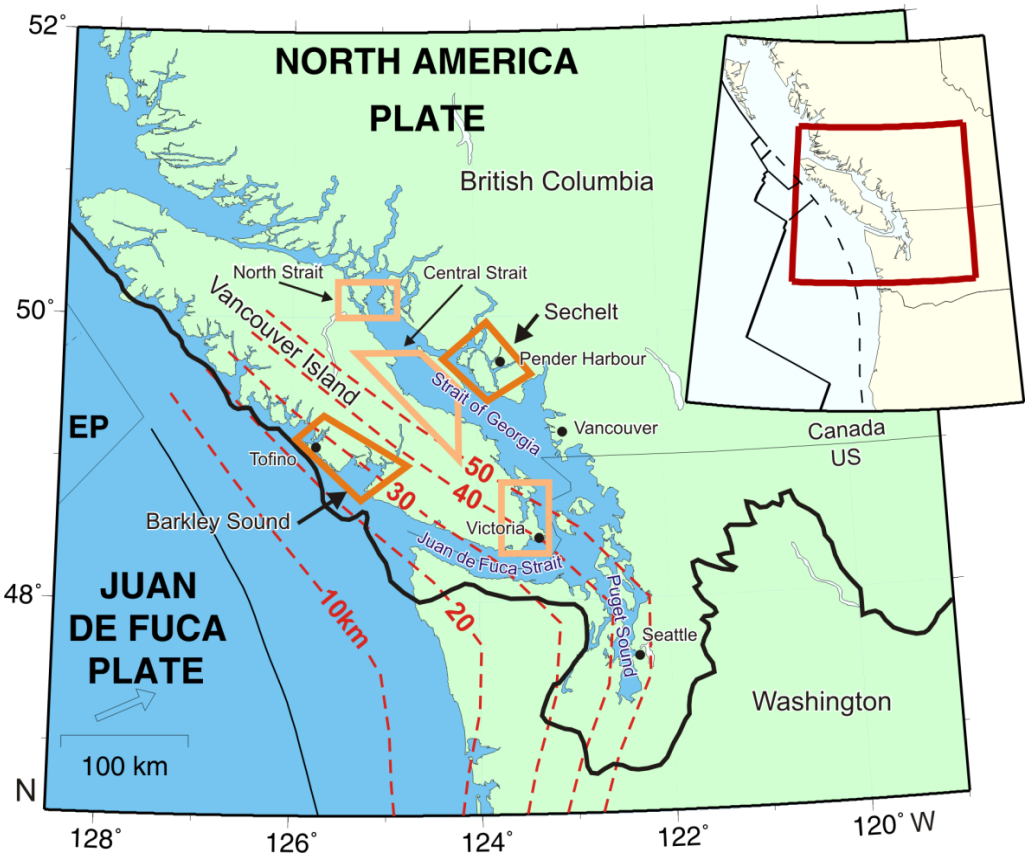

Figure 4.1. Location map showing regions for which relative sea-level curves are newly defined (Sechelt) or extended (Barkley Sound) (dark orange quadrilaterals) in this study. Three previously published curves (pale orange) for Victoria (James *et al.* 2009a), central Strait of Georgia (Hutchinson *et al.* 2004a), and northern Strait of Georgia (James *et al.* 2005) are also located over the northern Cascadia subduction zone in the Straits of Georgia and Juan de Fuca (figure after James *et al.* 2009a).

New data presented here and in Chapter 3 for Sechelt, BC, define a second profile that is approximately perpendicular to the existing profile. The new profile is oriented southwest-northeast across Vancouver Island and the Strait of Georgia. They intersect in the central Strait of Georgia, where Hutchinson *et al.* (2004) described the sea-level history.

As described in Chapter 3, the CIS had a source region in the Coast Mountains and spilled over onto coastal lowlands. It flowed south along the Strait of Georgia and overtopped Vancouver Island, extending offshore onto the continental shelf (Clague and James 2002). Sea-level observations over this region show how sea-level change differed with distance from the edge of the ice-sheet. This chapter presents new information on the timing and amplitudes of sea-level change during CIS deglaciation for the west coast of Vancouver Island that are then used to refine existing models of ice-sheet history in Chapter 5.

4.1 Summary of prior sea-level investigations on the west coast of Vancouver Island, British Columbia

Late Quaternary sea-level fluctuations on the British Columbia coast are constrained by radiocarbon ages and interpretations of terrestrial and marine sediments and landforms (Clague 1975; Clague *et al.* 1982). The sea-level history of mainland BC and eastern Vancouver Island (inner coast) is quite different from that of Haida Gwaii and western Vancouver Island (outer coast), especially during late Pleistocene emergence. The rapid uplift of submerged coastal lowlands evident on both coasts of the Strait of Georgia between about 13 cal kyr BP and 10 cal kyr BP appears to be absent in Haida Gwaii. Instead, shorelines on Haida Gwaii were identified to have been below present from before 13.7 cal kyr BP until approximately 10 cal kyr BP. Maximal transgression during the late Pleistocene was interpreted to be about 15 m in Haida Gwaii at about 7.5-8.5 cal kyr BP.

The sea-level history of the west coast of Vancouver Island exhibits characteristics of both the inner and outer patterns. The late Pleistocene marine maximum was about 27 m at Cape Scott, 19-20 m on Brooks Peninsula, and 32-34 m above present at Hesquiat Harbour, where a late Holocene sea-level curve was constrained by radiocarbon samples (Fig. 10 in Clague *et al.* 1982). Two late Pleistocene dates from the study are included in Table 4.1 and plotted with the present analysis of sea-level around Barkley Sound. The pattern of sea-level change between 13 ^{14}C kyr BP and 4 ^{14}C kyr BP was not constrained by available data.

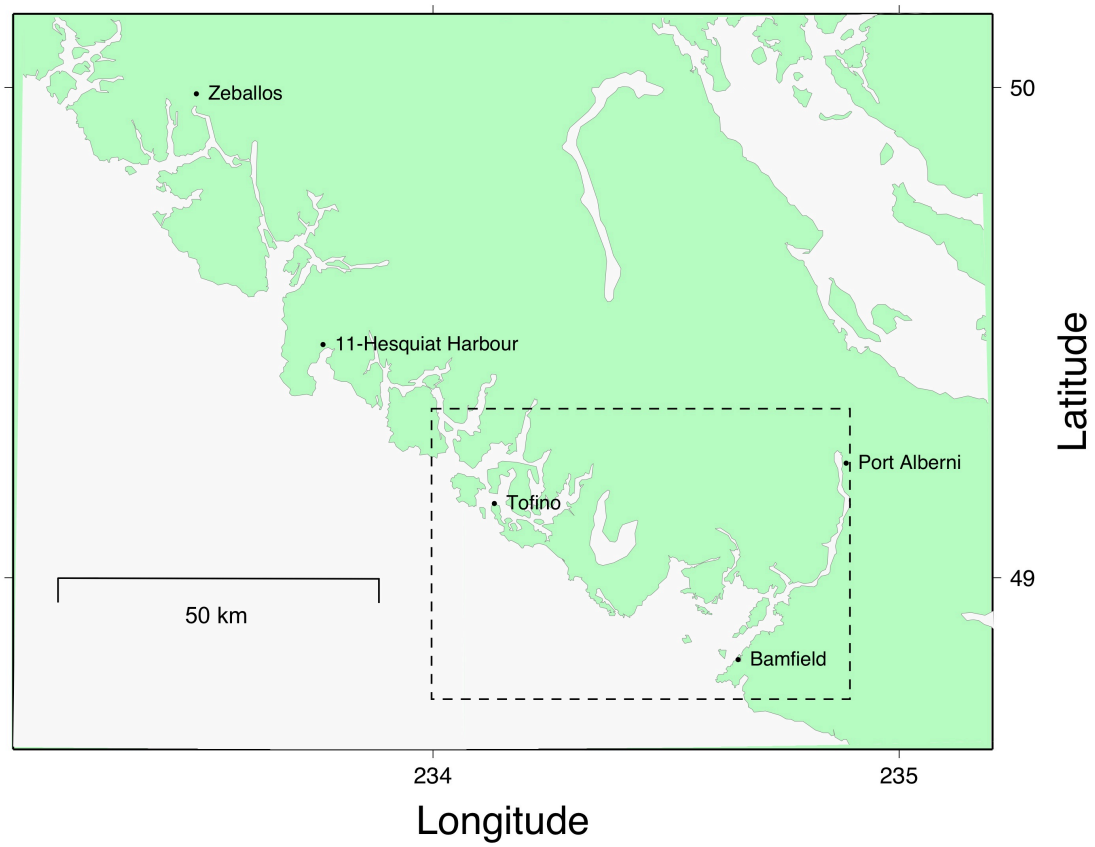

Figure 4.2. Location map of the central west coast of Vancouver Island. With the exception of Hesquiat Harbour (Site 11 in this study), the locations of study sites are given in Figure 4.5 (dashed-line box).

Hutchinson (1992) catalogued existing Holocene radiocarbon ages. Friele and Hutchinson (1993) used the catalogue and new radiocarbon ages around Tofino, BC to propose a new Holocene RSL curve for the central west coast of Vancouver Island, based on topographic surveys of coastal landforms and the stratigraphy of coastal deposits. Twenty-three previously unpublished radiocarbon ages were presented for Vargas Island and both the Esowista and Ucluth peninsulas near Tofino, BC. RSL rose steadily from an unconstrained, early Holocene lowstand sometime before 7 ^{14}C kyr BP, as indicated by dates on tree stumps in the intertidal zone and salt-marsh peats and forest-floor deposits buried by marine sands and gravels. One late

Pleistocene and two early Holocene dates from the study are listed with other dates from the present study (Table 4.1) and plotted with the present analysis of sea-level around Barkley Sound (Bobrowsky and Clague 1992; Friele and Hutchinson 1993). The sea-level history for the west coast of Vancouver Island was unconstrained between 13 ^{14}C kyr BP and 9 ^{14}C kyr BP.

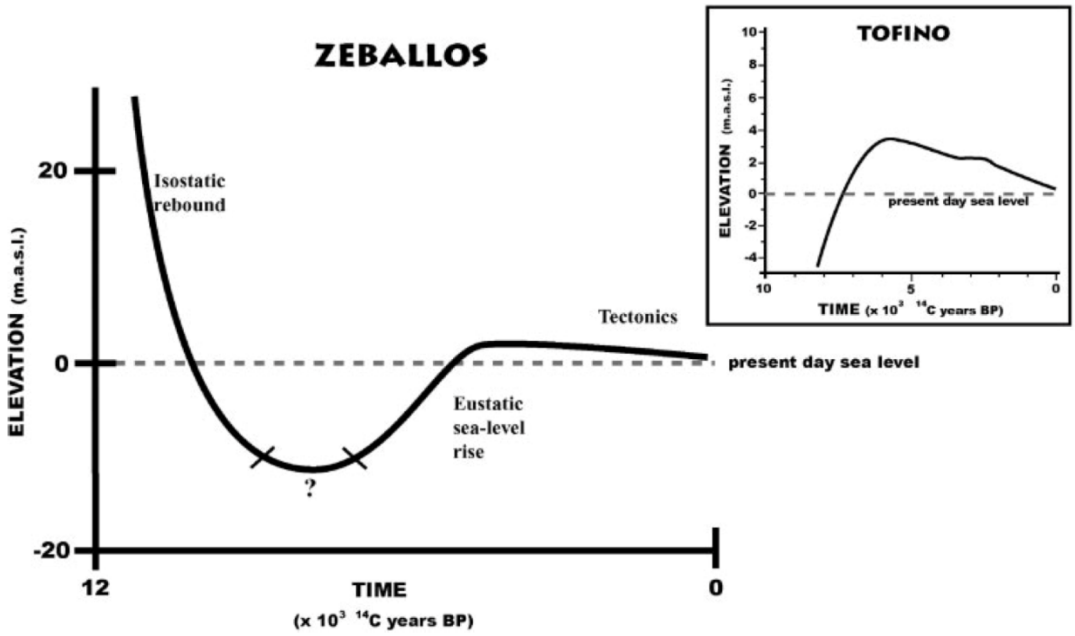

Figure 4.3. Relative sea-level curve for Zeballos (Gutsell *et al.* 2004). Inset shows Holocene relative sea-level curve for the Tofino area (Friele and Hutchinson 1993). The relative sea level curve is annotated with a progression of dominant regimes from late Pleistocene isostatic rebound to early Holocene eustatic sea-level rise to late Holocene tectonics.

Additional studies of Holocene sea-level change near Tofino (Clague *et al.* 1982; Bobrowsky and Clague 1992; Friele and Hutchinson 1993; Gutsell *et al.* 2004) indicate a drop in sea level from over 30 m elevation sometime before 12 ^{14}C kyr BP to below present levels around 11 ^{14}C kyr BP (Figure 4.3). Gutsell *et al.* (2004) presented the architectural framework and Holocene evolution of the Zeballos fjord-head delta on the west coast of northern Vancouver Island. Deltaic morphology and a

ground-penetrating radar survey allowed inferences to be drawn about Late Quaternary sea-level change at Zeballos. The deltaic sediments were found to be composed of two deltas: an older, elevated, incised, late Pleistocene delta and a younger, inset Holocene delta that has been graded to present sea level. Both the Pleistocene and Holocene deltas exhibit classic Gilbert-type structure (flat top and bottom-sets with inclined fore-set). The elevated, late Pleistocene delta was constructed when relative sea level was about 21 m higher than today, well below the 46 m marine limit inferred by Howes (1981a) for the region. The older delta was dissected when sea-level fell rapidly after the onset of Fraser deglaciation. During the early Holocene, relative sea-level at Zeballos reached an uncertain lowstand position about 20 m below present levels sometime around 9 ^{14}C kyr BP. Sea-level rose likely rose to a mid-Holocene highstand of about 4 m, producing the younger delta plain and remnant shoreline surfaces along valley margins.

Dallimore *et al.* (2009) constructed a 14 cal kyr RSL history for the west coast of Vancouver Island by combining new data from a marine core in Effingham Inlet, Barkley Sound with information from Hutchinson's (1992) catalogue of radiocarbon dates near Tofino, BC. The new local sea-level curve indicated a lowstand of -46 m around 13.5 cal kyr BP. Re-submergence began about 500 years later at 13.0 cal kyr BP and continued until sea level stabilized at a Holocene highstand about 3 m above present around 5.5 cal kyr BP. The current study will present new data from around Barkley Sound and interpret the new data combined with existing radiocarbon dates compiled and presented by Hutchinson (1992), Dallimore *et al.* (2009), and others.

4.2 Geological Setting

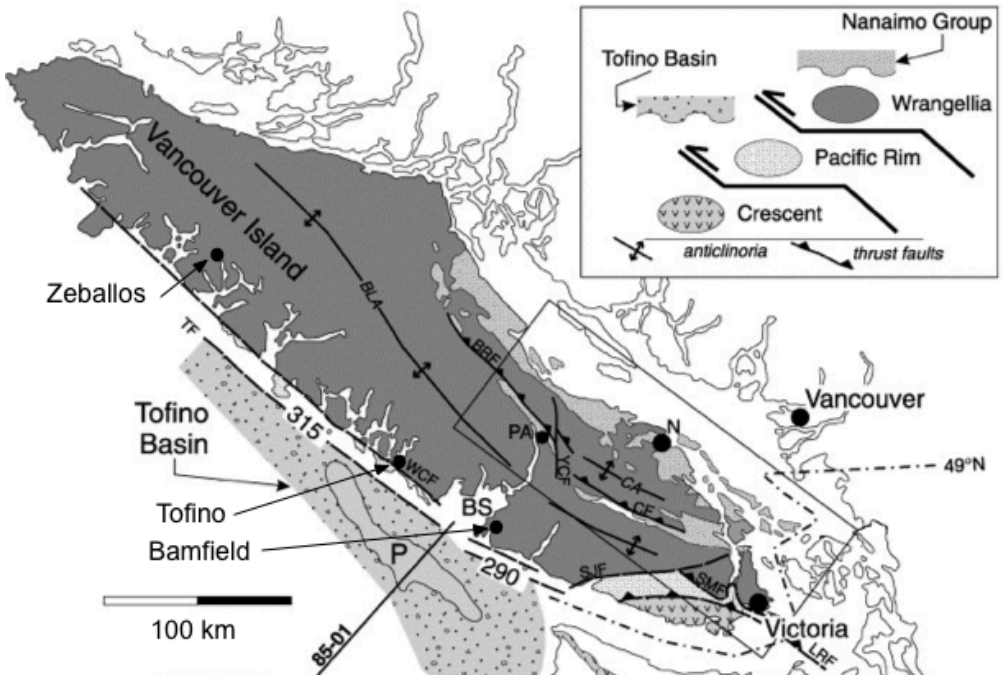

Figure 4.4. Regional geology and faults (F) of Vancouver Island: West Coast (WCF), Tofino (TF), San Juan (SJF), Survey Mountain (SMF), Trial Island (TIF), Beaufort Range (BRF), Yellows Creek (YCF), Cowichan (CF),Leech River (LRF). Communities are Bamfield, Tofino, Zeballos, Port Alberni (PA), Nanaimo (N). (after Johnston and Acton 2003).

Barkley Sound is a large bight at the mouth of the 60-km long, 330 m deep Alberni Inlet. It nearly bisects Vancouver Island, leaving a 25-km wide isthmus from Port Alberni at the inlet's head, over Mt. Arrowsmith of the South Vancouver Island Ranges to Parksville in the Nanaimo Lowlands. The Nanaimo Lowlands border the Georgia Strait on the east coast of Vancouver Island, and run from Campbell River to Victoria. (Yorath and Nasmith 1995).

The Estevan Lowlands run in a narrow band along the west coast of Vancouver Island from the Brooks Peninsula to Port Renfrew. Barkley Sound

interrupts the otherwise continuous, rocky coastline of small, irregular, steep-sided hills between Ucluelet and Bamfield, where the high mountains and deep inlets of the West Vancouver Island Fjord-land meet the lower hills of the South Vancouver Island Ranges (Yorath and Nasmith 1995).

Barkley Sound has been interpreted to be a small-scale, Eocene-aged, Southern Vancouver Island orocline (Johnston and Acton 2003). A deflection formed in the otherwise northwest to southeast fault-controlled (fault parallel) coastline of southwestern Vancouver Island. The upper plate responded to the collision of the Crescent Terrane seamount chain with Vancouver Island by rotating counterclockwise around an axis just northeast of Port Alberni. Both the Pacific Rim and Crescent Terranes were accreted to Vancouver Island during the Eocene Epoch of the Tertiary Period by the same convergent tectonic processes that remain active today; sediments accrete to the overriding North American continental plate as they are scraped off the subducting Juan de Fuca oceanic plate. However, southern Vancouver Island appears to have remained structurally stable during at least three Quaternary glaciations (Yorath and Nasmith 1995).

4.3 Barkley Sound

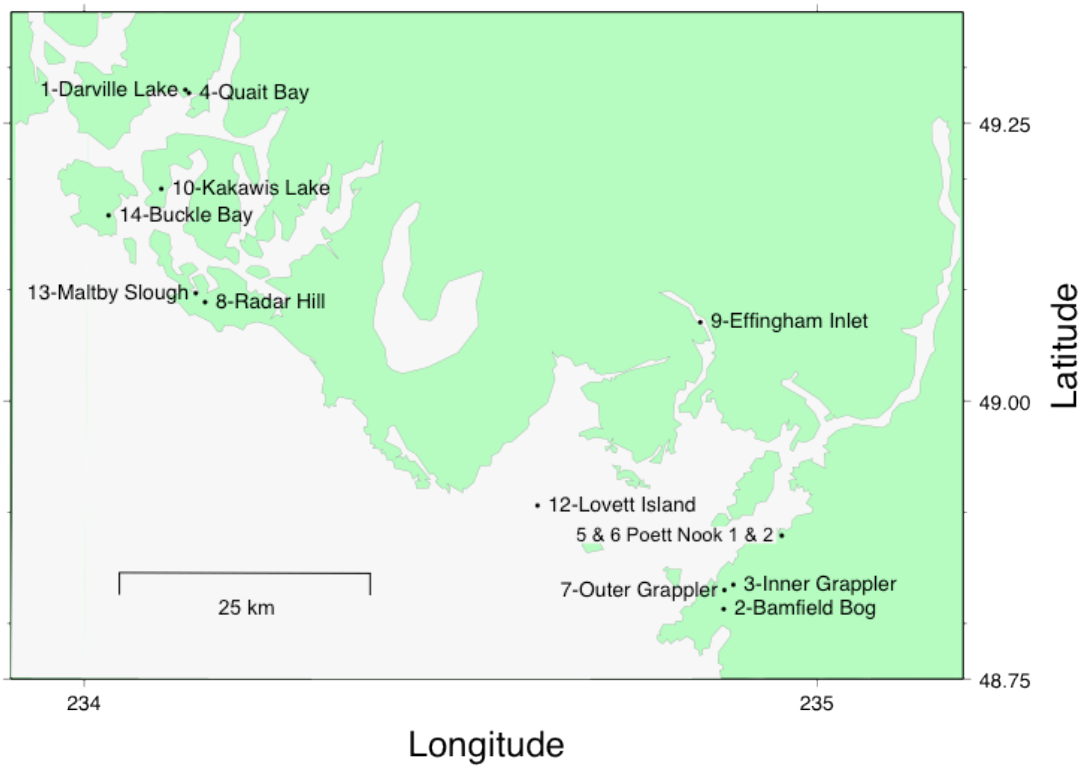

Figure 4.5. Location map of sample sites 1-10 and 12-14 in the Barkley Sound region. Site 11-Hesquiat Harbour is plotted separately in Figure 4.2 above.

For this study, eleven cores were recovered at six locations: four marine basins (Inner and Outer Grappler Inlet, Quait Bay, Poett Nook), one bog (Bamfield Bog), and one lake (Darville Lake). Core samples were collected by Thomas James, Ian Hutchinson, Bill Hill, Amber Church, Eric Geall, and Peter Locher. Sedimentology was described by Thomas James and Ian Hutchinson. Seven of the cores yielded a total of 21 samples of plants, shells, and other organic matter (seeds, gyttja, etc.) that were radiocarbon dated along with a marine shell that was obtained in 2004 from Brent Ward (Simon Fraser University), who sampled a creek-bed near Radar Hill in Tofino, BC. Fifteen radiocarbon ages were compiled from six cores

taken at Kakawis Lake (López 2002). Eight wood and ten marine shell dates were compiled from a giant core taken at Effingham Inlet in 2002 (Dallimore *et al.* 2009).

Table 4.1. Summary of radiocarbon ages of samples constraining postglacial sea level around Barkley Sound, BC: unpublished and published data (Clague *et al.* 1982; Blake 1983; Bobrowsky and Clague 1992; Friele and Hutchinson 1993; López 2002).

Location	Site (Fig. 2)	Latitude (ºN)	Longitude (ºW)	Elevation (m)	Material dated	Sample id	Lab no.	Radiocarbon age	Corrected age	Calibrated age (1 S.D.)	Sea-level position
Darville Lake	1	49.28	125.862	27	organic mud	CIA-98-07-264/265	TO-10849	12370 ± 90	11745 ± 108	14144-14582	above
Darville Lake	1	49.28	125.862	27	*Nuculana fossa*	CIA-98-07-569/574	TO-10850	13960 ± 100	13010 ± 112	15162-15551	below
Hesquiat Harbour	11	49.475	125.442	25	*Pinus contorta*	GSC-2976	GSC-2976	13000 ± 55	13000 ± 55	15158-15541	below
Bamfield Bog	2	48.813	125.127	21	spruce cone	CIA-02-08-175/177	TO-10847	12390 ± 90	12390 ± 90	14168-14610	above
Radar Hill	8	49.089	125.835	18	shell	04-TOFINO-RH	Beta-242125	13550 ± 70	12600 ± 86	14241-14676	below
Lovett Island	12	48.906	125.381	14	marine shells	GSC-3617	GSC-3617	13400 ± 55	12450 ± 74	14241-14676	below
Kakawis Lake	10	49.191	125.895	4	twigs	Kakawis-01	TO-7634	2340 ± 50	2340 ± 50	2320-2375	marginal
Kakawis Lake	10	49.191	125.895	4	cone	Kakawis-02	TO-7636	3220 ± 50	3220 ± 50	3380-3478	marginal
Kakawis Lake	10	49.191	125.895	4	bark frags	Kakawis-03	TO-7637	3540 ± 50	3540 ± 50	3724-3754	marginal
Kakawis Lake	10	49.191	125.895	4	twig	Kakawis-04	TO-7638	3410 ± 60	3410 ± 60	3574-3722	marginal
Kakawis Lake	10	49.191	125.895	4	twig	Kakawis-05	TO-8186	4120 ± 120	4120 ± 120	4522-4824	marginal
Kakawis Lake	10	49.191	125.895	4	twig	Kakawis-06	TO-7641	3300 ± 50	3300 ± 50	3462-3580	marginal
Kakawis Lake	10	49.191	125.895	4	twig	Kakawis-07	TO-7642	7160 ± 60	7160 ± 60	7884-7885	above
Kakawis Lake	10	49.191	125.895	4	wood fragment	Kakawis-08	TO-8187	7430 ± 80	7430 ± 80	8183-8340	above
Kakawis Lake	10	49.191	125.895	4	wood fragment	Kakawis-09	TO-7644	11620 ± 80	11620 ± 80	13369-13576	above
Kakawis Lake	10	49.191	125.895	4	shell fragment	Kakawis-10	TO-7645	13260 ± 80	12310 ± 94	14030-14439	below
Kakawis Lake	10	49.191	125.895	4	shell fragment	Kakawis-11	TO-7646	13810 ± 90	12860 ± 103	15005-15336	below
Kakawis Lake	10	49.191	125.895	4	gyttja	Kakawis-12	TO-8188	7560 ± 120	6935 ± 134	8201-8267	above
Kakawis Lake	10	49.191	125.895	4	cone	Kakawis-13	TO-7647	7870 ± 70	7870 ± 70	8558-8571	marginal
Kakawis Lake	10	49.191	125.895	4	twig	Kakawis-14	TO-7648	6990 ± 90	6990 ± 90	7733-7876	marginal
Kakawis Lake	10	49.191	125.895	4	wood fragment	Kakawis-15	TO-7722	9690 ± 70	9690 ± 70	10874-10945	above
Buckle Bay	14	49.167	125.967	2.5	Barnacle	Beta-42922	Beta-42922	12970 ± 80	12020 ± 94	13770-13974	below
Maltby Slough	13	49.097	125.848	0	wood (Picea)	CIA-90-111	GSC-5106	7870 ± 100	7870 ± 100	8551-8781	above
Maltby Slough	11	49.097	125.848	0	wood	PTB90-94-01	AECV-1205C	7070 ± 120	7070 ± 120	7762-7772	above
Maltby Slough	11	49.097	125.848	0	wood	SFU-856	SFU-856	9450 ± 110	9450 ± 110	10522-10533	above
Inner Grappler	3	48.835	125.114	-2	seed, plant detritus	CIA-02-06-063	TO-10841	5720 ± 60	5720 ± 60	6440-6567	below
Inner Grappler	3	48.835	125.114	-2	twigs	CIA-02-06-081	TO-10842	6220 ± 60	6220 ± 60	7020-7123	below
Inner Grappler	3	48.835	125.114	-2	*Pododesmus machrochisma*	CIA-02-06-153	69304	7845 ± 25	7125 ± 93	7903-8106	below
Inner Grappler	3	48.835	125.114	-2	*Panomya sp.*	CIA-02-06-164/166	TO-10843	12960 ± 90	12010 ± 103	13766-13972	below
Inner Grappler	3	48.835	125.114	-2	*Mytilus trossulus*	CIA-02-06-171	69305	12525 ± 30	11575 ± 58	13319-13459	below
Inner Grappler	3	48.835	125.114	-2	*Mya truncata*	CIA-02-06-179	69306	12850 ± 25	11900 ± 56	14047-14279	below
Inner Grappler	3	48.835	125.114	-2	shell fragments	CIA-02-06-203/204	TO-10844	11100 ± 90	10150 ± 103	11417-11504	below
Inner Grappler	3	48.835	125.114	-2	*Mya truncata*	CIA-02-06-243	69307	12600 ± 35	11650 ± 61	13408-13582	below

Location	Site (Fig. 2)	Latitude (ºN)	Longitude (ºW)	Elevation (m)	Material dated	Sample id	Lab no.	Radiocarbon age	Corrected age	Calibrated age (1 S.D.)	Sea-level position
Quait Bay	4	49.277	125.857	-5	plant fragments	CIA-98-06-534/541	TO-10848	3780 ± 70	3780 ± 70	3995-4037	below
Poett Nook 1	5	48.879	125.048	-8	hemlock cone	CIA-02-01-165	TO-10836	3750 ± 60	3750 ± 60	3989-4045	below
Poett Nook 1	5	48.879	125.048	-8	wood & bark	CIA-02-01-182/184a	TO-10838	4190 ± 60	4190 ± 60	4627-4638	below
Poett Nook 1	5	48.879	125.048	-8	butter clam	CIA-02-01-182/184b	TO-10837	4850 ± 60	4130 ± 108	4567-4841	below
Poett Nook 1	5	48.879	125.048	-8	root or twig	CIA-02-01-274/278	TO-10839	4060 ± 60	4060 ± 60	4438-4489	below
Poett Nook 2	6	48.879	125.047	-8	wood chunk	CIA-02-02-487	TO-10840	5180 ± 60	5180 ± 60	5770-5785	below
Outer Grappler	7	48.83	125.126	-8	bark fragments	CIA-02-07-195	TO-10845	8670 ± 80	8670 ± 80	9539-9707	below
Outer Grappler	7	48.83	125.126	-8	littleneck clam	CIA-02-07-256	TO-10846	1350 ± 50	630 ± 103	366-499	below

Table 4.1. Summary of radiocarbon ages of samples constraining postglacial sea level around Barkley Sound, BC (continued).

Study locations are numbered and presented in order of decreasing elevation (and then increasing core depth) from 33 m elevation (1-Darville Lake) to -46 m (9-Effingham Inlet). Lake elevations were determined from altimeter readings calibrated to the high-tide mark as the zero-meter datum. A total of 21 new samples were radiocarbon-dated and are presented together in Table 4.1 with 20 previously published samples from Kakawis Lake (López 2002), Hesquiat Harbour (Clague *et al.* 1982; Blake 1983), Lovett Island (Clague *et al.* 1982; Blake 1988), Maltby Slough (Bobrowsky and Clague 1992), and Buckle Bay on Vargas Island (Friele and Hutchinson 1993).

Twenty previously published ages from Effingham Inlet (Dallimore *et al.* 2009) are presented separately in Table 4.2. In their study, Dallimore *et al.* (2009) specify the marine reservoir correction to be 810 years. Corrected radiocarbon ages were given, but radiocarbon laboratory ages were not provided. In Table 4.2, the Inferred Laboratory Age was determined by adding 810 years to their published radiocarbon age. As described in Chapter 2, Pleistocene marine samples in this study are corrected by 950 ± 50 years, so the present study interprets shell ages from Effingham Inlet as 140 years younger (950 minus 810 years) than Dalllimore et al. (2009).

4.3.1 Darville Lake

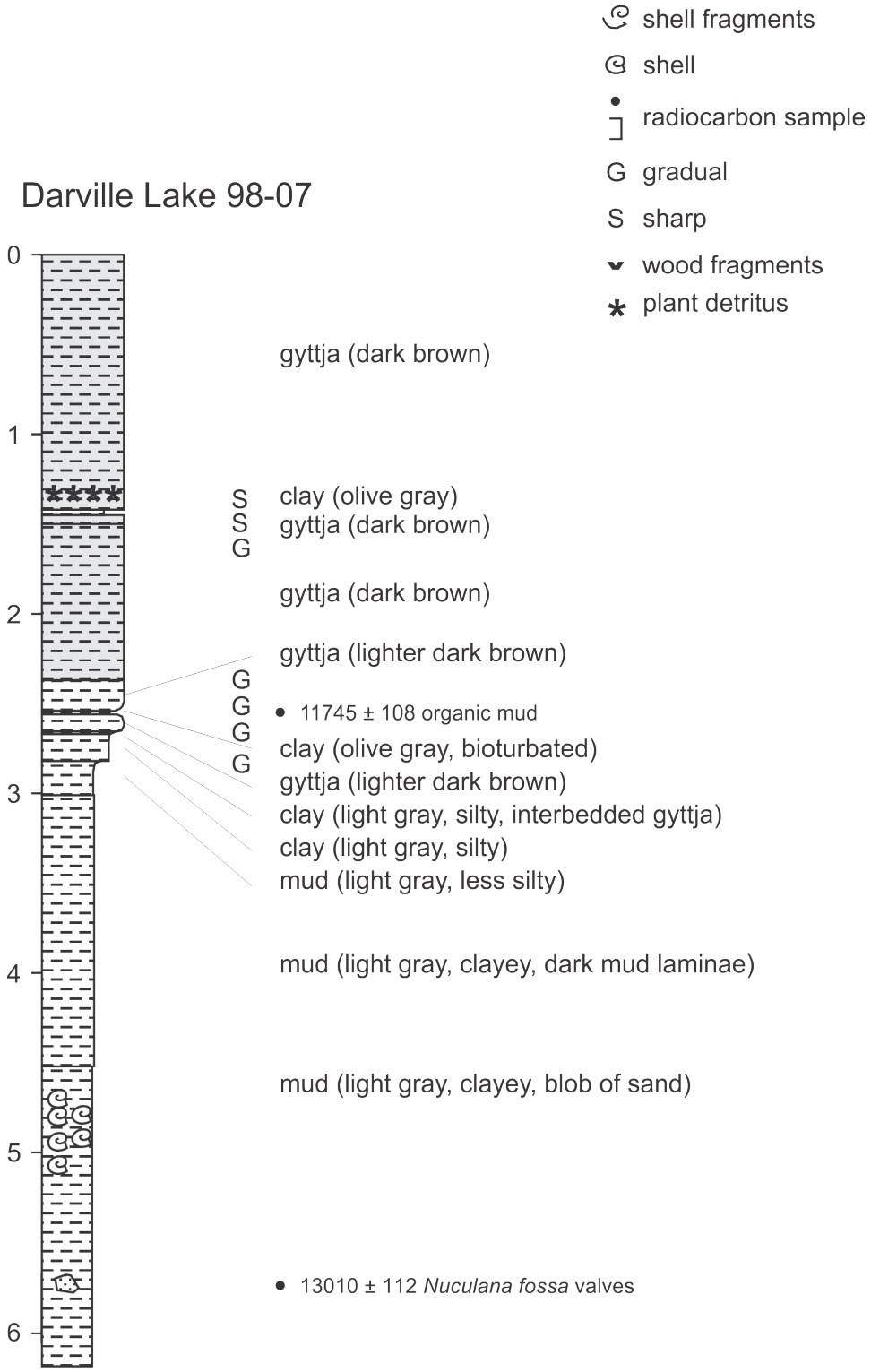

Figure 4.6 Stratigraphy (m) and radiocarbon ages (yr) for core taken at Darville Lake.

The sill elevation at Darville Lake was determined to be 26.8 m. Water depth at the core site was 9.4 m. The core pipe penetrated 8.2 m and recovered 6.2 m of core (25% compaction). The core was logged as dark brown gyttja, whose water content decreased downward. Abundant plant detritus at 136-140 cm was sampled (CIA-98-07-247/267) and yielded an age of 8370 ± 170 ^{14}C yr BP.

A sample of organic mud (CIA-98-07-264/265) was taken from the lighter brown, basal gyttja unit at 237-254 cm, whose upper contact was delineated by a bioturbated, broken, olive-gray clay layer a few millimetres thick. This basal gyttja indicates that sea-level must have fallen below Darville Lake by 11745 ± 108 corrected ^{14}C yr BP. *Nuculana fossa* valves (CIA-98-07-569/574) sampled from near the bottom of the core indicate that sea-level must have remained above Darville Lake until at least 13010 ± 112 corrected ^{14}C yr BP.

4.3.2 Hesquiat Harbour

A piece of wood (GSC-2976) sampled from marine silt at 25 m elevation near Hesquiat Harbour dated to 13000 ± 55 ^{14}C yr BP (Clague *et al.* 1982; Blake 1983). The wood provides a minimal age constraint: sea-level must have remained at least 25 m higher than today until at least 13000 ± 55 corrected ^{14}C yr BP.

4.3.3 Bamfield Bog

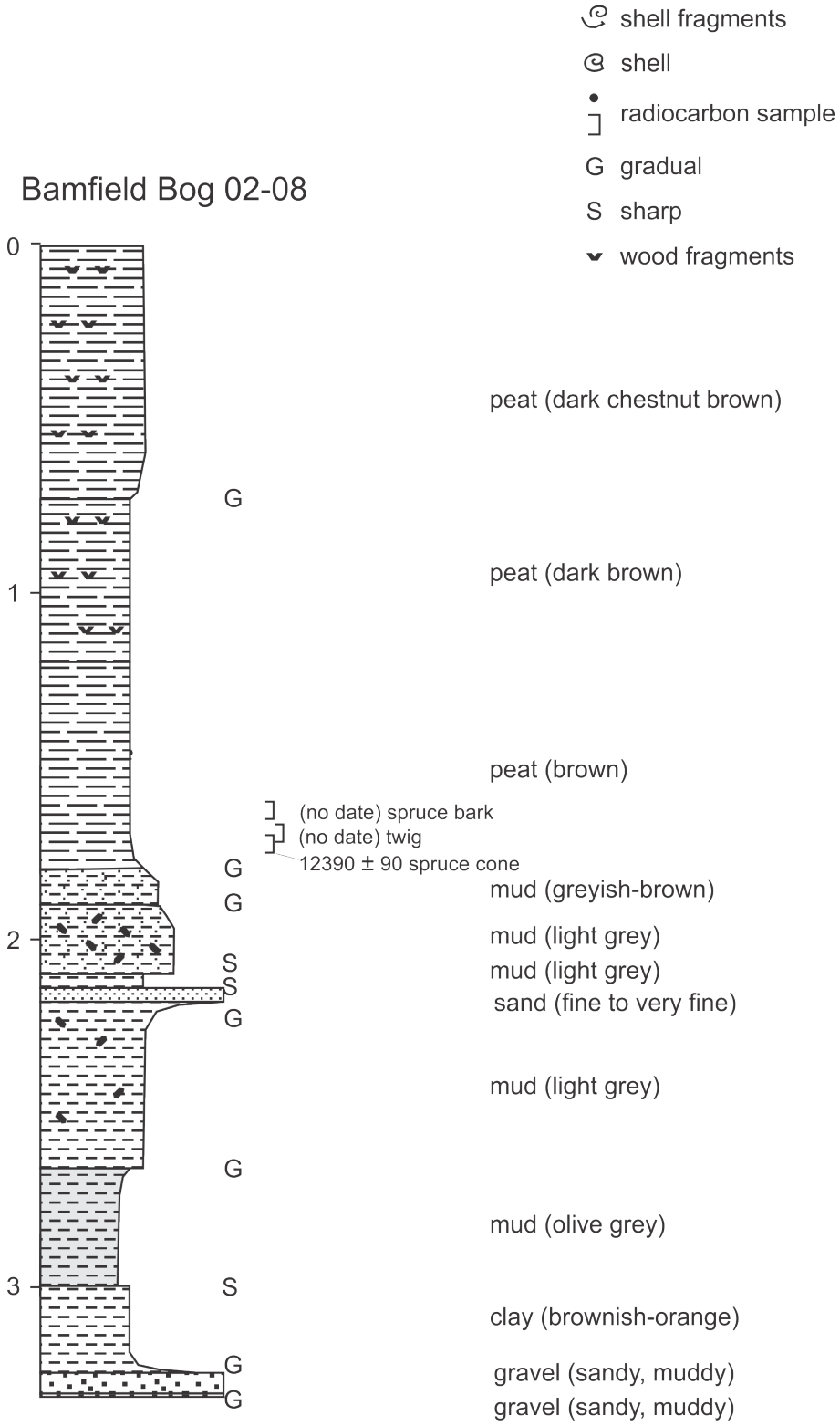

Figure 4.7. Stratigraphy and radiocarbon age (yr) for core taken at Bamfield Bog.

A vibracore was taken in a boggy area fringing a small pond (Bamfield Bog). The sill elevation was determined to be 18.0 m. A spruce cone (CIA-02-08-175/177) was sampled above a gradational contact at 180 cm found between brown sedge peat with wood fragments and underlying, organic-rich, grayish-brown sandy mud. The cone dated at 12390 ± 90 ^{14}C yr BP, by which time the sea surface had fallen below the elevation of Bamfield Bog.

4.3.4 Radar Hill

Professor Brent Ward (Simon Fraser University) provided a marine shell (04-TOFINO-RH, unpublished) sampled from a small exposure on a creek-bed near Radar Hill in Tofino, BC, at 16 m elevation. The shell was sampled from a blue grey massive mud with abundant thin-walled, articulated shells and isolated clasts. The shell provides a minimal age constraint: sea-level must have remained at least 16 m higher than today until at least 12600 ± 86 corrected ^{14}C yr BP.

4.3.5 Lovett Island

Marine shells (GSC-3617) sampled at 13.5 m elevation on Lovett Island in Barkley Sound dated to 13400 ± 55 corrected ^{14}C kyr BP (Clague *et al.* 1982, Blake 1988). The shells provide a minimal age constraint: sea-level must have remained at least 13.5 m higher than today until at least 13400 ± 55 corrected ^{14}C kyr BP.

4.3.6 Kakawis Lake

Kakawis Lake is situated at 4 m elevation on Meares Island, about 4.5 km north of Tofino, BC. Fifteen radiocarbon samples were compiled from six cores taken at Kakawis Lake by López (2002) as part of a study of inferred tsunami deposits. While such deposits can sometimes complicate stratigraphic interpretation, the cores yielded valuable samples whose radiocarbon dates span 14 ^{14}C kyr, helping constrain both late Pleistocene emergence and Holocene submergence.

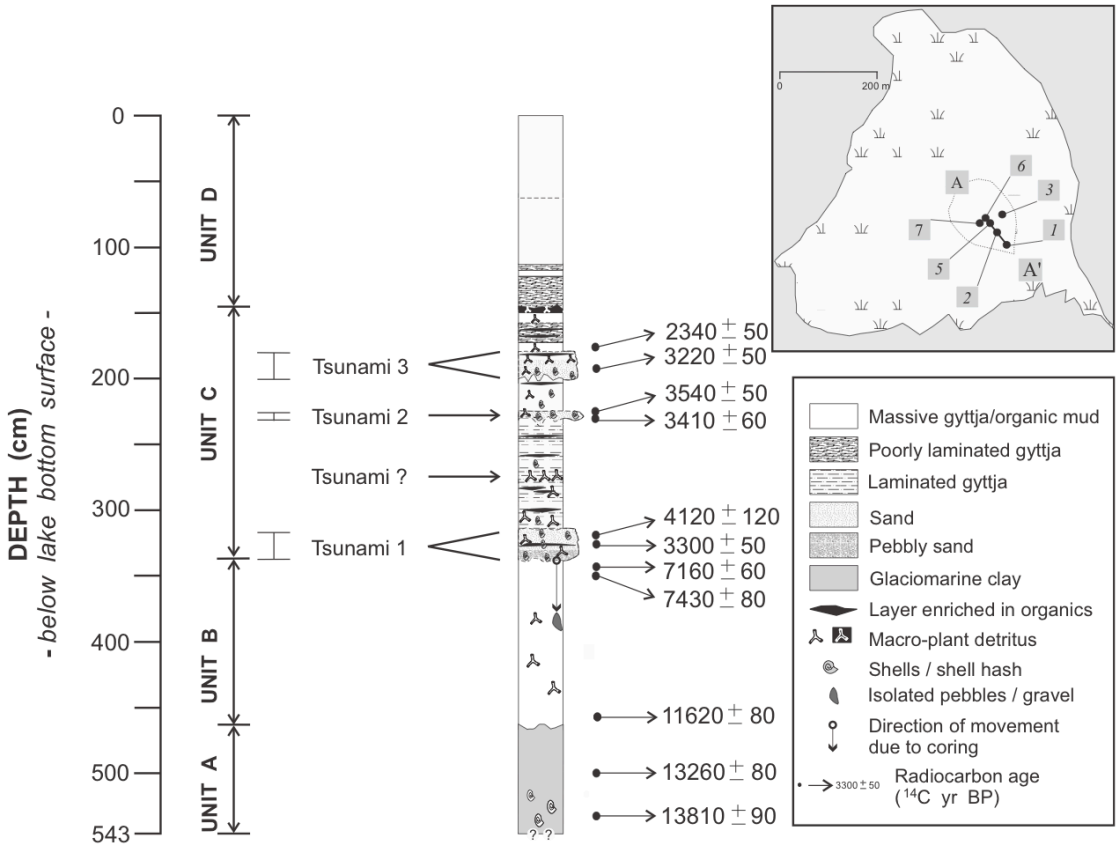

Figure 4.8. Stratigraphy and radiocarbon age for Kakawis Lake. The composite core is based on six cores taken at locations shown in the top-right box. Unit A: light bluish-grey clay with marine shell fragments. Unit B: dark brown to black gyttja with sharp but undulating lower contact. Unit C: laminated to horizontally bedded olive grey organic mud with a few shells and abundant plant detritus. Unit D: massive gyttja (López and Bobrowsky 2001).

The two oldest shells (TO-7645, TO-7646) dated to 12310 ± 94 corrected ^{14}C yr BP and 12860 ± 103 corrected ^{14}C yr BP, respectively. Sea-level must have been higher than Kakawis Lake until at least 12.3 ^{14}C kyr BP. A wood fragment sampled from gyttja dated to 11620 ± 80 ^{14}C yr BP, indicating that sea-level fell below the elevation of Kakawis Lake before 11.6 ^{14}C kyr BP (TO-7644).

4.3.7 Buckle Bay (Vargas Island)

An in-situ barnacle sampled from stony mud at 2.5 m elevation dated to 12020 ± 94 corrected ^{14}C kyr BP. The barnacle provides a minimal age constraint: sea-level must have remained above its present level until at least 12020 ± 94 corrected ^{14}C kyr BP (Friele and Hutchinson 1993).

4.3.8 Maltby Slough

An in-situ tree stump at 0 m elevation dated to 7870 ± 50 corrected ^{14}C kyr BP. The tree stump provides a minimal age constraint: sea-level was below its present level at 7870 ± 50 corrected ^{14}C kyr BP (Bobrowsky and Clague 1992).

4.3.9 Inner Grappler Inlet

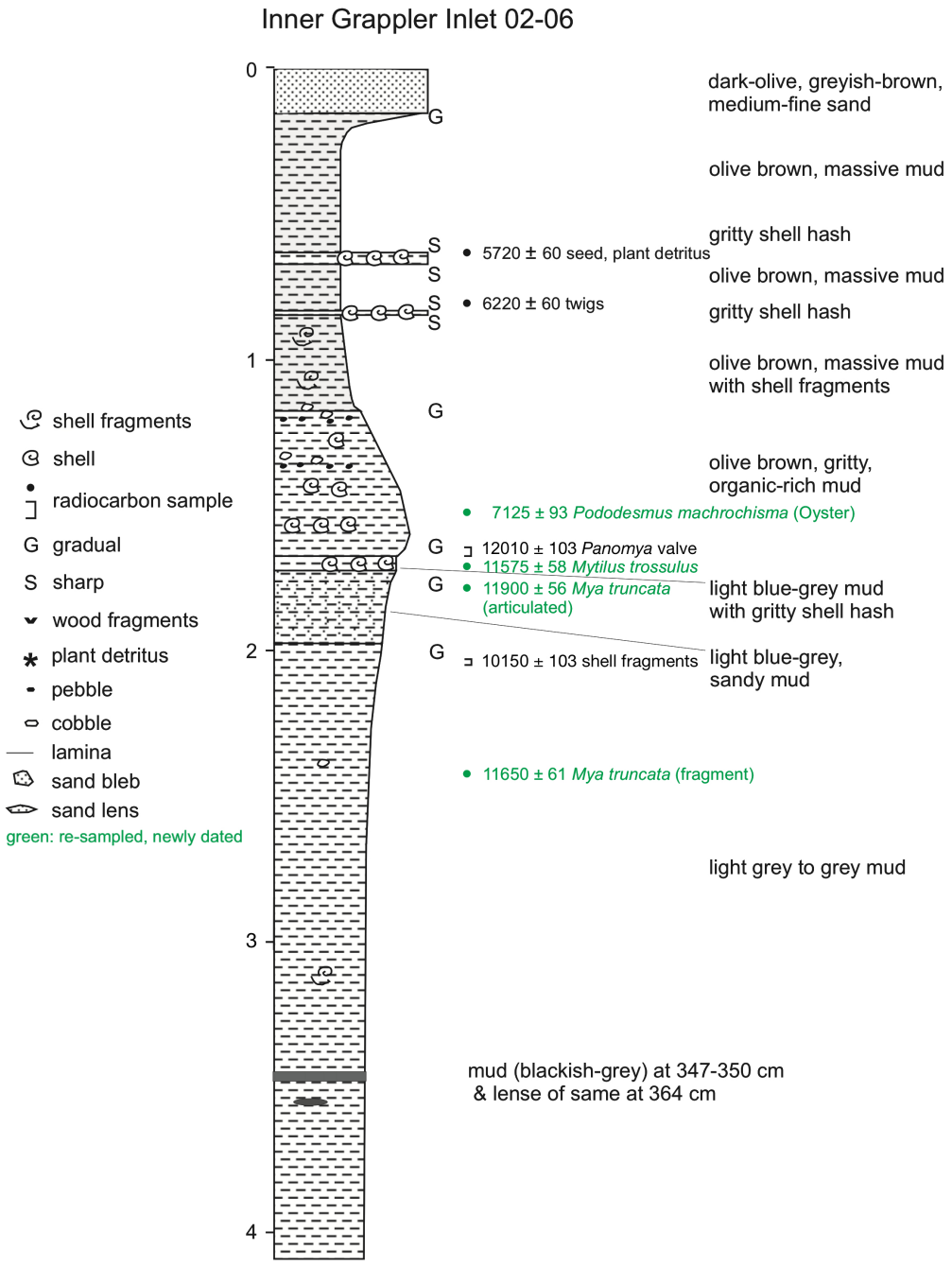

Figure 4.9. Stratigraphy (m) and radiocarbon ages (yr) for core taken at Inner Grappler Inlet.

Grappler Inlet (Figures 4. 9 and 4.13) is comprised of an inner segment with a shallow sill at about -2 m depth, and an outer segment with a deeper sill (see below). A core taken in the inner segment penetrated. 450 cm and yielded a 400 cm core (11% compaction).

A total of four samples were initially dated. Two shell samples were taken from two lower units of light blue-grey, sandy mud. A nearly whole *Panomyasp.*Valve (CIA-02-06-164/166) dates the top of the transitional unit to 12010 ± 103 corrected ^{14}C yr BP. Three shell fragments (CIA-02-06-203/204) returned a date of 10150 ± 103 corrected ^{14}C yr BP for the top of the blue-grey mud. The younger age is located below the older age from the top of the unit.

Plant samples were also taken from gritty shell hash in an upper unit of olive brown organic mud. Plant detritus (CIA-02-06-63), including eroded hemlock needles and bark fragment were combined with a seed and dated to 5720 ± 60 ^{14}C yr BP. Twigs (CIA-02-06-81) sitting on top of a lower gritty shell hash layer dated to 6220 ± 60 ^{14}C yr BP. The two coarse layers of gritty shell hash and plant detritus may record tsunamites or debris flows dating to the mid-Holocene.

Four additional samples were taken and dated. Age inversions are apparent in the four new ages, but the core appears to be comprised of an older portion, dating to 10150 ^{14}C yr BP and earlier, below about 1.7 m depth. Above this depth, there appears to be a hiatus in sedimentation (or erosion of previously deposited sediments), and the shallower sediments date to the mid-Holocene. Abundant shells throughout the core suggest marine conditions. Direct evidence of a lowstand is lacking, but the ages are consistent with sea-level dropping below -2 m some time

after 10150 ^{14}C yr BP and then rising above the sill elevation again before 7125 ^{14}C yr BP. If this is the case, lake sediments deposited during the lowstand were eroded during the mid-Holocene transgression.

4.3.10 Quait Bay

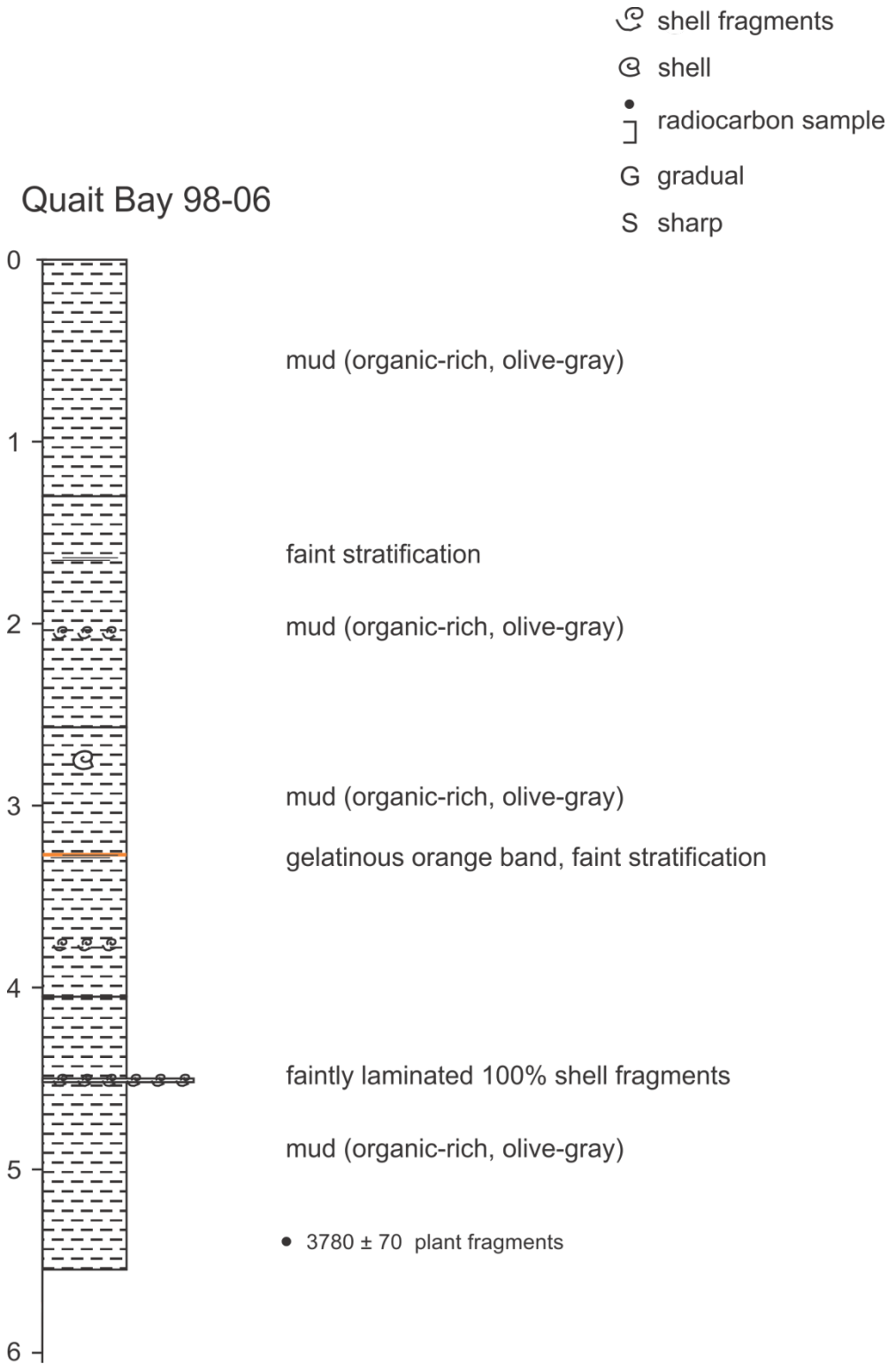

Figure 4.10. Stratigraphy (m) and radiocarbon age (yr) for core taken at Quait Bay.

Colleagues at Simon Fraser University (Ian Hutchinson and John Clague) granted access to a core taken in 1998. The sill elevation was determined to be -4.9 m. Water depth at the core site was 12.1 m. 885 cm penetration recovered a 548 cm core (38% compaction). A single sample of plant fragments (CIA-98-06-534/541) from the bottom section of olive-gray organic mud dated to 3780 ± 70 corrected ^{14}C yr BP. This age suggests high sedimentation rates (> 1 m/kyr). A longer core would be required to determine early Holocene and late Pleistocene conditions.

4.3.11 Poett Nook 1

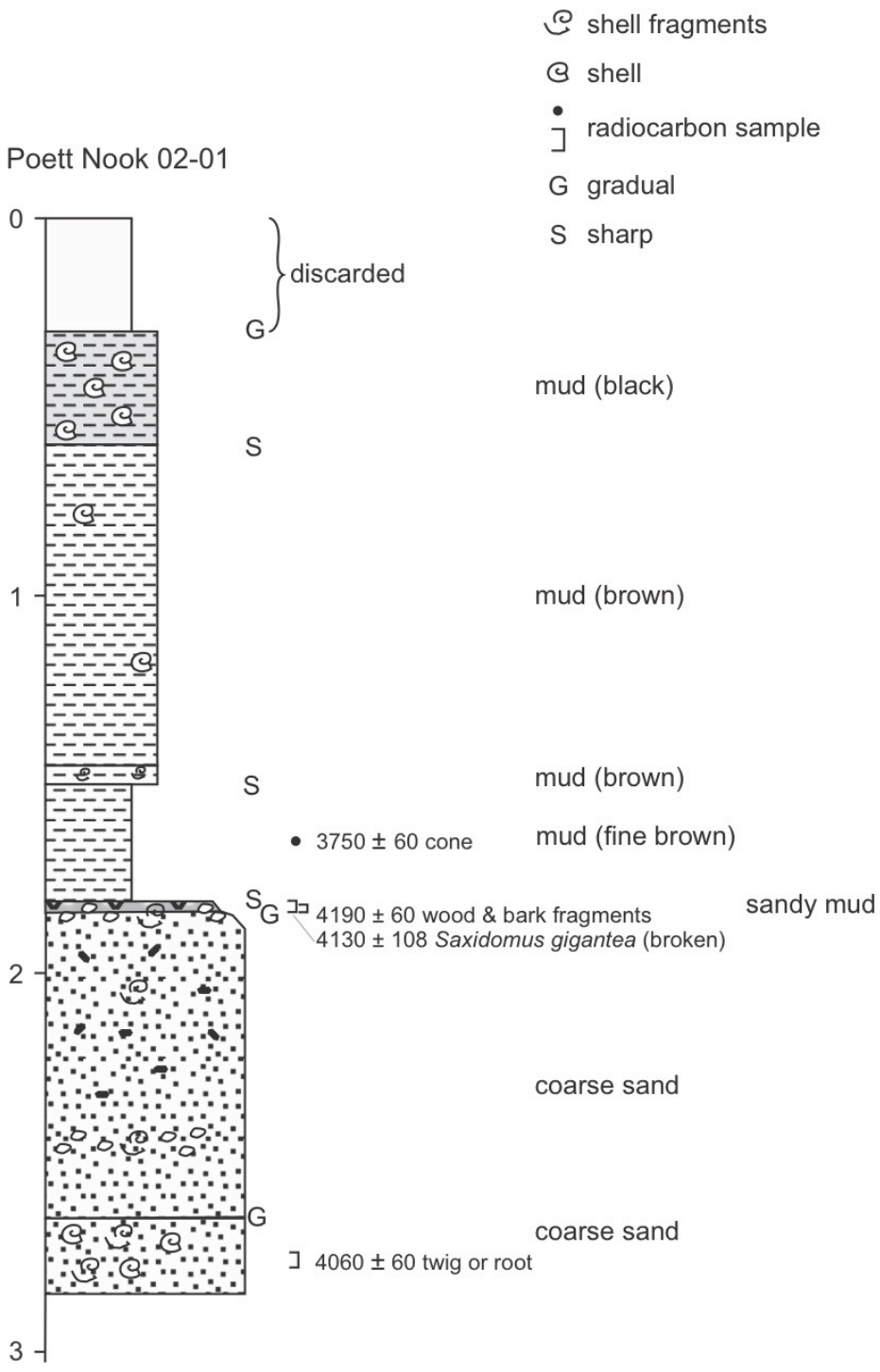

Figure 4.11. Stratigraphy (m) and radiocarbon age (yr) for core taken at Poett Nook, site 1.

A core was taken between the main dock and side docks. The depth of the sill (elevation) was determined to be about -8 m. 365 cm penetration yielded a 285 cm core (22% compaction). Shells and shell fragments are evident in both the basal coarse sand and the overlying mud and indicate marine conditions. Four samples were dated and indicate that the core dates to the mid-Holocene and younger.

4.3.12 Poett Nook 2

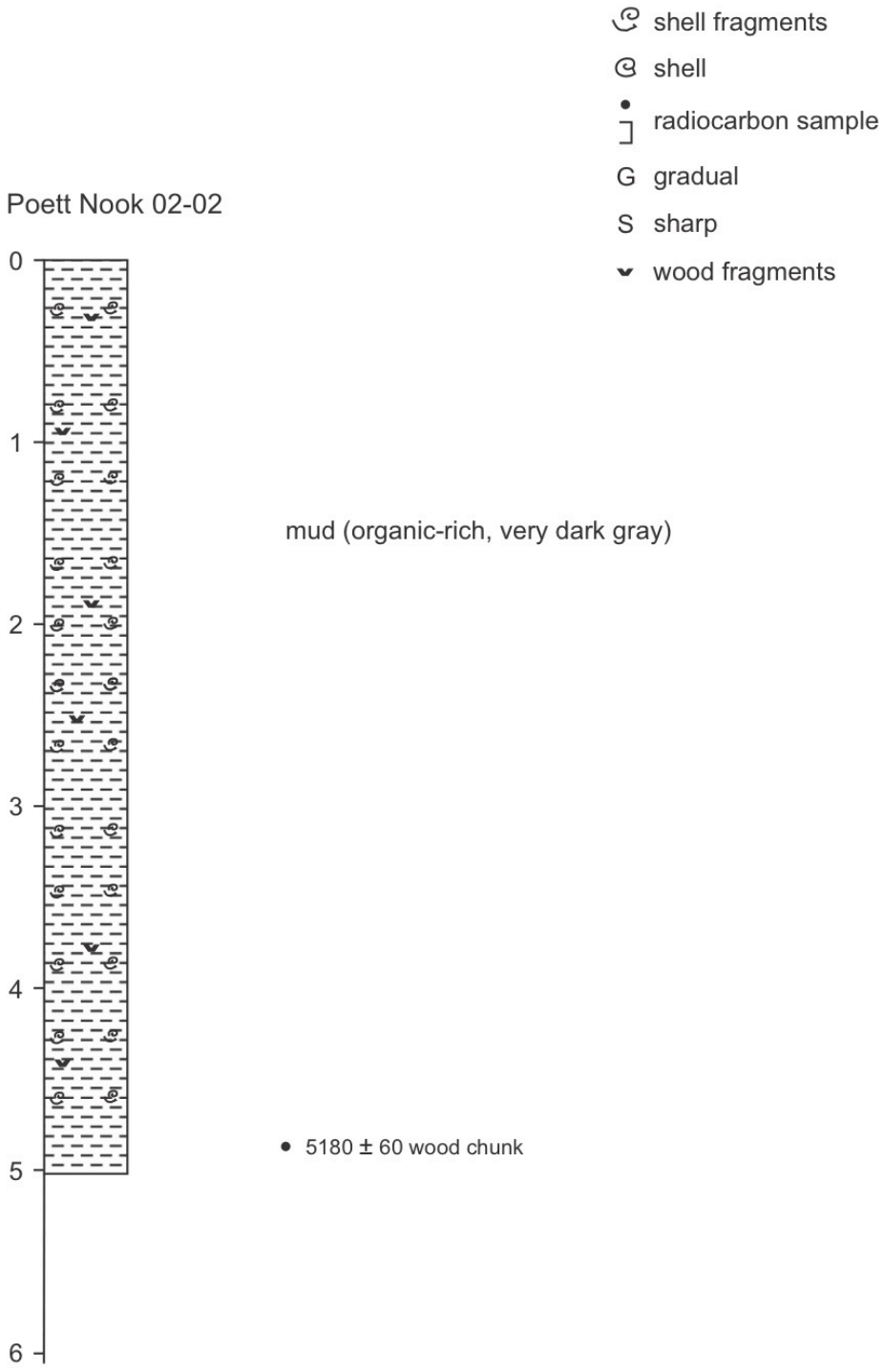

Figure 4.12. Stratigraphy (m) and radiocarbon age (yr) for core taken at Poett Nook, site 2.

A second core was taken at the middle of Poett Nook, about 100 m from the previous core (02-01), towards the centre of the basin. Sill depth (elevation) was determined to be -8 m. Penetration of 608 cm yielded a 502 cm core (17% compaction). A single sample from the base of the core was dated: a wood chunk (CIA-02-02-487) yielded an age of 5180 ± 60 ^{14}C yr BP. Apparently, the bay has experienced marine conditions at least since the mid-Holocene.

4.3.13 Outer Grappler Inlet

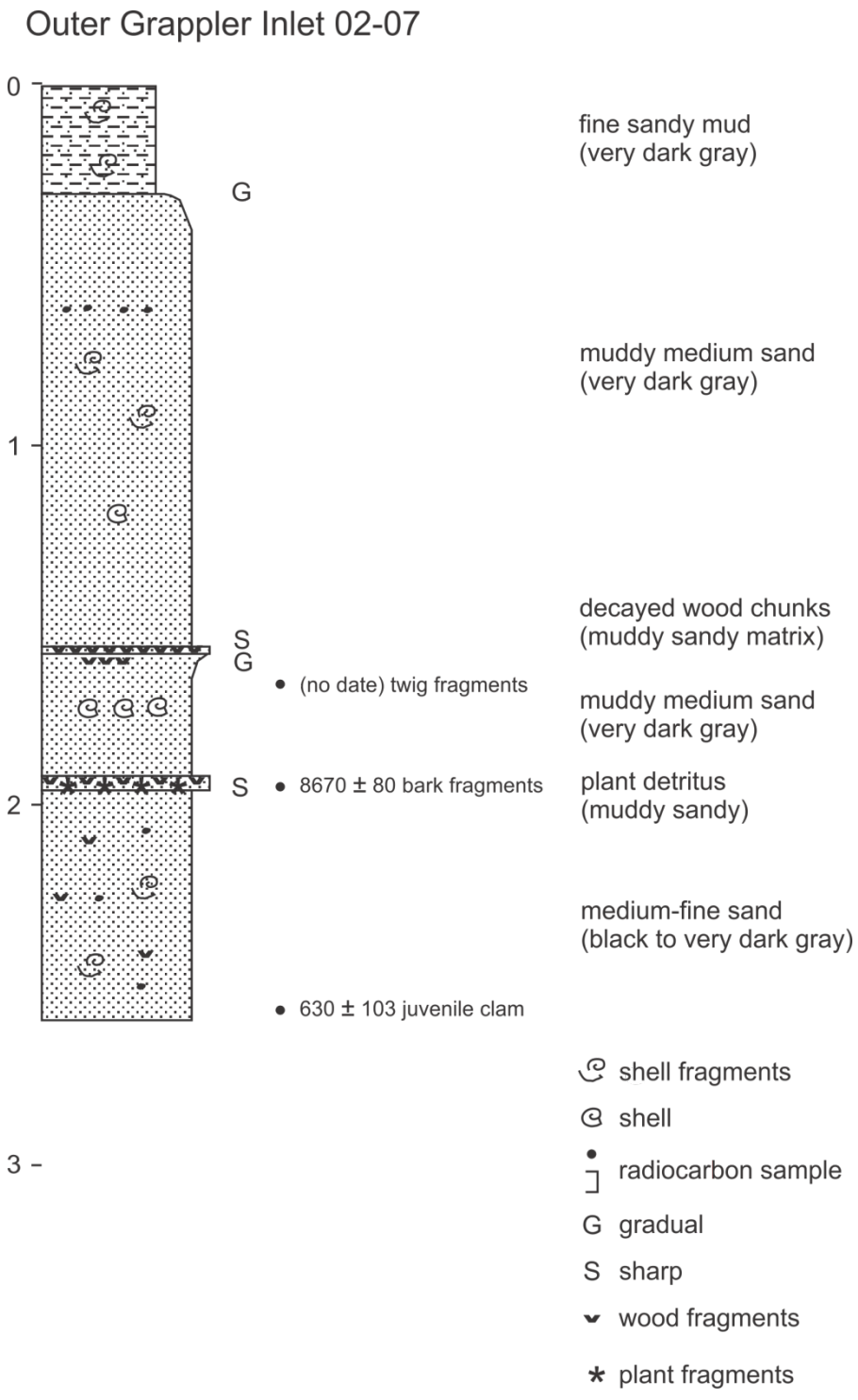

Figure 4.13. Stratigraphy (m) and radiocarbon ages (yr) for core taken at Outer Grappler Inlet.

A core was taken in the middle of Outer Grappler Inlet. Sill depth (elevation) was determined to be -8 m. 290 cm penetration yielded a 268 cm core (8% compaction). Gritty shell hash may record tsunamites or other debris flows and suggest substantial reworking of sediments in this basin (similar to Kakawis Lake).

Two samples were dated from the lower unit of organic-rich, muddy medium sand. Bark fragments (CIA-02-07-195) from a 4 cm layer of muddy, sandy plant detritus dated to 8670 ± 80 ^{14}C yr BP. The valve of a juvenile clam (*Mya arenaria sp.,* CIA-02-07-256) dated to 630 ± 103 corrected ^{14}C yr BP. The age of the juvenile clam at the base of the core is anomalous and may indicate either that the core catcher was contaminated during retrieval of the core or that shallow material lodged in the core catcher and was dragged down.

4.3.14 Effingham Inlet

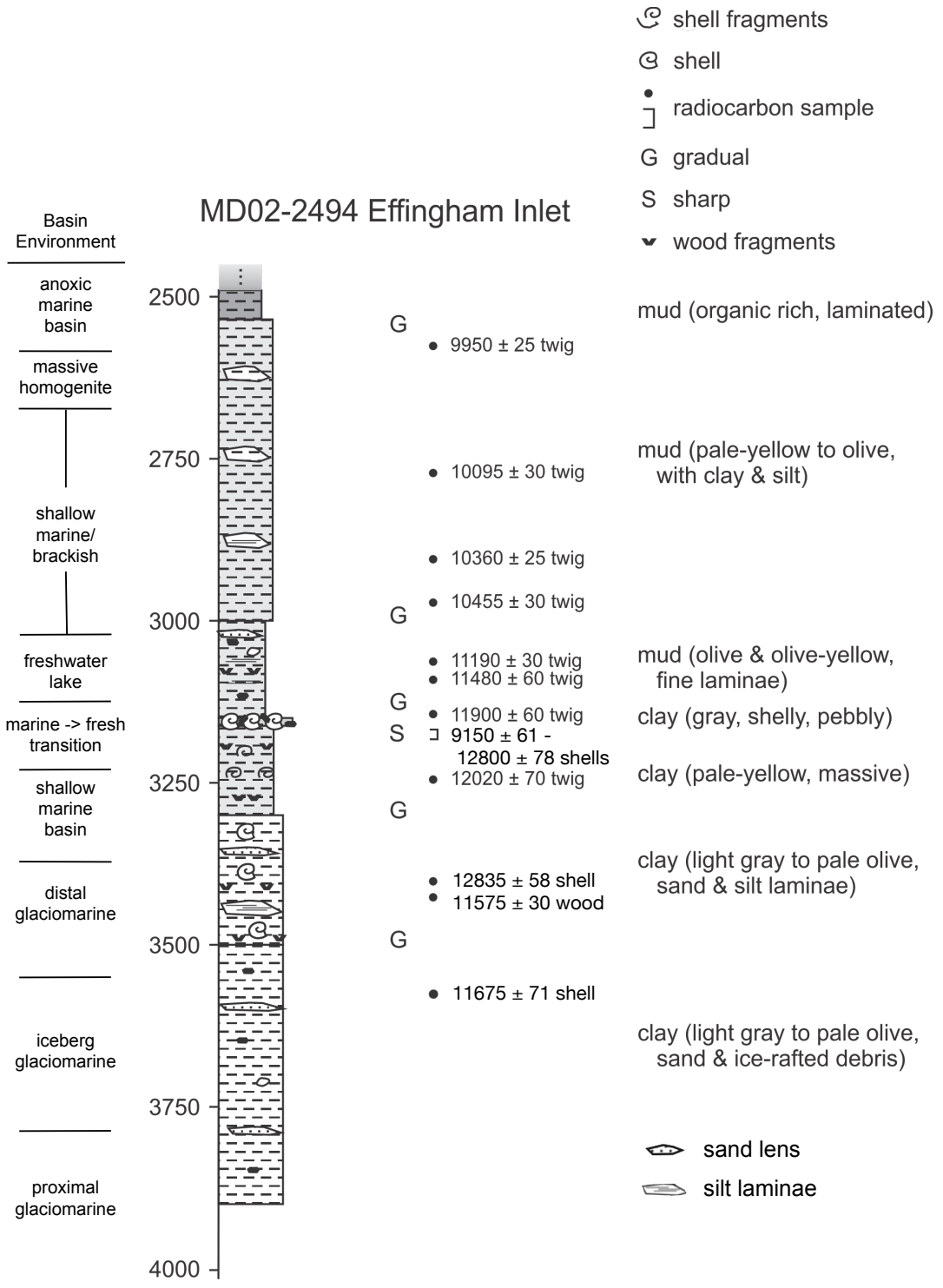

Figure 4.14. Stratigraphy (m) and radiocarbon ages (yr) for core MD02-2494 (after Dallimore *et al.* 2009).

Table 4.2. Stratigraphy and radiocarbon ages (yr) for core MD02-2494 (sampled at site 9-Effingham Inlet; after Dallimore *et al.* 2009).

Latitude (ºN)	Longitude (ºW)	Elevation (m)	Material dated	Sample id	Lab no.	Published radiocarbon age	Inferred radiocarbon lab age**	Corrected age (this study)	Calibrated age (1 S.D.)	Sea-level position
49.071	125.159	-46	twig	2576	10354*	9950 ± 25	9950 ± 25	9950 ± 25	11274-11355	marginal
49.071	125.159	-46	twig	2772	10355*	10095 ± 30	10095 ± 30	10095 ± 30	11510-11517	marginal
49.071	125.159	-46	twig	2905	10356*	10360 ± 25	10360 ± 25	10360 ± 25	12108-12239	marginal
49.071	125.159	-46	twig	2972	10357*	10455 ± 30	10455 ± 30	10455 ± 30	12245-12265	marginal
49.071	125.159	-46	twig	3063	10359	11190 ± 30	11190 ± 30	11190 ± 30	13061-13145	above
49.071	125.159	-46	twig	3091	2293	11480 ± 60	11480 ± 60	11480 ± 60	13270-13381	above
49.071	125.159	-46	twig	3151	2294*	11700 ± 70	11700 ± 70	11700 ± 70	13454-13642	marginal
49.071	125.159	-46	shell	3158	2296	12760 ± 60	13570 ± 60	12620 ± 78	13578-13767	marginal
49.071	125.159	-46	shell	3158	2297	11940 ± 50	12750 ± 50	11800 ± 71	12860-12969	marginal
49.071	125.159	-46	shell	3159	2298*	11130 ± 45	11940 ± 45	10990 ± 67	12719-12950	marginal
49.071	125.159	-46	shell	3159	2299	11430 ± 45	12240 ± 45	11290 ± 67	12313-12418	marginal
49.071	125.159	-46	shell	3159	2300	11415 ± 50	12225 ± 50	11275 ± 71	12255-12408	marginal
49.071	125.159	-46	shell	3160	2301	12940 ± 60	13750 ± 60	12800 ± 78	13962-14156	marginal
49.071	125.159	-46	shell	3160	2302	11740 ± 50	12550 ± 50	11600 ± 71	12784-12863	marginal
49.071	125.159	-46	shell	3161	2303	12720 ± 60	13530 ± 60	12580 ± 78	13506-13514	marginal
49.071	125.159	-46	shell	3161	2304	9290 ± 35	10100 ± 35	9150 ± 61	10337-10499	marginal
49.071	125.159	-46	twig	3245	2305	12020 ± 70	12020 ± 70	12020 ± 70	13798-13953	below
49.071	125.159	-46	shell	3402	10360	12975 ± 30	13785 ± 30	12835 ± 58	15069-15292	below
49.071	125.159	-46	wood	3410	10361	11575 ± 30	11575 ± 30	11575 ± 30	13352-13442	below
49.071	125.159	-46	shell	3611	2306	11815 ± 50	12625 ± 50	11675 ± 71	13414-13617	below

A 40.9 m giant (Calypso) piston core was taken at 120 m water depth in the inner basin of Effingham Inlet, during the 2002 Marges Ouest Nord Américaines (MONA) campaign (Dallimore *et al.* 2009). The sill depth (elevation) of the inner basin was determined to be -46 m using multibeam bathymetry.

Thirty-four plant and 15 shell samples were dated and correlated with analyses of diatoms and possible tephra deposits. Sediments at core depths between 3091-3161 cm record the transition from shallow marine basin to freshwater lake sediments. The freshwater lake sediments themselves occur above a gradational contact at core depths of 3063-3091 cm; shallow marine or brackish deposits are again found at 2500-3063 cm.

The age model was developed based only on terrestrial materials, since radiocarbon results for 9 marine shell samples from 3 cm of core at 3158-3161 cm returned a scattered range of dates from 9290 ± 35 to 12940 ± 60 corrected ^{14}C yr BP. In developing the age-depth model, wood dated to 11575 ± 30 ^{14}C yr BP at 3410 cm core depth (UCIAMS 10361) was treated as an outlier, as it does not follow stratigraphic sequence; it was proposed that the anomalously young sample may have been dragged down to the observed core depth during penetration.

The analysis concluded that marine conditions likely existed in Effingham Inlet before 11.3 ^{14}C yr BP and again since about 11 ^{14}C yr BP. Between 11.7-11.3 ^{14}C yr BP, diatom analysis indicated a transitional environment from a shallow marine basin to a freshwater lake at 11.3 - 11.0 ^{14}C yr BP (Fig. 3, Dallimore *et al.* 2009). More gradual inundation followed, returning the basin to marginal (brackish) marine conditions by 10455 ± 30 ^{14}C yr BP (twig, UCIAMS 2972). A sea-level

lowstand of 46 m below present datum was interpreted to have occurred in Effingham Inlet at ~11630 ^{14}C yr BP, 300 years before the observed age range of freshwater diatoms (11.3-11.0 ^{14}C yr BP).

An alternative approach can account for the majority of the reported shell ages, particularly those retrieved from gritty shell hash at depths of 3158 to 3161 that records the transition from marine to freshwater lake sediments. With one exception (UCIAMS 2304, 9290 ± 35), the ages range from 10990 to 12800 ^{14}C yr BP. Assigning an age of 10990 ^{14}C yr BP to the gritty shell hash then requires that freshwater and brackish sediments immediately overlying the gritty shell hash are younger than assumed by Dallimore *et al.* (2009). In particular, it implies that twigs retrieved from freshwater sediments above the gritty shell hash layer are older than the sediments that enclose them.

Two twigs above the gritty shell layer, dated to 11480 ± 60 ^{14}C yr BP and 11190 ± 30 ^{14}C yr BP, are located at 3063 and 3091 cm, respectively (UCIAMS 10359, 2293). The two twigs are out of stratigraphic sequence with one another (the older twig is higher in the core). A third twig just above the gritty shell hash layer at 3151 cm (the base of the transitional unit) dated to a similar age of 11700 ± 70 ^{14}C yr BP (UCIAMS 2294). This alternate interpretation suggests that the twig samples (UCIAMS 2293, 2294 and 10359) may be several hundred years older than the freshwater lake sediments they were deposited in. In other words, the minimum age of shells retrieved from the gritty shell hash layer (marine shell (UCIAMS 2298) at 10990 ± 67 corrected ^{14}C yr BP) constrains the age of the overlying freshwater sediments.

If so, the sea-level lowstand at Effingham Inlet may have occurred between 11.1-10.5 ^{14}C yr BP. This is several hundred years later than originally interpreted, but is consistent with the age range of freshwater diatom assemblages of 11.3-11.0 ^{14}C yr BP reported by Dallimore *et al.* (2009; see their Figure 3). This interpretation is consistent with all terrestrial and marine macrofossil dates, except the anomalously young shell dated to 9150 ± 61 corrected ^{14}C yr BP retrieved from the gritty shell hash layer.

4.4 Relative Sea-Level Curve

The radiocarbon ages and interpreted environments of deposition described above give the constraints on a regional relative sea-level curve (Figure 4.15). Previous studies of marine deposits and deltas on the west coast of Vancouver Island indicate that sea level during the late Pleistocene was at least 46 m above present (Howes 1981a). At Darville Lake, sea level remained at least 27 m above present until at least 13010 ± 112 but rapidly fell before 11745 ± 108 corrected ^{14}C yr BP (CIA-98-07-264/265 and 569/574). This corresponds well with regional data—about 50 km northwest along the coast at Hesquiat Harbour, sea level fell past 25 m elevation after 13000 ± 55 ^{14}C kyr BP; ~50 km southeast on Lovett Island in Barkley Sound, sea level remained above 13.5 m elevation until after 13400 ± 55 ^{14}C kyr BP (GSC-2976 and 3617; Clague *et al.* 1982; Blake 1983, 1988).

Sea-level at Radar Hill near Tofino, BC remained above 16 m elevation until at least 12600 ± 86 corrected ^{14}C yr BP. Sea level fell below 18 m elevation by 12390 ± 90 ^{14}C yr BP, when peat was deposited in Bamfield Bog (CIA-02-08-175/177). Sea-level remained higher than the 4 m elevation of Kakawis Lake until at least 12310 ± 94 corrected ^{14}C yr BP (TO-7645) and fell below 4 m by 11620 ± 80 ^{14}C yr BP. (TO-7644). Sea level remained above 2.5 m elevation at Buckle Bay (Vargas Island) until at least 12020 ± 94 corrected ^{14}C kyr BP (Friele and Hutchinson 1993).

Sea level then fell past the present level (0 m elevation) between 12.0-11.6 ^{14}C kyr BP. At Inner Grappler Inlet, sea level remained above the -2 m sill depth until at least 12010 ± 103 corrected ^{14}C yr BP (CIA-02-06-164/166). A younger marine

sample (CIA-02-06-203/204) lower in the same core is considered an outlier; it is 2,000 years out of stratigraphic sequence, and would require near present sea level at Inner Grappler Inlet around 10 ^{14}C kyr BP. This is roughly the same date as a -46 m lowstand at Effingham Inlet, only 27 km to the north. Differential crustal displacement of ~44 m across Barkley Sound is neither consistent with regional geology nor with the expected GIA response.

Sea level reached a lowstand of -46 m at Effingham Inlet between 11.1-10.5 ^{14}C kyr BP (UCIAMS 2298 and 2972). Sea level then rose to -8 m at Outer Grappler Inlet by 8670 ± 80 ^{14}C yr BP (CIA-02-07-195), reaching present levels at Maltby Slough sometime after 7870 ± 50 (GSC-5106; Bobrowsky and Clague 1992) and rising to within -2 m of present level by 7125 ± 93 ^{14}C yr BP at Inner Grappler Inlet (CIA-02-06-153). Based on the above constraints, Figure 4.15 plots relative sea-level change at Barkley Sound, BC since the late Pleistocene. Dashed blue lines represent loosely constrained portions of the curve.

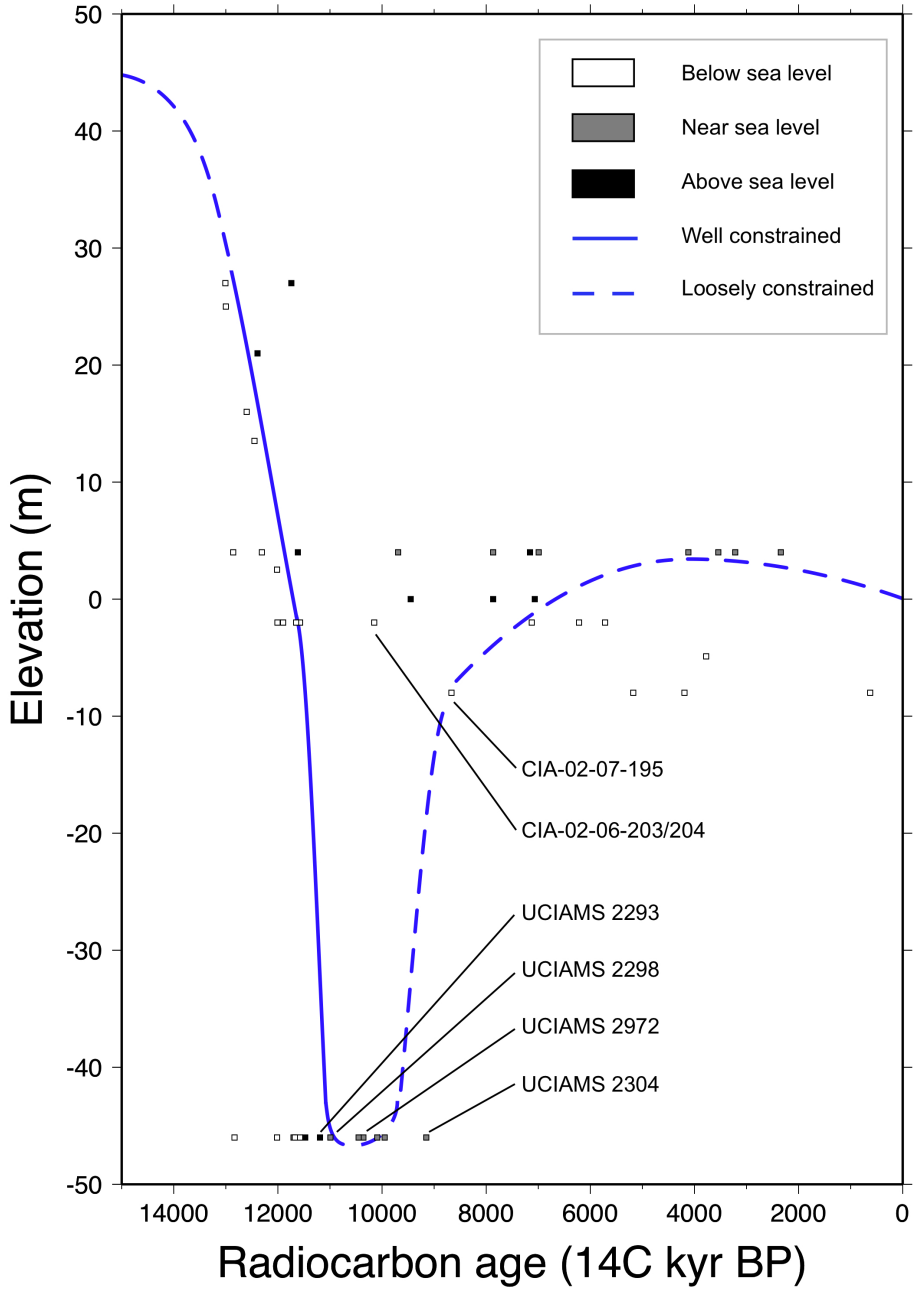

Figure 4.15. Postglacial relative sea-level change at Barkley Sound, BC, expressed in radiocarbon years. Dashed blue lines represent loosely constrained portions of the curve.

The revised sea-level history for Barkley Sound respects the majority of observed data in a regional analysis of relative sea-level. However, four data samples

fall on the wrong side of the proposed sea-level curve and have been interpreted as outliers; one was sampled from the core taken at Effingham Inlet (MD02-2494), two from Outer Grappler Inlet (02-07), and one from Inner Grappler Inlet (02-06). Each of these four anomalous data points is discussed below in the context of a regionally-consistent RSL history constrained by all the other observations (57 of 61 samples: 93%).

At Effingham Inlet, the proposed sea-level curve is consistent with the new, alternate interpretation presented above: that the reworking of shallow, near-shore sediments incorporated older materials, resulting in a range of dates at a given core depth. Excepting a single outlier (marine shell 2304 at 3161 cm, dated to 9150 ± 61 corrected ^{14}C yr BP), all terrestrial and marine shell dates sampled from core MD02-2494 are consistent with the revised sea-level curve. Marine conditions probably existed in Effingham Inlet before 11.1 ^{14}C yr BP and again around 10.5 ^{14}C yr BP. This suggests that the sea-level lowstand at Effingham Inlet may have occurred between 11.1-10.5 ^{14}C yr BP, several hundred years later than originally interpreted.

Two dates from the Outer Grappler Inlet core are outliers. Bark fragments (CIA-02-07-195) from Outer Grappler Inlet dated to 8670 ± 80 ^{14}C yr BP. This date is inconsistent with the proposed regional sea-level curve; only extremely rapid early Holocene submergence (>200 mm/yr)—about twice the accepted rate of eustatic sea-level rise—would resolve this datum at -8 m sill depth with the -46 m deep lowstand at Effingham Inlet. Moreover, the valve of a juvenile littleneck clam (*Mya arenaria sp.,* CIA-02-07-256) from the base of the same core dated to 630 ± 103 corrected ^{14}C yr BP. This very young date is contrary to expected stratigraphic sequence and likely

represents significant dating error such as insufficient radiocarbon sample size (0.0805 g) or natural reworking by a high-energy process such as a tsunamite mass-flow. The proposed regional sea-level curve suggests that marine conditions probably existed in Outer Grappler Inlet before 12 ^{14}C yr BP and after 8 ^{14}C yr BP.

At Inner Grappler Inlet, three shell fragments (CIA-02-06-203/204) were sampled together at a sill depth of -2 m and returned an age of 10150 ± 103 corrected ^{14}C yr BP. The sample was taken at the top boundary of the blue-grey (glacio-marine) mud; this date is approximately 2 kyr younger than expected according to stratigraphic sequence. Several other samples from the same core also returned ages contrary to expected stratigraphic sequence. These dates either represent dating error such as drag-down during coring or natural reworking by a high-energy process such as a tsunamite mass-flow. Excluding the above datum as an outlier, the proposed regional sea-level curve suggests that marine conditions probably existed in Inner Grappler Inlet before 12 ^{14}C yr BP and after 7 ^{14}C yr BP.

Corrected radiocarbon dates were calibrated to calendar years and plotted as probability density functions (PDFs) using the computer program Calib 5.0 (Stuiver and Reimer 1993); marine samples reference the Marine04 data-set (Hughen *et al.* 2004) and terrestrial samples the Intcal04 data-set (Reimer *et al.* 2004).

Figure 4.16 gives the relative sea-level curve in calendar years. Rapid deglaciation of Vancouver Island occurred between 17-16 cal kyr BP. Sea level in Barkley Sound fell quickly (~15 mm/yr) from a late Pleistocene marine maximum (Clague 1983) of about 46 m elevation (~100 m lower than the marine maximum at Sechelt) to near present levels by 13.5 cal kyr BP. This is about 1.5 kyr earlier than in

the central and northern Strait of Georgia (Hutchinson *et al.* 2004a; James *et al.* 2005). The steepest period of emergence followed—between 13.5-12 cal kyr BP—when sea level fell extremely rapidly (~30 mm/yr) from near present levels to a previously published lowstand of -46 m. Sea level in Barkley Sound rose quickly (~20 cm/yr) to -8 m by about 10 cal kyr BP (CIA-02-07-195) and then adopted the same trend as in the Strait of Georgia, returning to near present levels around 8 cal kyr BP (AECV-1205C, Bobrowsky and Clague 1992; CIA-02-06-153). A mid-Holocene high stand of about 4 m occurred about 5.5 cal kyr BP (TO-8186).

Barkley Sound emergence predated that in the central Strait of Georgia by at least 1 kyr; sea-level fell past present levels at least one thousand years earlier at Barkley Sound compared to Sechelt (13.5 vs. 12.4 cal kyr BP), and Barkley Sound experienced an earlier and much larger magnitude sea-level lowstand (-46 m versus -20 m) than Sechelt, returning to near present levels around 8 cal kyr BP. This is somewhat deeper than the maximum estimated lowstand of about -40 m for southern Vancouver Island (James *et al.* 2009a) and significantly deeper than the estimated lowstand of about -20 m in the central and northern Strait of Georgia (Hutchinson *et al.* 2004a; James *et al.* 2005), which occurred sometime between 12 - 10 cal kyr BP, up to one thousand years earlier in the central Strait than in the northern Strait.

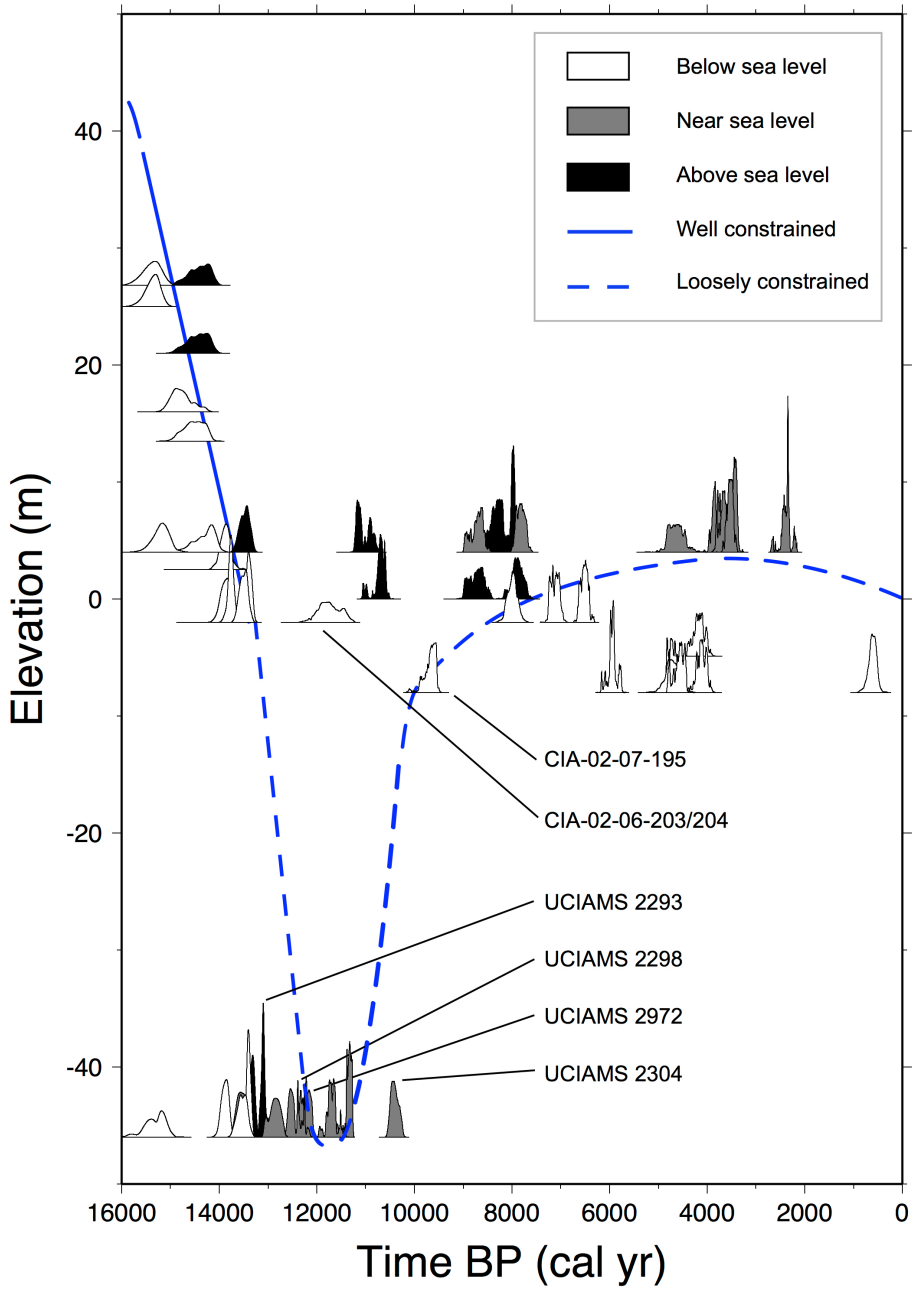

Figure 4.16. Postglacial relative sea-level change at Barkley Sound, BC, in calendar years. Dashed blue lines represent loosely constrained portions of the curve. White PDF (probability distributions) are expected to plot below the RSL curve, grey PDFs near/on the curve, and Black PDFs above it.

Chapter 5 - GIA Modeling

5.1 Introduction

A computational model of glacial isostatic adjustment, which is the solid Earth's response to ice loads, can be used to explore the characteristics of the lithosphere and mantle, the reconstruction of the glacial history, and their interactions. A well-constrained GIA model enables the separation of GIA effects from other processes, such as tectonic deformation. Geomorphic features and radiocarbon dating constraints on the size and extent of an ice sheet, through time, are used to establish a preliminary gridded ice sheet model.

The Earth's computed response to an ice load history depends largely on the viscosity of the mantle and the thickness of the lithosphere. These material properties are passed as parameters to a spherical Earth model. The GIA model and derived predictions based on it depend on the assumptions made about the ice model (time-dependent configuration of ice masses) and the parameterized Earth rheology. Frequently, a linear Maxwell viscoelastic response is assumed in GIA modeling.

The model is then run systematically over a wide range of values of model parameters (viscosity, lithospheric thickness, asthenospheric thickness, ice sheet history) to explore which combinations of ice-sheet history and Earth structure provide the best fit to the relative sea-level observed for a study region. When predictions disagree with observed data, the model assumptions are modified to produce better agreement between predicted and observed sea-level. For a given ice history, the primary objective is to find an Earth rheology that predicts observed relative sea level.

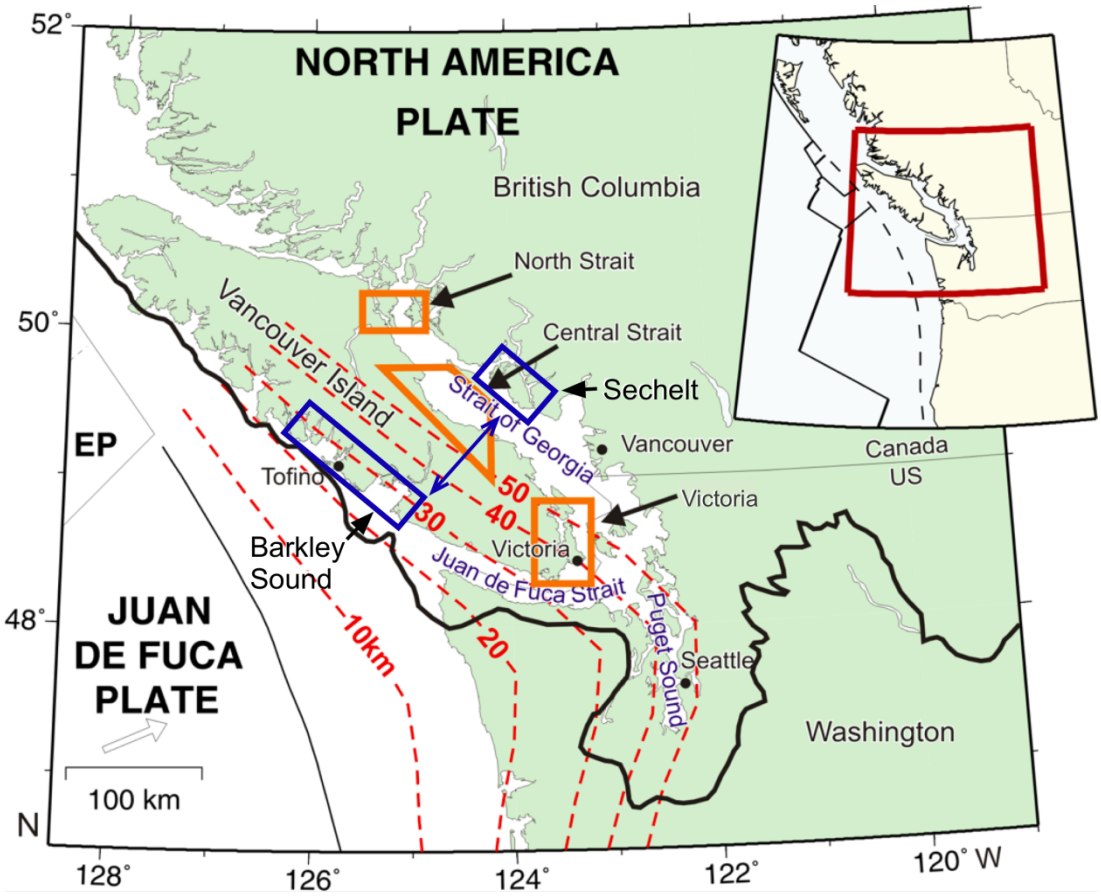

Figure 5.1. Map showing locations of a new relative sea-level curve at Sechelt and an extended sea-level curve at Barkley Sound (blue). Three previously published curves (orange) are also located over the northern CSZ (after James *et al.* 2009a). The new profile is oriented southwest-northeast across Vancouver Island and the Strait of Georgia (blue arrow). Variations along this profile are explored and related to the structure of the CSZ by modeling the Earth's response to the CIS.

Chapters 3 and 4 presented and discussed sea-level change during and after the retreat of the CIS for Barkley Sound and Sechelt. These new data widen the range of existing records to earlier times and create a new profile perpendicular to that of published observations. The new profile is oriented southwest-northeast across Vancouver Island and the Strait of Georgia.

Adding this second spatial dimension to regional sea-level modeling is important to our understanding of sea-level change for two main reasons. First, the CIS flowed roughly from northeast to southwest over the regions of interest.

Measurements along this path should indicate how sea-level change differed with distance from the edge to the centre of the ice-sheet. Relative timing and amplitudes of sea-level change are applied to refine existing models of ice-sheet history during rapid CIS deglaciation. Second, modeling the Earth's response to the CIS along a profile parallel to the tectonic subduction of the Juan de Fuca plate below the North American plate allows the exploration of spatial variations related to the structure of the CSZ.

5.2 Ice model

The ice-sheet model employed here is based on a sequence of models originated by James *et al.* (2000) and revised in studies by Clague and James (2002), Clague *et al.* (2005), Gowan (2007) and James *et al.* (2009a, 2009b). The CIS is represented with a coarse grid of elements with dimension 55 km × 55 km. The grid is further subdivided in four on Vancouver Island and adjacent mainland regions (Figure 5.2) where sea-level observations exist: central and south Vancouver Island, Puget Sound and the Straits of Georgia and Juan de Fuca.

The ice for each grid element is applied as a disk of equivalent area for computational simplicity. The thickness of each disk is varied over a model run through twenty time periods of varying duration from CIS inception at 35 cal kyr BP to the present interglacial (no ice) at 10.7 cal kyr BP. Eight time periods model the deglaciation of coastal Vancouver Island, including Puget Sound and the Straits of Georgia and Juan de Fuca, from 16.0 to 14.2 cal kyr BP. Four subsequent time periods model the downwasting of the CIS across southern BC from 14.4 to 12.9 cal

kyr BP. Limited re-advance of the CIS in mainland BC occurs between 12.9-11.5 cal kyr BP.

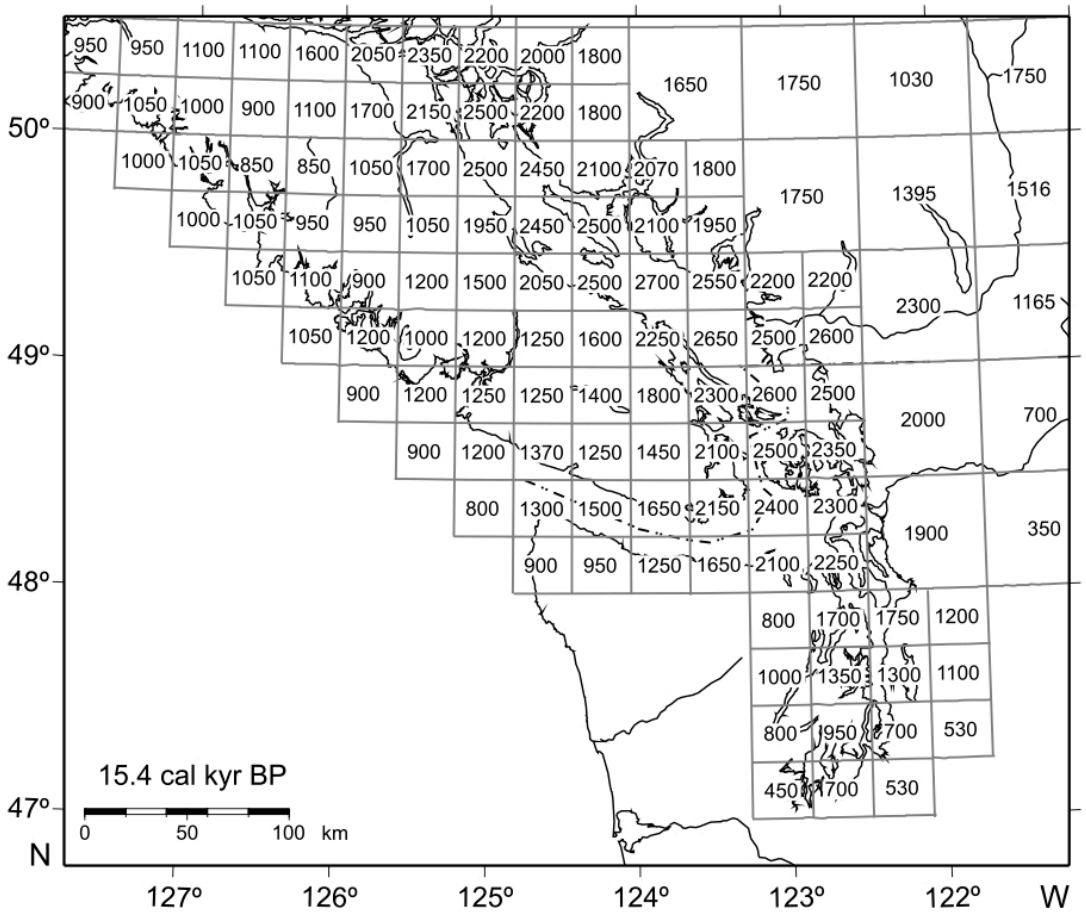

Figure 5.2. Ice-sheet model based on a sequence of models originated by James *et al.* 2000.

5.2.1 Ice history

Thickness, extent, and timing of the advance and retreat of the CIS is constrained by radiocarbon dates and geomorphic features that record ice-margin history and limit maximum ice-sheet elevation. Gowan (2007) refined the ice model by applying radiocarbon constraints on deglaciation in southwestern BC. Radiocarbon ages represent minimal ice-free ages. The present study updates the ice model

presented by Gowan (2007) with additional constraints on advance and retreat of the ice sheet from the literature—in particular on the west coast of Vancouver Island (Tables 5.1 and 5.2). Glaciological controls are also applied through consideration of the slope of the ice surface.

In western North America, the last major glacial cycle is called the Fraser Glaciation, which roughly correlates with the Wisconsinan glaciation of eastern and central North America. By 18 cal kyr BP, the Cordilleran Ice Sheet (CIS) covered most of British Columbia and northern Washington State, achieving a maximum thickness of about 3 km and forming the Puget Lobe in the southern Georgia Basin and the Juan de Fuca lobe between present-day Vancouver Island and the Olympic Peninsula. At its maximum, the CIS was sufficiently thick that its flow was nearly independent of topography: it overtopped mountain ranges on Vancouver Island at 2500 m elevation (Wilson *et al.* 1958; Mathews *et al.* 1970; Booth 1987; Stumpf *et al.* 2000; Clague and James 2002). Ice thickness exceeded 1.5 km in the Nanaimo Lowlands and Straits of Georgia and Juan de Fuca. The CIS became thinner towards its extremities but may have reached up to 1.2 km thick at its margin at the continental shelf off the west coast of Vancouver Island (Heusser 1973; Herzer and Bornhold 1982). Mathews *et al.* (1970) fixed maximum ice thickness of the CIS at 450 m elevation at the western entrance of the Juan de Fuca Strait.

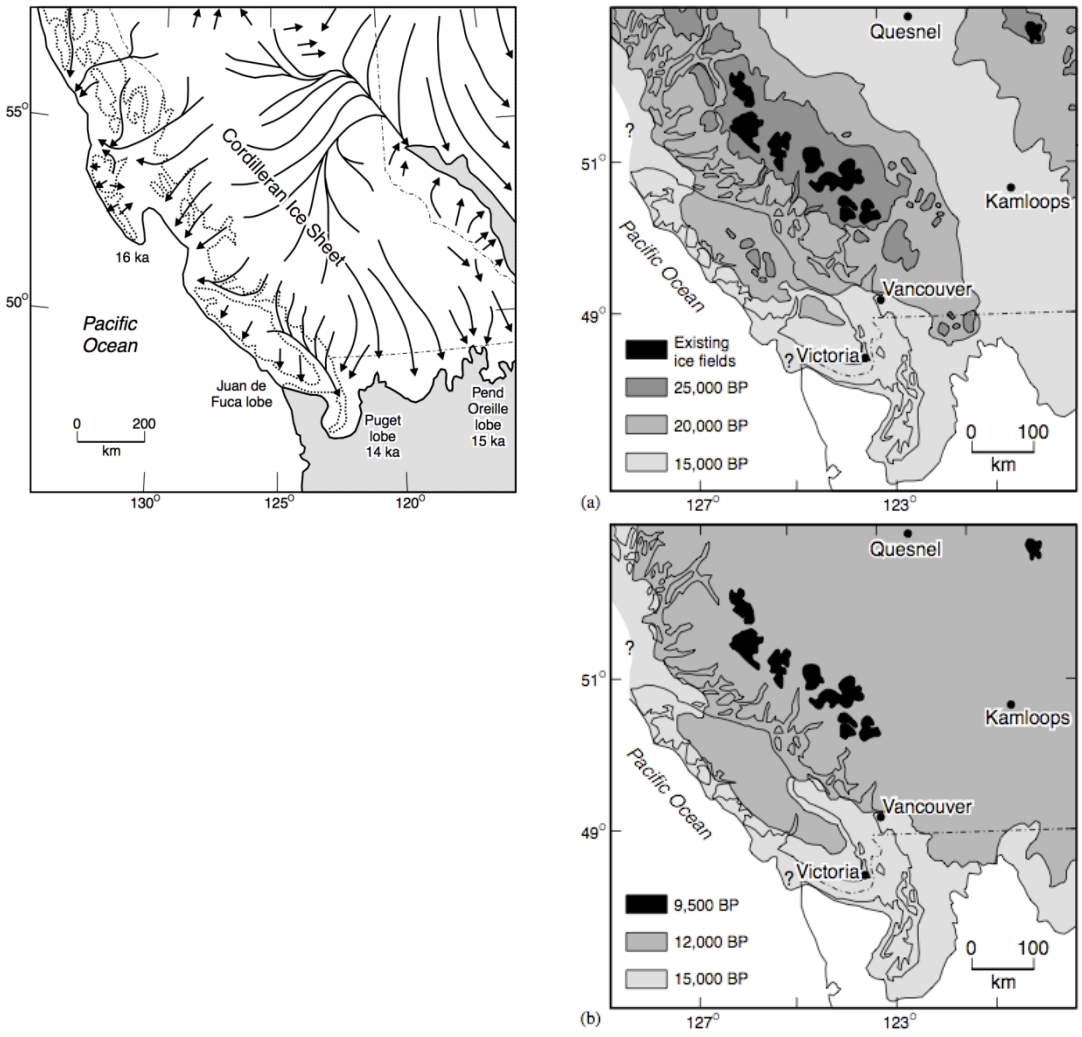

Figure 5.3. Left: general ice flow patterns of the southern CIS at the LGM (modified from Blaise *et al.* 1990, Fig. 11). Dates (ka) indicate times lobes achieved their maximum extent. Right: growth (a) and decay (b) of the CIS in southern BC during the Fraser Glaciation. Approximate glacier margins are depicted and unglaciated areas within the ice sheet are not shown (Fig. 4 and 5 in Clague and James 2002).

The CIS advanced and retreated several times during the Fraser Glaciation (30-10.5 cal kyr BP). Ice sheet advance and retreat is described in four stages (Clague and James 2002). Prior to the Fraser glaciation, alpine glaciation was dominant, as it is today. As the climate cooled, mountain glaciers advanced down into the lowlands. Valley glaciers coalesced into large ice-streams until the CIS covered all of southwestern BC except its very highest peaks, which remained exposed as nunataks.

The depositional history of CIS-related sediment is consistent with continuous sea-level rise (Clague *et al.* 2005). Sediments interpreted as being related to the CIS are grouped into four main units in southwest British Columbia: the Quadra Sand, the Coquitlam Drift, Vashon Drift, and Sumas Drift (Clague 1976; Armstrong 1981). The first of these units, Quadra Sand, contains well-sorted sand and gravel. The other three are composed of till, glaciofluvial, glaciolacustrine and ice-contact deposits.

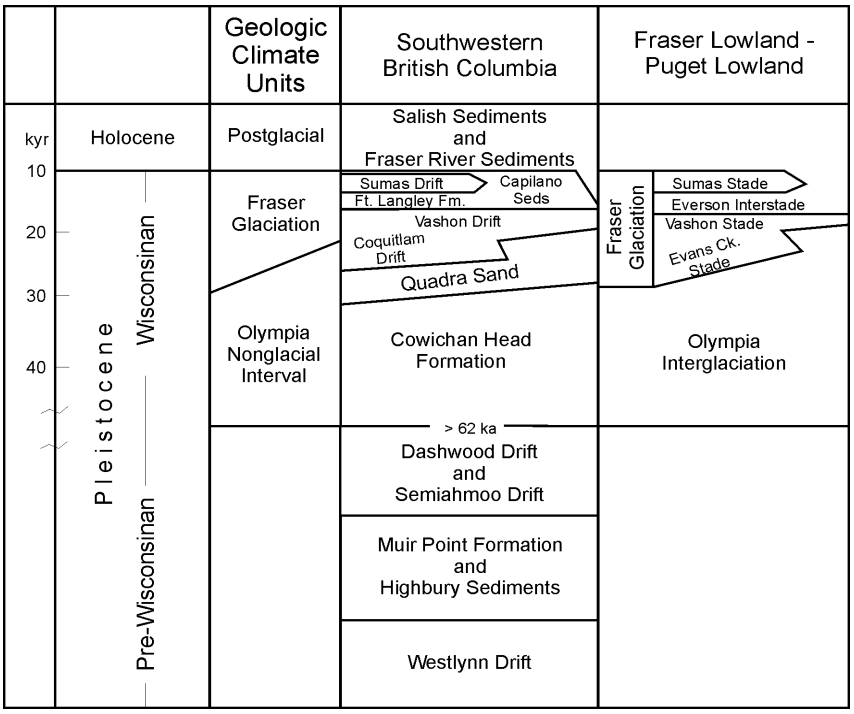

Figure 5.4. Late Pleistocene and Holocene stratigraphy of southwestern British Columbia (Clague 1994).

At the onset of the Fraser glaciation, the Quadra Sands record the advance of the CIS into the Georgia Basin, depositing fluvial sediments on a floodplain that likely extended across the present Strait of Georgia (Clague 1976). Materials were sourced from the Coast Mountains, and deposits age younger from north to south

from 34 cal kyr BP in the northern Strait of Georgia to 18 cal kyr BP in southern Puget Sound (Clague 1976).

The Fort Langley Formation includes interbedded glaciomarine and marine sediments as well as till, and is interpreted as marking the retreat of the CIS after the last glacial maximum (LGM). The Capilano Sediments are composed of glaciofluvial, glaciomarine and marine sediments that include dropstones but lack tills.

The largest advance between 20 and 15 cal kyr BP is known as the Vashon Stade, when the CIS extended south across the Fraser Lowlands of BC and the Puget Lowlands of northwestern Washington State, filled the Straits of Georgia and Juan de Fuca, and overtopped Vancouver Island (Armstrong *et al.* 1965; Clague 1981). A commonly accepted reference age range for the global LGM is 21 to 17 cal kyr BP (Denton and Hughes 1981).

The maximum extent of the CIS occurred around 15-18 cal kyr BP, several thousand years later than the Wisconsinan LGM of the Laurentide Ice Sheet (LIS) at about 21.5 cal kyr BP (Porter and Swanson 1998; Dyke 2002). Porter and Swanson (1998) and Kovanen and Easterbrook (1997, 2002b) reconstructed ice-flow patterns during the advance and retreat of the Puget Lobe of the CIS into northern Washington State. The analysis presented wood and bulk organic (gyttja) deposits as constraints to establish rapid advance and retreat across the Seattle area between 17.6-16.0 cal kyr BP and a maximal terminus of the CIS near Olympia, WA between 17.0-16.8 cal kyr.

Deglaciation along the coast occurred rapidly: the CIS remained at its furthest extent for only a few hundred years before the rapid collapse of the Juan de Fuca and Puget Lobes around ~17 cal kyr BP (Kovanen and Easterbrook 1997, 2002b; Cosma

et al. 2008; Hendy 2009). In contrast, the LIS persisted near its maximum extent for over 10 kyr. By ~10 cal kyr BP, the CIS extent was similar to modern alpine conditions. A submarine moraine in Howe Sound (south of Sechelt Inlet) marks the withdrawal of the CIS from the coastal lowlands of BC around 9.5 cal kyr BP (Fulton 1967).

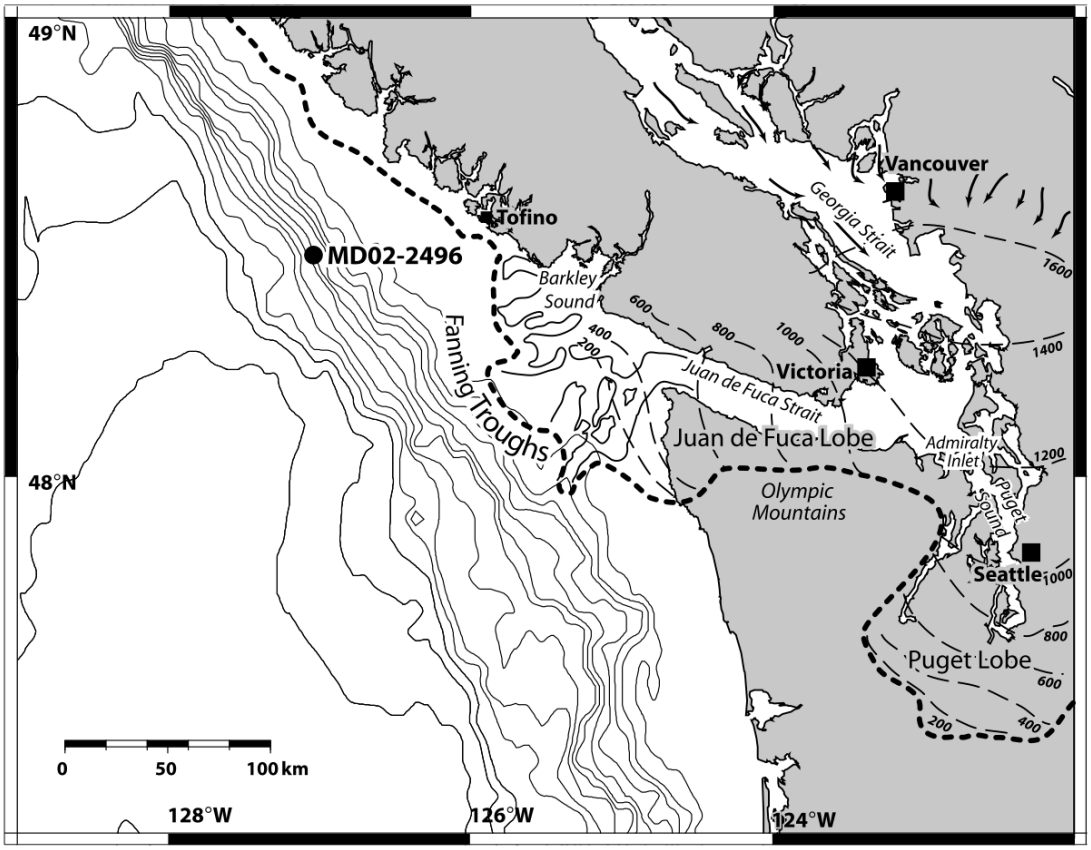

Figure 5.5. Location of core site MD02-2496 (1243 m water depth, 48.9745°N, 127.0357°W) on the west coast of Vancouver Island. Heavy dashed line represents the maximum extent of the Cordilleran Ice Sheet at 15.0 ^{14}C kyr BP. (Clague and James 2002). Thin dashed lines represent ice sheet thickness, and arrows represent ice flow direction (Porter and Swanson 1998). Troughs outside the Juan de Fuca Strait indicate locations of grounded ice (Herzer and Bornhold 1982). Fig 1. in Cosma *et al.* 2008.

Deglaciation of the CIS occurred primarily by down-wasting and stagnation rather than retreat (Fulton 1967; Alley and Chatwin 1979; Clague and James 2002).

Although not prevalent around Vancouver Island during CIS deglaciation, some evidence of iceberg calving exists. Extensive iceberg scour is observed in the Queen Charlotte Basin but not in the Straits of Georgia or Juan de Fuca, although ice-rafted debris (pebbles) were observed in ice-proximal Capilano Sediments sampled in the two cores TUL97B042 and TUL92A058 (Barrie and Conway 2002; Vaughn Barrie, personal communication, 2009). At its marine margins, ice shelves likely broke up quite rapidly just after the LGM at 18-17 cal kyr BP. Freshwater outburst flooding (meltwater plumes) carried glacial sediment including ice-rafted debris (IRD) that record short intervals of significant iceberg calving in core MD02-2496 (Cosma *et al.* 2008; Hendy 2009).

Away from the coast, the primary method of retreat was by downwasting. Large volumes of the ice sheet melted down rapidly and stagnated as they were cut off from the distant ice-centers they had flowed from. Stagnant valley ice thickness was reduced to less than 700 m by 14.8 cal kyr BP on southern Vancouver Island (Alley and Chatwin 1979), and topographically-controlled alpine glaciation came to dominate. The CIS diminished to its modern extent by about 11.5 cal kyr BP (Clague, 1981).

Causes of fast decay likely included 2 kyr of warming immediately preceding CIS collapse as well as the feedback cycle of rising global sea level, decreased ice cover, and a subsequently lowered albedo. Several local re-advances have been correlated to the Younger Dryas climatic event (Osborn *et al.* 1995; Friele and Clague 2002).

5.2.4 Radiocarbon constraints on ice history

Tables 5.1 and 5.2 give the radiocarbon ages used to constrain the advance and retreat of the Cordilleran ice sheet, respectively. These dates are based on and extend a comprehensive compilation by Gowan (2007), with a focus on the data relevant to the present study area. Gowan presented an analysis of CIS history, including a new compilation of radiocarbon samples corrected for marine reservoir effects (Hutchinson *et al.* 2004b). Previous analyses either used earlier reservoir corrections or did not correct for these effects (Alley and Chatwin 1979; Clague 1981; Booth 1987; Easterbrook 1992; Dethier *et al.* 1995; Porter and Swanson 1998; Swanson and Caffee 2001). Gowan's reanalysis of marine reservoir effects presents a retreat history that differs from previous studies by as much as 1000 years.

The present study conservatively adapts the ice model originated by James *et al.* (2000) and most recently revised by James *et al.* (2009b). New constraints in the study regions (Tables 5.1 and 5.2) are applied, while maintaining maximal ice thicknesses and preserving a smoothly sloping ice surface.

A timestep was added to the starting ice model of James *et al.* (2009b) at 19.0 kyr to model an earlier advance (at 19.0 instead of 18.0) of the CIS across southwestern BC. Compared to the starting model, ice was thinned in the northern Strait of Georgia to better predict slightly earlier emergence and a shallower lowstand than that observed at Sechelt. At Sechelt, peak ice thicknesses occurred at 14.2-13.5 cal kyr BP rather than 15.4-14.5 cal kyr BP. Ice thicknesses of 200-800 m were maintained for a longer period of near Sechelt from 14.4-13.4 (disks 320-323).

Glaciation was also delayed for the central and northern Strait of Georgia. Ice was thinned earlier in the northern Strait of Georgia by 100-1800m from 15.2-13.4 kyr (disks 156-159, 392-399). The central Strait of Georgia became ice-free at 14.5 cal kyr BP, Howe Sound and the northern Strait of Georgia at 14 cal kyr BP, and Sechelt at 13.5 cal kyr BP.

The LGM was set to 17.1 cal kyr BP (was 15.4) for the west coast of Vancouver Island (Cosma *et al.* 2008). Ice was thickened at LGM by 200-500 m on the west coast of Vancouver Island (disks 400-408, 383-391, 364-382, 304-306, 160,177,178) and in the Strait of Juan de Fuca (disks 340-347). New grid elements were added (disks 409, 410, 411) to model the westernmost extent of the Juan de Fuca Lobe over the present day fanning troughs at the continental shelf. Deglaciation to ice-free conditions for the Strait of Juan de Fuca and the west coast of Vancouver Island (especially north of Barkley Sound) was modeled from 17.1-15.4 cal kyr BP, significantly earlier than the previous model (15.4-14.8 cal kyr BP).

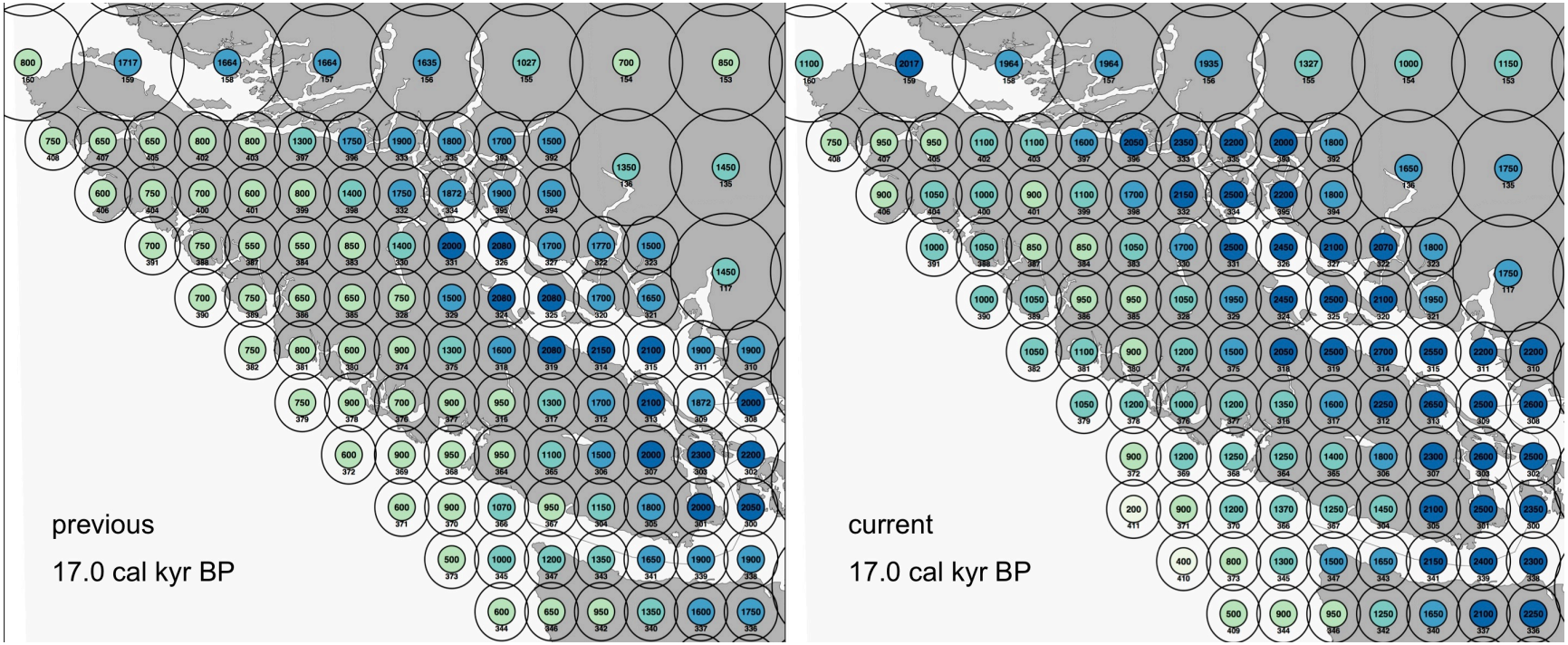

Figure 5.6a. Comparison of previous ice model (James *et al.* 2009b) vs. current ice model at ~17 cal kyr BP.

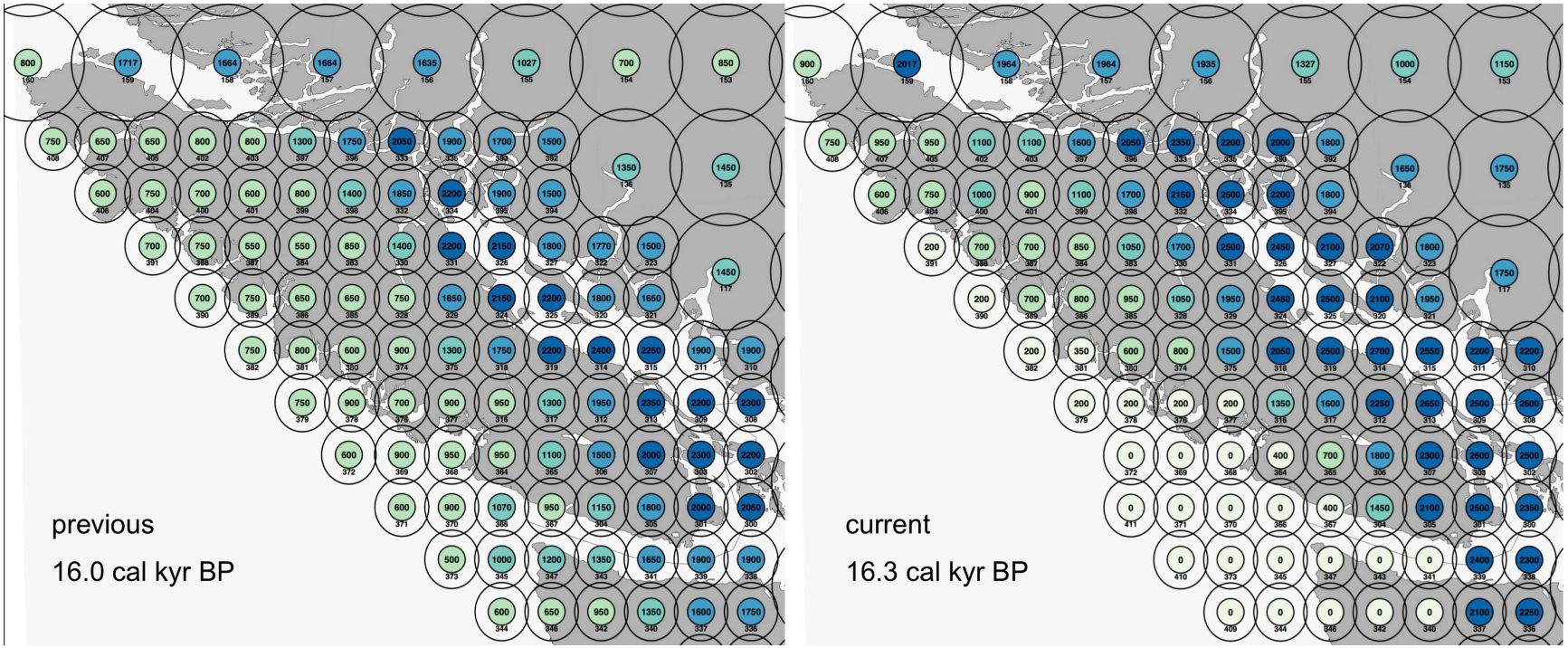

Figure 5.6b. Comparison of previous ice model (James *et al.* 2009b) vs. current ice model at ~16 cal kyr BP.

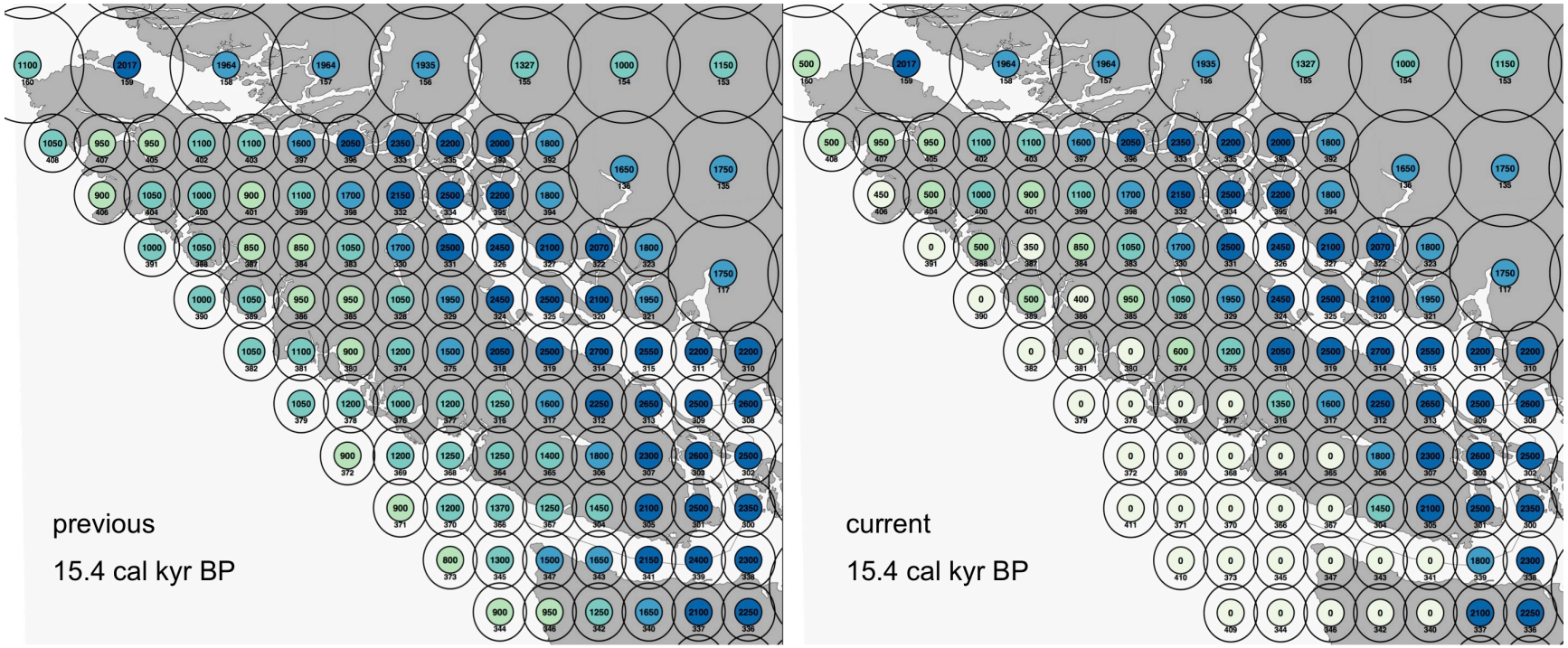

Figure 5.6c. Comparison of previous ice model (James *et al.* 2009b) vs. current ice model at ~15 cal kyr BP.

Table 5.1. Dates and elevations pertaining to the advance of the Cordilleran Ice Sheet.
[a] All dates have a 1-sigma error. Reservoir corrections include -950±50 for marine organisms and -650±60 for basal gyttja and peat
[b] Dates calibrated using Calib 5.0 (Stuiver and Reimer 1993). Age range is 1-sigma limits.

Location	Elevation (m)	Lab no.	Material	Radiocarbon age	Calibrated age	Error (kyr)	Constraint	Reference
Cowichan Tongue	n/a			19.00			minimum glaciation	Halstead 1968
Holberg Inlet	n/a	GSC-2505	shells	20.60		330	minimum glaciation	Howes 1981b
Puget Lobe	n/a				17.00		LGM	Porter and Swanson 1998
Puget Lobe	n/a				16.00	1		Porter and Swanson 1998
Victoria Peak	1550				LGM		ice thickness	Howes 1981b
Pinder Peak	1371				LGM		ice thickness	Howes 1981b
Gold River	1335				LGM		ice thickness	Howes 1981b
Houpsitas	1112				LGM		ice thickness	Howes 1981b
Yuquot	1005				LGM		ice thickness	Howes 1981b
Howe Sound	1000				14.00		ice thickness	Friele and Clague 2002
Zeballos	701				LGM		ice thickness	Howes 1981b
Zeballos	700				16.00		ice thickness	Gutsell et al. 2004
Kitimat	200						upper marine limit	Clague 1983
Vancouver (Fraser Lowland)	200						upper marine limit	Clague 1983
Bellingham	180						upper marine limit	Mathews et al. 1970
Sechelt	180						upper marine limit	Clague 1983
Campbell River	175						upper marine limit	Clague 1983
Eve - Adam River	175		deltaic & marine silts				upper marine limit	Howes 1981a
Vancouver	175						upper marine limit	Mathews et al. 1970
Bella Bella	165						upper marine limit	Clague 1983
Eve - Adam River	152		deltaic & marine silts				upper marine limit	Howes 1981a
Courtenay	150						upper marine limit	Mathews et al. 1970
Stewart (Observatory Inlet)	150						upper marine limit	Clague 1983
Qualicum Beach	140						upper marine limit	Clague 1983
Queen Charlotte Sound	120						upper marine limit	Clague 1983
Port Alberni	100						upper marine limit	Clague 1983
Port Hardy	100						upper marine limit	Clague 1983

Location	Elevation (m)	Lab no.	Material	Radiocarbon age	Calibrated age	Error (kyr)	Constraint	Reference
Port Hardy	95		fossil marine silts				upper marine limit	Howes 1981a
Alberni (Port)?	90						upper marine limit	Mathews et al. 1970
Port McNeill	90		deltaic				upper marine limit	Howes 1981a
Port Eliza	85			16.30	19.30	0	minimum glaciation	Al Suwaidi and Ward 2006
Victoria	75						upper marine limit	Mathews et al. 1970
Port McNeill	53	WSU-2019	shell	12.25		220	min marine maximum	Howes 1981b
Tofino	50						upper marine limit	Clague 1983
Esperanza Inlet Head	46		deltaic				upper marine limit	Howes 1981a
Zeballos	45						upper marine limit	Clague et al. 1982
Tofino	37	GSC-2768	log in gravel	16.70			maximum onset of glaciation	Clague et al. 1980
Hesquiat Harbour	33						upper marine limit	Clague et al. 1982
Hesquiat Harbour	32		beach strandlines & marine silts				upper marine limit	Howes 1981a
Esperanza Inlet Mouth	30		deltaic				upper marine limit	Howes 1981a
Hesquiat Harbour	30		beach strandlines & marine silts				upper marine limit	Howes 1981a
Cape Scott	27						upper marine limit	Clague et al. 1982
Brooks Penninsula	25						upper marine limit	Clague 1983
Brooks Penninsula	25		beach strandlines				upper marine limit	Howes 1981a
Cape Scott	25						upper marine limit	Clague 1983
Cape Scott	25		wave cut bench				upper marine limit	Howes 1981a
Zeballos	21						highstand	Gutsell et al. 2004
Brooks Penninsula	20						upper marine limit	Clague et al. 1982
Queen Charlotte Islands (Dixon Entrance)	20						upper marine limit	Clague 1983
Port McNeill	17	WSU-1710	shell	12.93		160	min marine maximum	Howes 1981b
South Van. Isl.	0			18.00			advance	Alley and Chatwin 1979

Table 5.1. Dates and elevations pertaining to the advance of the Cordilleran Ice Sheet (continued).

Table 5.2. Dates and elevations pertaining to the retreat of the Cordilleran Ice Sheet.
[a] All dates have a 1-sigma error. Reservoir corrections include -950±50 for marine organisms and -650±60 for basal gyttja and peat
[b]Dates calibrated using Calib 5.0 (Stuiver and Reimer 1993). Age range is 1-sigma limits.

Location	Elevation (m)	Lab no.	Material	Radiocarbon age (kyr)	Calibrated age (kyr)	Error (kyr)	Constraint
Coast Mtns	n/a			10.50			minimum deglaciation
Coast Mtns	n/a			13.00			maximum deglaciation
Cowichan Tongue	n/a			12.80	14.00		ice-free
Hecate Strait	n/a			14.16			shelf retreat
Olympic Penninsula	n/a		lodgepole pine	14.50			minimum deglaciation
Queen Charlotte Sound	n/a			12.91			shelf retreat
Queen Charlotte Sound	n/a			15.00			shelf retreat
Queen Charlotte Sound	n/a			13.50			ice-free
Strait of Georgia	n/a			9.20			lowstand
Strait of Georgia	n/a			11.30	13.50	50	ice free
Strait of Georgia	n/a			13.00			calving embayment
Strait of Georgia	n/a			13.10			calving embayment
Strait of Georgia	n/a			12.50			calving embayment
San Juan Ridge	762			11.20		110	minimum deglaciation
Lens Creek	700			12.20		140	minimum deglaciation
Howe Sound	450				13.50		ice thickness
South Van. Isl.	400			13.00			minimum deglaciation
Harris Creek	396			13.10		130	minimum deglaciation
Artlish River Cave (A-1)	285	GSC-2435	wood	8.30		70	
Lake Cowichan	200			10.28		150	minimum deglaciation
Port Eliza	85			12.30	14.80	0	minimum deglaciation
Texada Island	80		raised beach	11.94		50	minimum deglaciation
Texada Island	80		raised beach	11.25		50	minimum deglaciation
Bear Cove, Port Hardy	30				16.00		deglaciation
Bear Cove, Port Hardy	30		earliest record of humans	8.00		110	minimum anthropogenic
Bear Cove, Port Hardy	30		lodgepole pine	13.63	15.00	0	minimum deglaciation
Zeballos	4						holocene-highstand

Location	Elevation (m)	Lab no.	Material	Radiocarbon age (kyr)	Calibrated age (kyr)	Error (kyr)	Constraint
Buckle Bay, Vargas Isl.	3	Beta-42922		12.97		80	min marine maximum
Howe Sound	0				12.70		ice thickness
Zeballos	-20				9.00	1000	lowstand
Hornby Island	-24			11.02		50	max lowstand
Queen Charlotte Strait	-100			12.90		400	IRD #3 (min)
Juan Perez Sound	-145	CAMS59768	in situ pine tree stump	12.24		50	lowstand
Juan Perez Sound	-150	CAMS22276	wood in marine setting	12.38		70	lowstand
Goose Island Trough	-200			13.60		400	IRD# 3 (max)
Queen Charlotte Strait	-200			12.00		400	maxiumum lowstand
Queen Charlotte Strait	-200			10.20		400	minimum lowstand
IRD #1	-1243	MD02-2496			16.20		IRD #1 (min)
IRD #1	-1243	MD02-2496			17.10		IRD #1 (max)
IRD #2	-1243	MD02-2496			15.30		IRD #2 (max)
West Coast	-1243	MD02-2496			14.70		IRD #2
West Coast	-1243	MD02-2496			14.60		IRD #2 (min)

Table 5.2. Dates and elevations pertaining to the retreat of the Cordilleran Ice Sheet (continued).

5.3 Earth model Parameters

The Earth's response to an ice load depends largely on the viscosity profile of the mantle and the elastic thickness of the lithosphere. These material properties are incorporated into a spherical Earth model.

5.3.1 Rheology of the Mantle

The Earth's response to stress depends on its mechanical and rheological properties and the time scale over which the stress is applied. The lithosphere is relatively cold and it behaves elastically, like a spring shortening immediately under a compressive force and relaxing to its original state once the force is removed (Turcotte and Schubert 2002). The mantle also acts elastically on short time scales (less than an hour): seismic shear waves experience very little attenuation as they travel through the mantle (Turcotte and Schubert 2002). However, at longer time scales (millions of years), tectonic plates are driven by a convecting mantle that flows as a viscous fluid. At intermediate times (thousands of years), relative sea-level observations document a continuing response of the Earth to the removal of the surface load imposed by ice sheets. Because the mantle acts elastically at short time periods and viscously at long periods, a linear viscoelastic Maxwell rheology is chosen to model the Earth's GIA response. The effect of nonlinear rheologies on GIA observables has also been investigated (Karato and Wu 1993; Peltier 1998), but no strong requirement to incorporate nonlinear rheologies when undertaking modeling to explain GIA observables has yet been demonstrated.

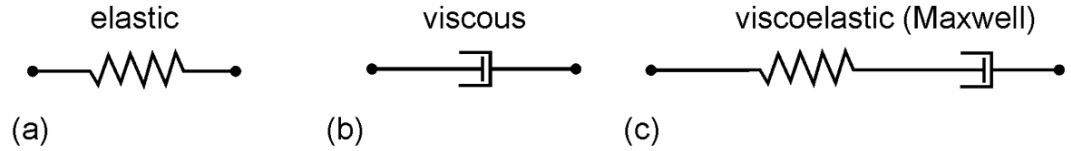

Figure 5.7. Mechanical equivalents of simple rheological models (Ranalli 1995): (a) elastic (Hooke's Law), (b) Newtonian viscous (dashpot), (c) viscoelastic Maxwell (combined spring and dashpot), after Fig. 4.1 of Gowan (2007).

The present study models the lithosphere as responding elastically to ice loading. Because the mantle flexes elastically at short time periods (like a spring) but flows viscously over long periods, we model the GIA response of the mantle with a viscoelastic Maxwell rheology. The fundamental rheological law for a Maxwell viscoelastic material (Turcotte and Schubert, 2002) is:

$$\frac{\partial \varepsilon}{\partial t} = \frac{1}{2\mu}\sigma + \frac{1}{E}\frac{\partial \sigma}{dt} \tag{1}$$

The total strain, ε, for a viscoelastic material is the sum of both elastic and fluid strains. The strain rate, $d\varepsilon/dt$, depends on the applied uniaxial stress, σ (the component of the stress tensor normal to the surface of the half-space), as well as the rate of change of the applied stress ($d\sigma/dt$). When we initially apply or remove a stress, the stress rate term dominates and we observe elastic behaviour ($\sigma_0 = E\varepsilon_0$, where E is Young's modulus). When a constant stress is maintained—or removed following isostatic equilibrium—the stress-rate term is zero; stress is then linearly related to strain rate as for a viscous fluid, where μ is the viscosity.

Turcotte & Schubert (2002) describe the relaxation of a uniform, incompressible viscous half-space (i.e., the Earth's mantle in a GIA model) subject to an initial surface disturbance under the influence of gravity as:

$$\omega = \omega_m e^{-\frac{t}{\tau_r}} \tag{2}$$

where ω is the surface displacement from an initial position ω_m at time t = 0, and the characteristic relaxation time τ_r is given by:

$$\tau_r = \frac{4\pi\mu}{\rho g \lambda} \tag{3}$$

where ρ is the density of the mantle, g is the surface acceleration due to gravity, λ is the sinusoidal wavelength of the surface displacement, and μ is the viscosity.

In characteristic regions of slow rebound such as Hudson's Bay, Canada (Figure 5.8) and the Gulf of Bothnia between Finland and Sweden, GIA exhibits a relatively long relaxation time of >3 kyr, and residual decay continues to generate present-day relative sea-level fall.

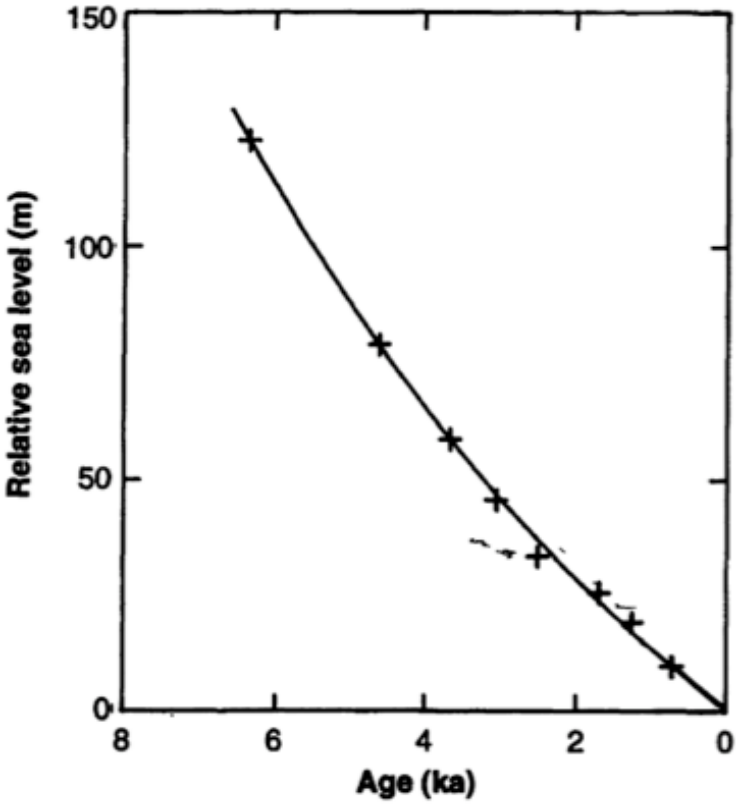

Figure 5.8. Post-glacial rebound in Hudson's Bay (Peltier 1994).

In contrast, GIA response to the collapse of the CIS in southwestern BC was extremely rapid. Very little residual signal due to postglacial rebound remains today, with estimates of the vertical motion due to GIA being less than 0.1 mm/yr (James *et al.* 2009b).

Relative sea-level change in southwestern BC provides a reliable constraint on postglacial rebound during the late Pleistocene and early Holocene, as the rate of sea-level fall after deglaciation was fast enough (>100 mm/a) that tectonic motions are considered negligible. By contrast, the tectonic component of present day crustal motion—about 2 mm/yr on Vancouver Island (Mazzotti *et al.* 2003)—obscures the < 0.1 mm/yr residual signal due to postglacial rebound (James *et al.* 2009a).

Simplified Earth models composed of six layers are employed for the analyses described here: a fluid core, three mantle layers of fixed viscosity, one upper mantle layer of variable viscosity, and an elastic lithosphere of variable thickness (Figure 5.9). The lithospheric thickness is based on the structural setting of the Sechelt and Barkley Sound regions. Rigidity and density parameters are based on the Preliminary Reference Earth Model (PREM) (Dziewonski and Anderson 1981). Rigidity and density are volumetrically averaged for each rheological layer, including the core and lithosphere.

The Earth models used by the present study define spherically symmetric layers with uniform properties of elasticity, density and viscosity. The GIA response is calculated as described by James (1991) and James and Ivins (1998). Formally, the conservation equations for mass and momentum, as well as Poisson's equation for gravitational potential, are linearized and decomposed in terms of Legendre functions or spherical harmonics. There are a number of exponentially decaying responses for each spherical harmonic (or Legendre function) degree with differing amplitudes.

5.3.2 Asthenospheric thickness and viscosity

This study uses the same family of Earth models as James *et al.* (2009b) to explore the viscosity of the asthenosphere relative to GIA and subduction dynamics at the northern CSZ (Figure 5.9). The Earth models feature a fluid core, a lower mantle divided into 2 layers, an upper mantle divided into 2 layers, and an elastic lithosphere. The thickness of the lithosphere and the thickness and viscosity of the asthenosphere (uppermost upper mantle layer) can vary. Except for the asthenosphere, viscosity values are based on the VM2 model (Peltier 1998). In the upper mantle, below the asthenosphere, the viscosity is 4.0×10^{20} Pa s. Below the 670 km discontinuity, two lower mantle layers are bounded at 1291 km depth, the upper with viscosity 1.6×10^{21} Pa s, the lower with 3.2×10^{21} Pa s. A fluid core begins at 2891 km depth.

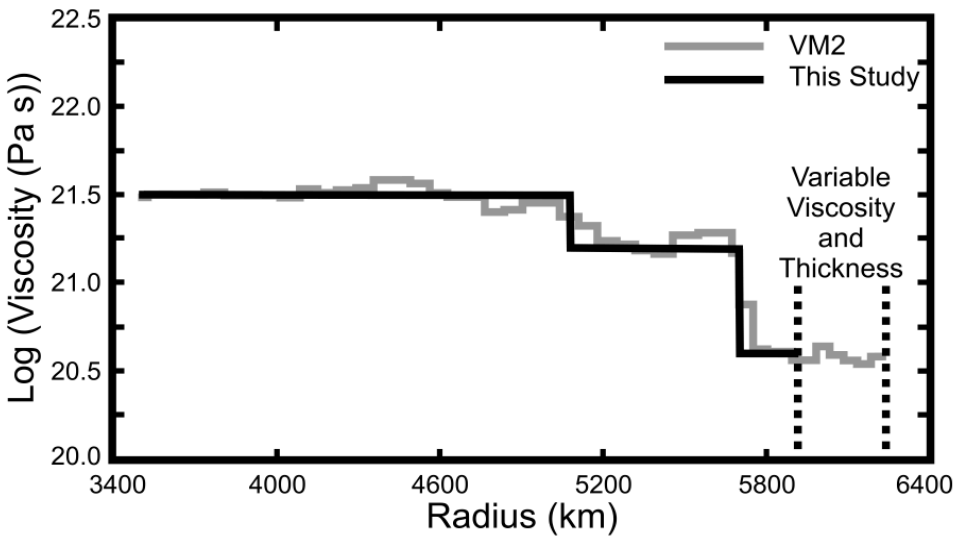

Figure 5.9. Viscosity profile of the mantle. The gray line is the VM2 model of Peltier [2004], and the black line is the simplified model used in this study. The uppermost mantle (asthenosphere) has variable viscosity and thickness (after Figure 2 of James *et al.* 2009b).

A series of previous studies explored mantle viscosity, asthenospheric thickness and lithospheric thickness to model GIA in the CSZ. James *et al.* (2000) modeled

regional effective mantle viscosities of 5×10^{18} to 5×10^{19} Pa s. Clague and James (2002) confirmed that an upper mantle viscosity $< 10^{20}$ Pa s fits observed RSL patterns and shoreline tilts in the region. A lithospheric thickness of 60 km was inferred from heat flow and seismic data to best represent the combined flexural rigidity of the continental crust and oceanic slab. Predictions of the GIA model (James *et al.* 2009b) are in good agreement with previously-published sea-level observations at Victoria and in the central and northern Strait of Georgia for asthenospheric thicknesses varying from 140 to 380 km and for viscosities around 10^{19} Pa s (Figure 5.9).

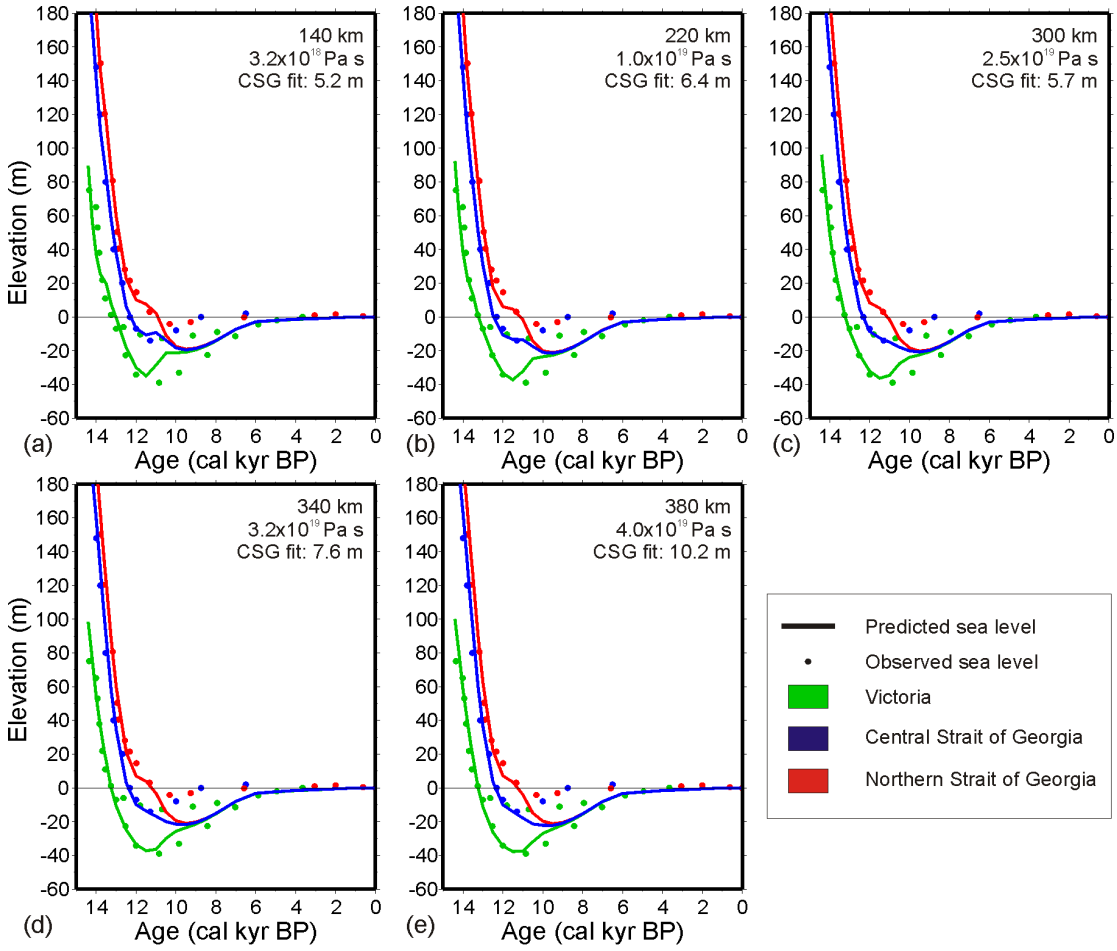

Figure 5.10. Predictions of a previous GIA model (James *et al.* 2009b) are in good agreement with previously-published sea-level observations for a range of asthenospheric thicknesses (km) and viscosities (Pa s) around 10^{19} Pa s. Diffusive channel flow theory predicts lower viscosity with a thinner asthenosphere (James *et al.* 2009b).

The present study uses the same earth models and parameters to explore agreement between model predictions and the new sea-level observations at Barkley Sound and Sechelt.

5.3.3 Effective elastic thickness of the lithosphere

Southwestern BC overlies the northern CSZ. In the backarc, asthenospheric convection and water from slab dehydration produce high rates of heat flow that result in a relatively thin lithosphere (Hyndman 2010). In the forearc, low measured heat flow suggests larger lithospheric thicknesses. The lithospheric thickness parameter of Earth models used by the present study is interpreted as an effective elastic thickness, which is a measure of the average depth to the transition between brittle-elastic and ductile response of the lithosphere or mantle (Flück *et al.* 2003). Effective lithospheric thickness is expected to vary from location to location.

Episodic tremors during silent slip events occur under southern Vancouver Island at depths of over 40 km (Kao *et al.* 2005). Such events occur within the subducting oceanic crust and upper mantle, which, on the time scale of the GIA response, is decoupled from the overriding continental plate for depths of less than 25 km (James *et al.* 2009b). Down-dip, to the northeast—where the plate interface is already several tens of km deep—seismicity within the subducting slab has been observed from the plate interface to depths of 65 km (Cassidy and Waldhauser 2003). For example, an effective elastic thickness ranging from 31-39 km was established for Seattle, WA by a study of crustal tilting in Puget Sound. The study first considered seismogenic depths and then applied thermal modeling constraints on the subducting slab (Clague and James 2002).

Near Barkley Sound (at Port Renfrew) on the west coast of Vancouver Island, a lithosphere thickness of about 30 km was determined by seismic tomography, based on the depth to the top of the subducting Juan de Fuca slab (Figure 5.10; Ramachandran *et al.* 2005). While some studies of gravity and topography data estimate an effective elastic thickness of 40 km for southern Vancouver Island (Flück *et al.* 2003), a 60 km depth to the top of the Juan de Fuca plate provides a good fit to GIA models for southern Vancouver Island and the Strait of Georgia (Gowan 2007; James *et al.* 2009b).

Sechelt overlies the transition between the forearc and backarc of the CSZ, where the Juan de Fuca slab has subducted below the forearc mantle wedge. An effective elastic thickness of 60 km was found in previous modeling in the central and northern Strait of Georgia (Hutchinson *et al.* 2004a; James *et al.* 2005) and southern Vancouver Island (James *et al.* 2009b) to produce a good fit to the observations. The present study models the lithosphere at Sechelt with an effective elastic thickness of 60 km.

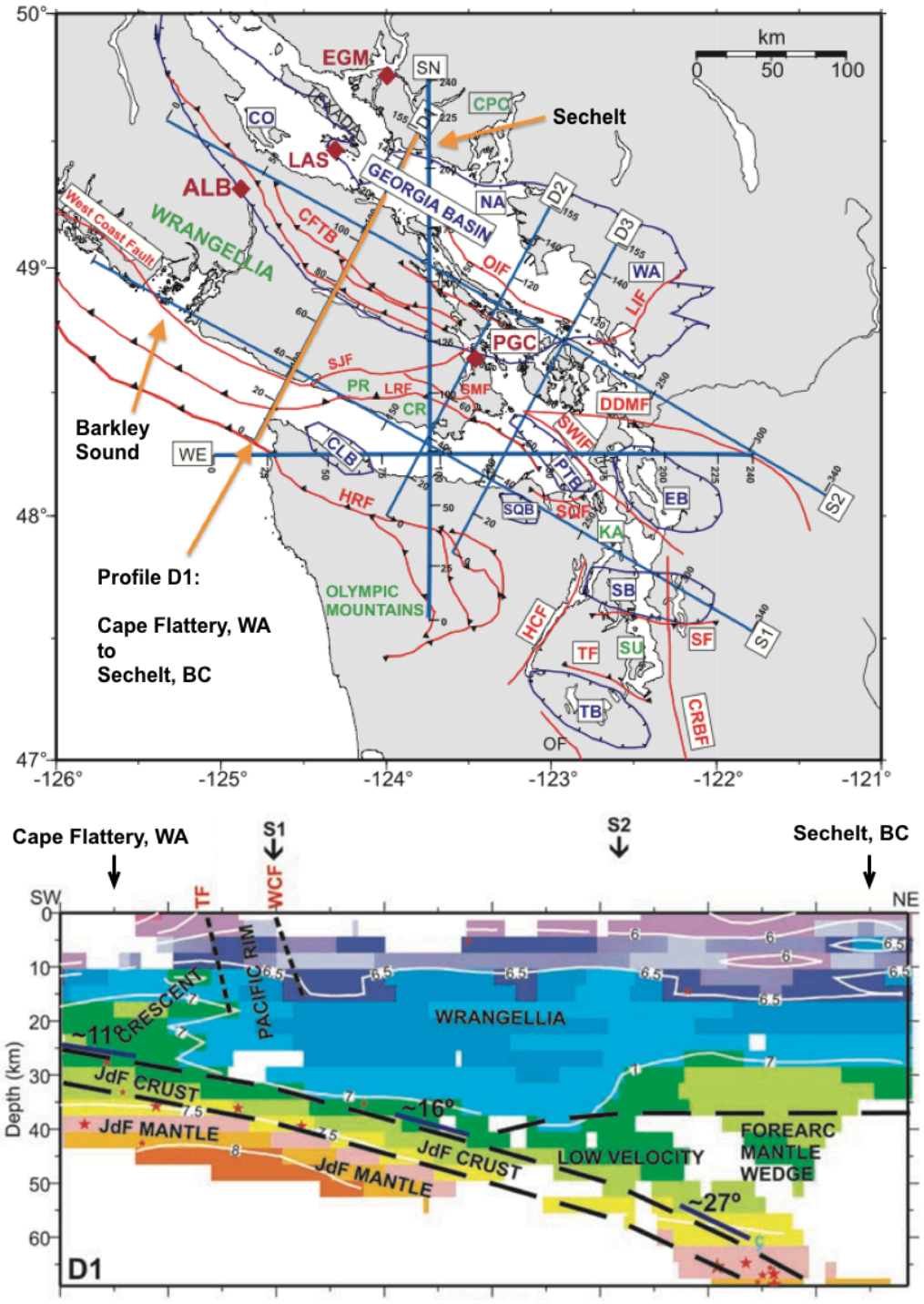

Figure 5.11. Vertical seismic velocity tomography along-dip for Juan de Fuca (JdF) plate subduction. Profile D1: Cape Flattery, WA to Sechelt. WCF (Westcoast Fault) bisects profile S1 at Barkley Sound. TF (Tofino Fault) is offshore. Sechelt is near the NE end of Profile D1 (Figures 2 and 7a in Ramachandran *et al*. 2005).

Barkley Sound lies above the forearc of the CSZ in a region of relatively low heat flow and frequent seismic activity. Seismicity is an indicator of brittle behavior and thus provides another constraint on the effective elastic thickness of the lithosphere: the depth ranges of active seismicity indicate the portion of each plate that behaves like an elastic-brittle material (James *et al.* 2000).

Effective elastic thickness for the CSZ may pertain solely to the continental lithosphere or to the combined elastic thickness of the overriding plate, t_c, and subducting oceanic lithosphere, t_o. Since the resistance of an elastic plate to bending varies with the cube of its thickness (Turcotte and Schubert 1982), the combined elastic thickness can be expressed as:

$$t_e^3 = t_c^3 + t_o^3 \qquad (2)$$

Crustal seismicity is distributed from the surface to the plate interface at a depth of 30 km. The subducting Juan de Fuca plate below Barkley Sound is relatively young and is expected to exhibit seismicity over only a few km of thickness (Figure 5.10). The bottom of crustal seismicity occurs at 30 km depth. Setting t_0 to a relatively small value like 5 or 10 km and t_c to 30 km results in an effective elastic thickness that is essentially equal to the t_c thickness (30.05 - 30.37 km). The present study models the lithosphere with an effective elastic thickness of 30 km below Barkley Sound.

5.3.5 The Sea-level Equation

Farrell and Clark (1976) presented a method of calculating postglacial sea level for elastic and viscoelastic non-rotating Earth models that continues to be used, with modifications, up to the present day. It states:

$$S(\theta,\lambda,t) = G(t) - R(t) - \left[\frac{M_I}{\rho_w A_O}\right] - \langle G(t) - R(t)\rangle_0 \qquad (3)$$

The sea-level equation describes sea level S as it changes over time (t), co-latitude (θ), and longitude (λ). The quantity G is the geoid, R is the deflection of the surface of the solid earth, A_o the ocean's surface area, ρ_w the density of water, and M_I the total change in ice-sheet mass from initial melting to time (t). Sea level is the difference between the geoid G and the surface of the solid Earth R, modified to include eustatic sea-level change (the middle term in square braces) and to conserve mass (the right-hand term). GIA generates changes through time of these surfaces (Farrell and Clark 1976; Mitrovica and Peltier 1991; Mitrovica and Milne 2003).

The sea-level equation applies the ocean function C(t) such that sea-level is only defined where C(t) = 1 and assumes (1) a closed hydrologic cycle: mass from ice-melt must be added to the ocean and (2) a constant ocean surface-area. The 'steep-shoreline approximation' does not account for the increase of ocean area resulting from an increase in the volume of water. This effect can be significant where near-shore bathymetry is shallow (such as southern Patagonia) but is an acceptable approximation on Vancouver Island and the mainland coast north of Vancouver.

5.3.6 Eustatic Sea Level

The crustal displacement due to GIA can be estimated by removing a globally averaged, or eustatic, sea level from observed relative sea level (Farrell and Clark 1976).

Conversely, if crustal displacements due to GIA are generated from a model calculation, the corresponding relative sea-level change can be approximated by adding the eustatic sea-level to the crustal displacement.

To calculate relative sea level in southwestern BC, the present study uses a published Barbados sea-level curve based on radiocarbon-dated coral (Figure 5.11; Fairbanks 1989; Bassett *et al.* 2005), similar to the approach of Gowan (2007) and James *et al.* (2009a). This approximation is valid because sea level fell rapidly and the precise eustatic contribution is not needed to determine vertical motion rates and thus generate estimates of Earth rheology. A more complete treatment (for future study) would incorporate the CIS model into a global model and calculate globally self-consistent sea-level change.

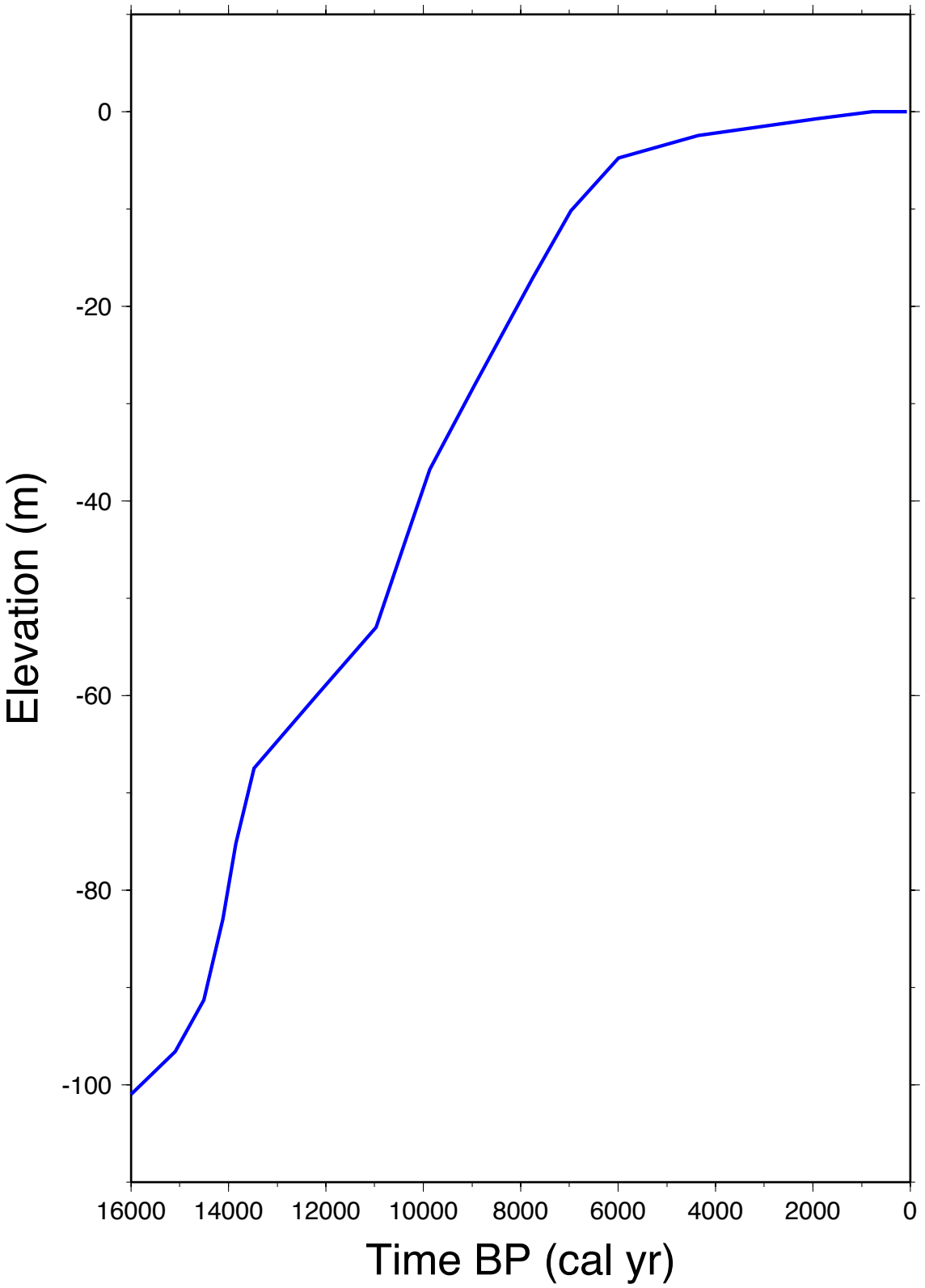

Figure 5.12. Eustatic sea-level curve for Barbados (Bassett *et al.* 2005).

5.4 GIA Model Results

To explore combinations of ice-sheet history and Earth structure, the GIA model described in section 5.3 was run systematically over the same range of model mantle viscosity and asthenospheric thickness values explored by James *et al.* (2009b). The sea-level history predicted by each run was compared to observed sea-level change at Barkley Sound and Sechelt. When predictions disagreed with observed data, model assumptions were modified to produce better agreement between predicted and observed sea level. Ice surface elevations were computed to ensure that the surface slopes smoothly to its edges.

As discussed (Section 5.2.4), to establish good agreement between predicted and observed RSL at Barkley Sound and Sechelt, modifications were made to the ice model originated by James *et al.* (2000) and most recently revised by James *et al.* (2009b). Revisions to the ice models are consistent with radiocarbon constraints on ice sheet history (Tables 5.1 and 5.2) and provide good agreement with observed sea-level history for both study regions as well as the Strait of Georgia and southern Vancouver Island.

5.4.1 Sechelt Peninsula

The observed Sechelt sea-level curve, especially the rapid fall from the initial high-stand position before 12 cal kyr BP, is well predicted by an earth model with a 60-km thick lithosphere and 380-km thick asthenosphere and model viscosity of 4.0×10^{19} Pa s (Figure 5.13). If lithospheric thickness is decreased from 60 km to 40 km or 30 km or asthenospheric thickness and viscosity are decreased below 340 km and 3.2×10^{19} Pa s (model variants not shown), the fit to the observations worsens significantly; predicted

emergence is earlier and faster and the predicted lowstand is significantly deeper and earlier than observed.

In contrast to the good fit obtained for the initial large-amplitude sea-level fall, the timing and magnitude of the predicted lowstand differs from the observed sea-level curves at central and northern Strait of Georgia, as well as Sechelt. The lowstand fit for Victoria is good. These departures during the Holocene have been previously noted for the central and northern Strait of Georgia and require further modeling (James *et al.* 2009b). It is possible that lateral Earth structure, or perhaps alternative choices for asthenospheric thickness and viscosity, could provide a better fit while preserving the good fit of the earlier portions of the curves.

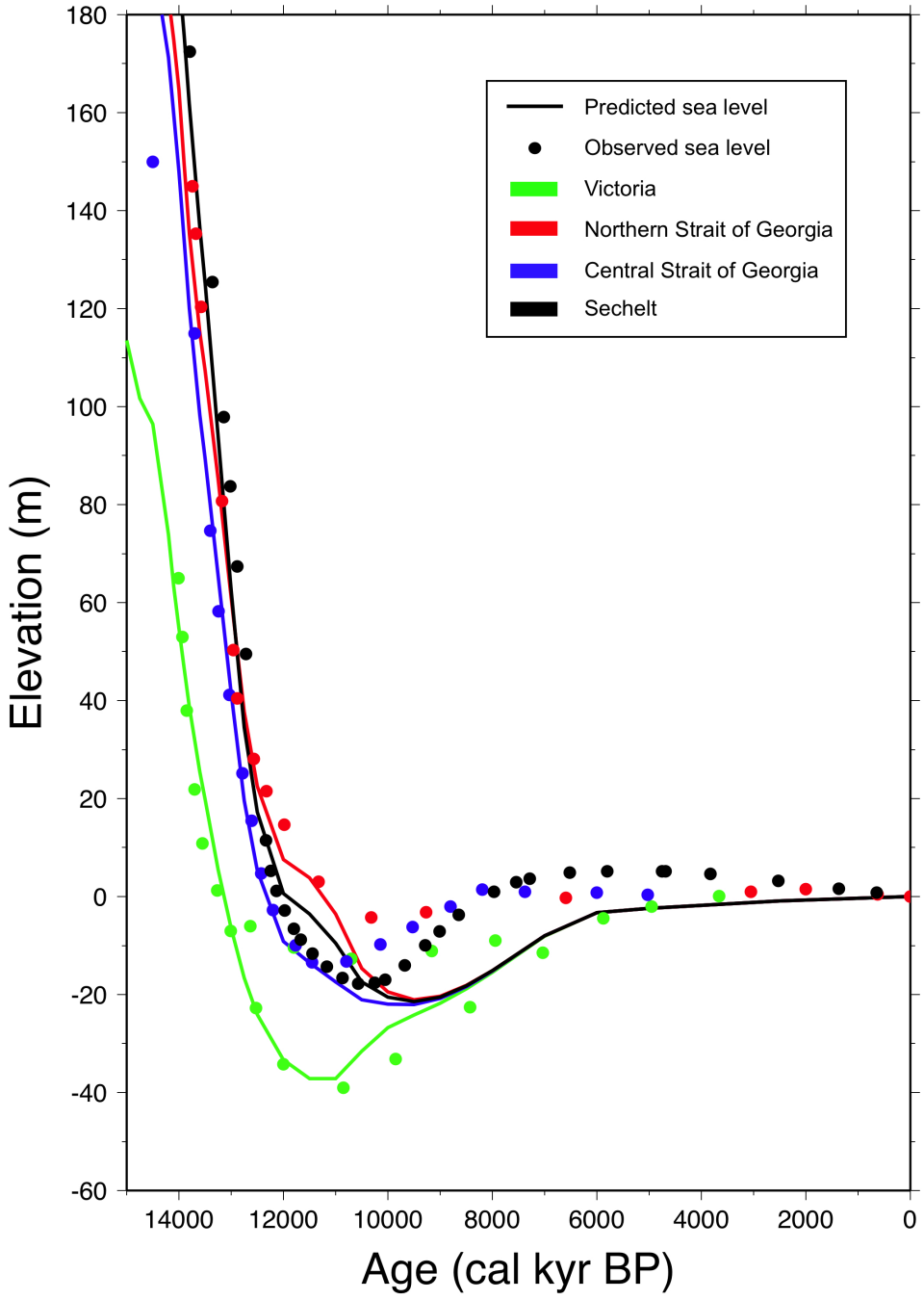

Figure 5.13. Relative sea-level predictions (solid lines) compared to the observed relative sea-level curve (circles) for the new Sechelt RSL curve and three previously modeled regions. Earth model parameters include a 60-km thick lithosphere and a 380-km thick asthenosphere with viscosity of 4.0×10^{19} Pa s.

5.4.2 Barkley Sound

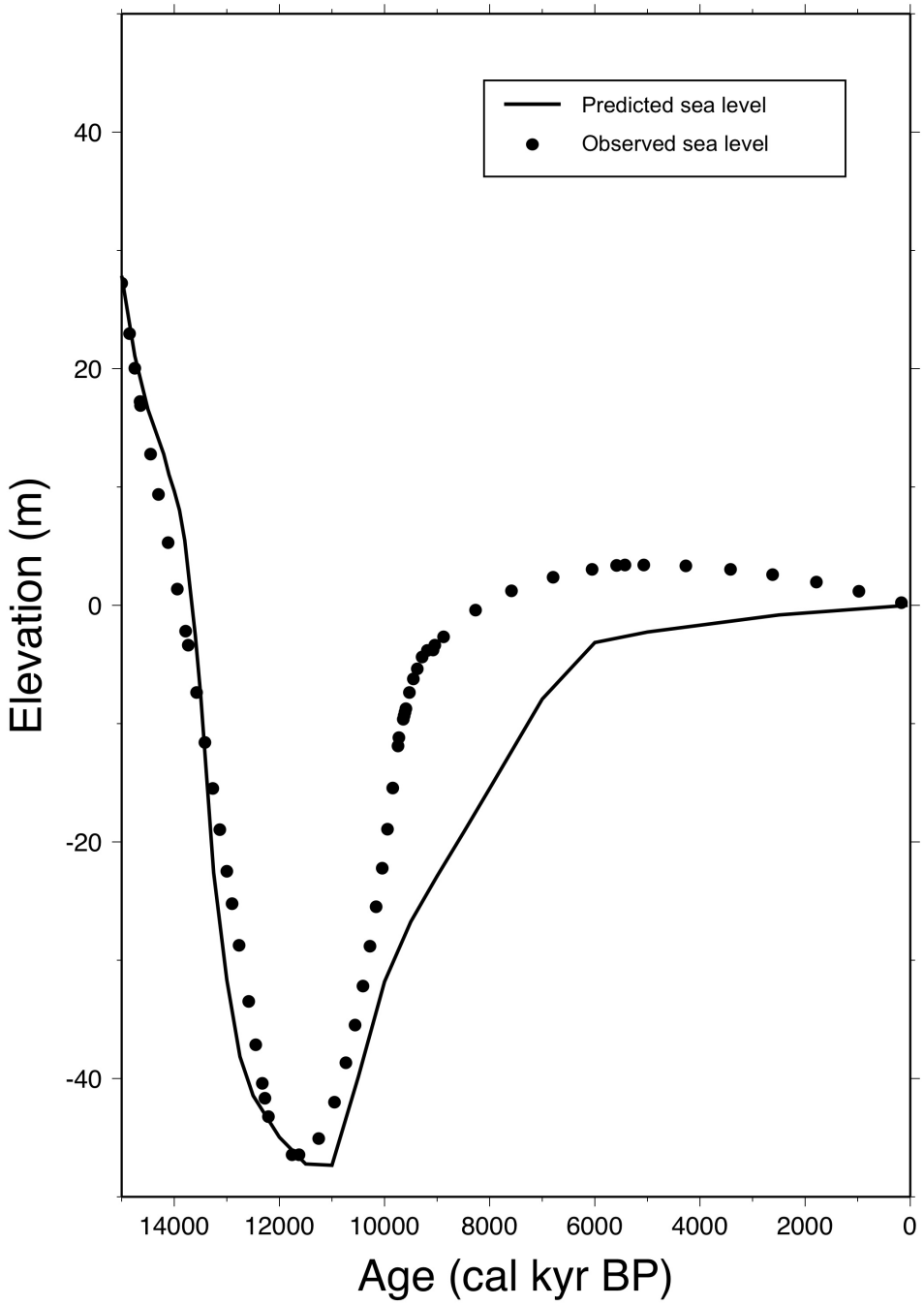

Figure 5.14. Relative sea-level predictions (solid line) compared to observed relative sea-level curve (circles) for Barkley Sound. Earth model parameters include a 30-km thick lithosphere and 380-km thick asthenosphere with model viscosity 4.0×10^{19} Pa s.

The observed Barkley Sound relative sea-level curve can be reasonably well fit by the GIA response of an Earth model with a 30-km thick lithosphere and 410-km thick asthenosphere with a model viscosity 4.0×10^{19} Pa s (Figure 5.14). If lithospheric thickness is increased from 30 km to 35 km or 40 km (not shown), the model fit worsens significantly as predicted emergence is later and faster than observed and the predicted lowstand is significantly deeper and earlier than observed. The fit to the observations also worsens significantly if asthenospheric thickness and viscosity are decreased to 340 km and 3.2×10^{19} Pa s or lower, as predicted emergence is later and faster, and the predicted lowstand is significantly shallower and later than observed.

During early emergence from the marine maximum to the present datum between 16-13.5 cal kyr BP, there is very good agreement between predicted and observed RSL. (Figure 5.14). Subsequently—between 13.5-12.0 cal kyr BP—the model prediction suggests even more rapid emergence than originally interpreted from 0 m to the -46 m lowstand. After the lowstand, the predicted curve approaches present levels much more slowly than the observed curve, similar to the Strait of Georgia sites.

A sensitivity analysis explored potential differences in predicted relative sea-level history between Barkley Sound and Tofino to determine if it is valid to combine data along the west coastal of Vancouver Island to construct the regional observed sea-level curve. The maximum distance between data sites is about 118 km from Hesquiat Harbour (site 11) to either Poett Nook 1 (site 5) or Bamfield Bog (site 2). Sea level predictions for Barkley Sound were calculated at Stopper Islands and Tofino sea level was calculated at the location of Darville Lake (Table 4.1). It was not possible to obtain an appreciable

difference in RSL history between Barkley Sound and Tofino, even after experimenting with extreme ice loads that would violate thickness and timing constraints.

Thus, the results of the present study suggest that RSL history along the west coast of Vancouver Island does not vary greatly in phase or amplitude between regions separated by distances on the order of 100 km. In other words, the relative sea-level history presented for Barkley Sound represents a regional pattern that is consistent with observations constraining sea-level change along the central west coast of Vancouver Island from Bamfield to Tofino, Hesquiat Harbour, and possibly Zeballos.

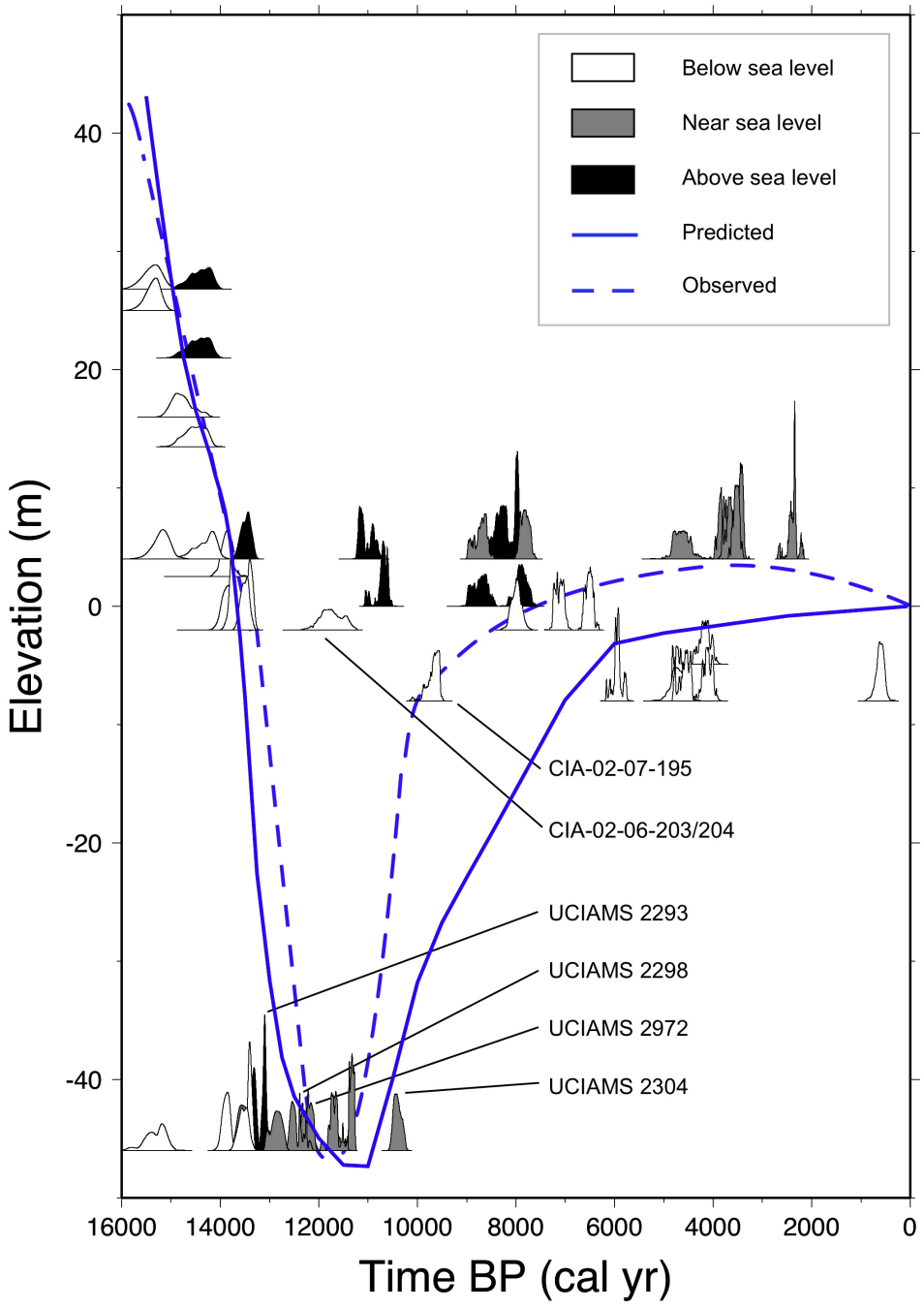

Figure 5.15. GIA-predicted sea level (solid line) plotted with observed sea-level curve (dashed line) for Barkley Sound, BC.

5.4.3 Discussion of Modeling Results

The sea-level predictions of the present study are in good agreement with previously-published best fit analyses for sea-level observations around Vancouver Island. Mantle viscosities around 10^{19} Pa s, which fit the sea-level observations described here, are two orders of magnitude smaller than model viscosities (~10^{21}) that fit regions with significant residual (present day) GIA uplift such as Hudson's Bay and the Gulf of Bothnia. A 30-km thick lithosphere Earth model predicts an acceptable fit to the GIA response for Barkley Sound. A 60-km thick lithosphere earth model predicts an acceptable fit to GIA response for Sechelt. There is very good agreement in both study regions between predicted and observed RSL during early emergence from the marine maximum to the present datum. After the lowstand, the predicted curves for Barkley Sound and the Strait of Georgia sites (central Strait of Georgia, northern Strait of Georgia, and Sechelt) approach present levels much more slowly than the observed curves.

Chapter 6 - Conclusions

6.1 Sea-level Observations

This study presents a new relative sea-level curve at Sechelt and extends and revises the sea-level curve at Barkley Sound on the west coast of Vancouver Island. New radiocarbon ages were obtained primarily from nineteen cores recovered in 2002 near Sechelt, Pender Harbour, and Bamfield and from two cores recovered near Tofino in 1998. Considered alongside previously published data, the new samples provide tight constraints on relative sea level at Sechelt and Barkley Sound during late Pleistocene emergence. Re-submergence during the early Holocene is only loosely constrained due to limited observations from shallow marine basins.

At Sechelt, sea level dropped from at least 150 m before 14 cal kyr BP to below present levels by about 12 cal kyr BP. A poorly constrained lowstand occurred between 12 and 9 cal kyr BP, after which sea level returned to near present levels. An analysis of the isostatic depression and its decay generates a preferred lowstand magnitude of about -25 m at 10.5 cal kyr BP. Similar analyses for the central Strait of Georgia (Hutchinson *et al.* 2004a) established a preferred lowstand magnitude of approximately -10 m at about 11.5 cal kyr BP. In the northern Strait of Georgia the preferred lowstand is about -5 m at 10 cal kyr BP (James *et al.* 2005).

The initial crustal uplift rate at Sechelt during late Pleistocene deglaciation (from 14 to 12 cal kyr BP) was at least 85 mm/yr. The analysis of isostatic depression suggests 2 exponentially-decaying terms, one with a characteristic decay time τ of 800 years, and a second decay time of 3700 years. The faster decay time is attributed to a low-viscosity asthenosphere and the slower decay time to a more viscous deeper mantle. Vertical

crustal motion then decreased to about 50 mm/yr from 12-10 cal kyr BP (10.5-9.0 ^{14}C kyr BP), when the fast component had decayed sufficiently that the dominant response shifted to the slower, more-viscous deeper mantle (τ = 3700 years). By 10 cal kyr BP, remnant effects of GIA were less than 0.1 mm/yr, whereafter sea-level change was dominated by eustatic sea-level rise until the late Holocene. Current sea level change is dominated by regional tectonics.

Relative sea level at Sechelt closely followed the same trend as the central and northern Strait of Georgia. Relative sea level at all three locations dropped from at least 150 m before 14 cal kyr BP (Hutchinson *et al.* 2004a: Fig. 5; James *et al.* 2005: Fig. 6 and 7). A maximum lowstand magnitude for the Central Strait of Georgia is inferred by a core taken at -24 m depth recording continuous marine deposition, with no indication of subaerial exposure (Barrie and Conway 2000). Sea level at all three locations returned to near present levels around 9 cal kyr BP.

A revised sea-level history on the west coast of Vancouver Island near Barkley Sound (from Bamfield to Tofino) includes the observed lowstand at Effingham Inlet (Dallimore *et al.* 2009), but revises the timing slightly. The new timing is between 12.0-11.5 cal kyr BP (11.1-10.5 ^{14}C kyr BP), which is several hundred years later than originally interpreted. Sea-level change near Barkley Sound most likely preceded the Sechelt, central and northern Strait of Georgia trends by at least 1000 years.

Rapid deglaciation of Vancouver Island occurred between 17-16 cal kyr BP. Sea level in Barkley Sound fell quickly (~15 mm/yr) from a late Pleistocene marine maximum (Clague 1983) of about 46 m elevation (~100 m lower than the marine maximum at Sechelt) to near present levels by 13.5 cal kyr BP. This is about 1.5 kyr

earlier than at Sechelt (this study) and central and northern Strait of Georgia (Hutchinson *et al.* 2004a; James *et al.* 2005). The steepest period of emergence followed—between 13.5-12 cal kyr BP—when sea level fell extremely rapidly (~30 mm/yr) from near present levels to a previously published lowstand of -46 m. Sea level then rose to present levels in the early Holocene. A mid-Holocene high stand of about 4 m occurred about 5.5 cal kyr BP.

New constraints on late Pleistocene emergence are established for both study regions. At Barkley Sound sea level fell past the present level around 13.5 cal kyr BP, at least 1000 years earlier than at Sechelt, where sea level fell past the present level sometime after 12.4 cal kyr BP, most likely around 11.7 cal kyr BP. Age ranges—from maximal to preferred (most likely)—for the time that sea level dropped below present are: Barkley Sound: 13.5 cal kyr BP, central Strait of Georgia: 13.0-12.4 cal kyr BP, Sechelt: 12.4-11.7 cal kyr BP, and northern Strait of Georgia 12.4-11.0 cal kyr BP (Hutchinson *et al.* 2004a; James *et al.* 2005). Preferred ages are consistent with a noted trend of relatively early and deep lowstands toward the (south-west) periphery of the CIS and later and shallower lowstands towards its (north-east) interior. However, determining the actual sequence of emergence requires the establishment of further constraints, particularly in the northern Strait of Georgia.

Barkley Sound experienced an earlier and much larger magnitude sea-level lowstand (-46 m versus -20 m) than Sechelt, returning to near present levels around 8 cal kyr BP. This is 10-20 m deeper than a lowstand of -30 ± 5 m estimated for southern Vancouver Island (James *et al.* 2009a) and ~25 m deeper than the estimated lowstand of

about -20 m in the central and northern Strait of Georgia (Hutchinson *et al.* 2004a; James *et al.* 2005), which occurred sometime between 12-10 cal kyr BP.

6.2 GIA modeling

The present study conservatively adapts the ice model originated by James *et al.* (2000) and most recently revised by James *et al.* (2009b). New constraints in the study regions are applied while maintaining maximal ice thicknesses and preserving a reasonably smooth ice surface. The LGM was modeled earlier at 17.5 cal kyr BP for the west coast of Vancouver Island (Cosma *et al.* 2008), and deglaciation to ice-free conditions was set to 15.4 cal kyr BP. At Sechelt, the LGM was modeled later at 14.2 cal kyr BP rather than 15.4-14.5 cal kyr BP. The central Strait of Georgia was modeled as ice-free by 14.5 cal kyr BP. Howe Sound and the northern Strait of Georgia were ice-free by 14 cal kyr BP and Sechelt by 13.5 cal kyr BP.

The new RSL history for Sechelt presented in Chapter 3 is well predicted by the GIA response of an earth model with a 60-km thick lithosphere and 380-km thick asthenosphere and model viscosity 4.0×10^{19} Pa · s. The GIA analysis is focused on the initial crustal response before 12 cal kyr BP. The model used by the present study is not tuned to model Holocene submergence.

The revised RSL history for Barkley Sound presented in Chapter 4 is reasonably well fit by the GIA response of an earth model with a 30-km thick lithosphere and 410-km thick asthenosphere and model viscosity 4.0×10^{19} Pa · s. The model fit worsens slightly if lithospheric thickness is increased from 30 km to 35 km or 40 km.

A preliminary sensitivity analysis explored potential differences in RSL history between Barkley Sound and Tofino by performing runs with significantly altered ice

history and a large range of parameters for lithosphere thickness and asthenosphere viscosity. Even experimentation with extreme ice loads that would violate thickness and timing constraints, it was not possible to obtain an appreciable difference in RSL history between Barkley Sound and Tofino. Thus, the results of the present study suggest that RSL history along the west coast of Vancouver Island does not vary greatly in phase or amplitude between regions separated by distances on the order of 100 km. In other words, the relative sea-level history presented for Barkley Sound represents a regional pattern that is consistent with observations constraining sea-level change along the central west coast of Vancouver Island from Bamfield to Tofino, Hesquiat Harbour, and possibly Zeballos.

6.3 Suggested future studies

At Sechelt, and in the central and northern Strait of Georgia, the marine lowstand could be better constrained by local marine cores at depths between -8 m and -51 m. To the author's knowledge, no such cores exist (Vaughn Barrie, personal communication). Specifically, to further constrain the lowstand, cores are needed from marine basins such as Hospital Bay and deeper basins, sampling late Pleistocene and early Holocene sediments.

At Barkley Sound, and for all of western and northern Vancouver Island, the marine maximum above 33 m elevation is difficult to constrain, since debris flows in steep terrain frequently disrupt the depositional history of isolation basins. Further sampling of late Pleistocene and early Holocene sediments from isolation basins between 20-60 m elevation are needed to further constrain late Pleistocene emergence.

In general, geodynamic processes at the CSZ could be explored in further detail by collecting more detailed observations to constrain relative sea level both seaward (along the west coast of Vancouver Island) and landward (along the mainland coast of BC and Washington State) and—as in the present study—relating them to the rheology of the oceanic mantle and continental arc and back-arc mantle wedge, respectively.

The GIA model used by this study is tuned to predict late Pleistocene emergence rather than Holocene re-submergence. A future study could incorporate the present CIS model into a global model and calculate global self-consistent sea-level change.

GIA modeling results could also be improved by incorporating lateral variability of CSZ structure. Sea-level observations in the present study were taken from sites located above the stagnant mantle wedge and relatively near the actively circulating continental mantle wedge (James *et al.* 2009b). Thus, the rapid sea-level fall observed is likely due to the combined response of the low viscosity oceanic mantle that directly underlies the sites (especially Barkley Sound) and the low-viscosity forearc and backarc mantle wedge immediately inland from Sechelt. The relative contribution of the oceanic mantle is expected to be higher seaward, on the west coast of Vancouver Island near Barkley Sound, and the relative contribution of the arc mantle wedge is expected to be higher landward, near Sechelt. A laterally variable model is needed to quantify this effect.

References

Alley, N.F. and Chatwin, S.C., 1979. late Pleistocene history and geomorphology, southwestern Vancouver Island, British Columbia. Canadian Journal of Earth Sciences, 16, 1645-1657.

Al-Suwaidi, M., Ward, B.C., Wilson, M.C., Hebda, R.J., Nagorsen, D.W., Marshall, D., Ghaleb, B., Wigen, R.J. and Enkin, R.J., 2006. Late Wisconsinan Port Eliza Cave Deposits and Their Implications for Human Coastal Migration, Vancouver Island, Canada. Geoarchaeology: An International Journal, 21, 307-332.

Armstrong, J.E., 1981. Post-Vashon Wisconsin glaciation, Fraser Lowland, British Columbia. Geological Survey of Canada, Bulletin 322, 34 p.

Armstrong, J.E., Crandell, D.R., Easterbrook, D.J. and Noble, D.J., 1965. Late Pleistocene stratigraphy and chronology in southwestern British Columbia and northwestern Washington. Geological Society of America Bulletin, 76, 321-330.

Balfour, N., Cassidy, J.F., and Dosso, S., 2008. Sources of Seismic Hazard in British Columbia, IRIS Annual Workshop, Skamania Lodge, WA, June 4-6, 2008.

Bard, E., 1988. Correction of accelerator mass spectrometry ^{14}C ages measured in planktonic foraminifera: paleooceanographic implications. Paleoceanography, 3, 635-645.

Barrie, J.V. and Conway, K.W., 2000. A preliminary interpretation of surficial marine geology of central and northern Strait of Georgia, British Columbia. Current Research 2000-A21, Geological Survey of Canada, Natural Resources Canada, Ottawa, 7p.

Barrie, J.V. and Conway, K.W., 2002. Contrasting glacial sedimentation processes and sea-level changes in two adjacent basins on the Pacific margin of Canada. *In* Glacier-Influenced Sedimentation on High-Latitude Continental Margins, *Edited by* J.A. Dowdeswell and C. Ó Cofaigh. Geological Society, London, Special Publication, 203, 181-194.

Bassett, S.E., Milne, G.A., Mitrovica, J.X. and Clark, P.U., 2005. Ice sheet and solid earth influences on far-field sea-level histories. Science, 309, 925-928.

Blaise, B., Clague, J.J. and Mathewes, R.W., 1990. Time of maximum late Wisconsin glaciation, west coast of Canada. Quaternary Research, 34, 282-295.

Blais-Stevens, A., Bornhold, B.D., Kemp, A.E.S., Dean, J.M. and Vaan, A.A., 2001. Overview of late Quaternary stratigraphy in Saanich Inlet, British Columbia: results of Ocean Drilling Program Leg 169S. Marine Geology, 174, 3-26.

Blake, W., 1983. Geological Survey of Canada radiocarbon dates XXIII. Geological Survey of Canada Paper 83-7, 34 p.

Blake, W., 1988. Geological Survey of Canada radiocarbon dates XXVII. Geological Survey of Canada Paper 87-7, 100 p.

Bobrowsky, P.T. and Clague, J.J., 1992. Neotectonic investigations on Vancouver Island (92B, F). British Columbia Geological Survey Branch, Geological Fieldwork 1991, Paper 1992-1, 325-329.

Booth, D.B., 1987. Timing and processes of deglaciation along the southern margin of the Cordilleran ice sheet. *In* The Geology of North America, v. K-3, North America and Adjacent Oceans During the Last Deglaciation, *Edited by* W.F. Ruddiman and H.E. Wright, Boulder, Colorado, Geological Society of America, 71-90.

Cassidy, J.F. and Waldhauser, F., 2003. Evidence for both crustal and mantle earthquakes in the subducting Juan de Fuca Plate. Geophysical Research Letters, 30, 1095, 4 p.

Clague, J.J., 1975. Late Quaternary sea-level fluctuations, Pacific coast of Canada and adjacent areas. In Report of activities, part C. Geological Survey of Canada, Paper 75-lC, pp. 17-21.

Clague, J.J., 1976. Quadra Sand and its relation to the late Wisconsin glaciation of southwest British Columbia. Canadian Journal of Earth Sciences, 13, 803-815.

Clague, J.J., Armstrong, J.E. and Mathews, W.H., 1980. Advance of the late Wisconsin Cordilleran Ice Sheet in southern British Columbia since 22,000 Yr B.P. Quaternary Research, 13, 322-326.

Clague, J.J., 1981. Late Quaternary geology and geochronology of British Columbia, part 2: summary and discussion of radiocarbon-dated Quaternary history. Geological Survey of Canada, Energy Mines and Resources Canada, Ottawa, Paper 80-35, 41 p.

Clague, J., Harper, J.R., Hebda, R.J. and Howes, D.E., 1982. Late Quaternary sea levels and crustal movements, coastal British Columbia. Canadian Journal of Earth Sciences, 19, 597-618.

Clague, J.J., 1983. Glacio-isostatic effects of the Cordilleran ice sheet, British Columbia, Canada. In: Smith, D.E., Dawson, A.G. (Eds.), Shorelines and Isostasy. Academic Press, London, pp. 321–343.

Clague, J.J., Saunders, I.R. and Roberts, M.C., 1988. Ice-free conditions in southwestern British Columbia at 16 000 years BP. Canadian Journal of Earth Sciences, 25, 938-941.

Clague, J.J., 1992. Quaternary glaciation and sedimentation, Chapter 12. *In* Geology of the Cordilleran Orogen in Canada, *Edited by* H. Gabrielse and C.J. Yorath. Geological Survey of Canada, Ottawa. No. 4, pp. 419-434.

Clague, J.J., 1994. Quaternary stratigraphy and history of south-coastal British Columbia. *In* Geology and Geological Hazards of the Vancouver Region, southwestern British Columbia. *Edited by* J.W.H. Monger. Geological Survey of Canada, Ottawa. Bulletin 481, pp. 181-192.

Clague, J.J. and James, T.S., 2002. History and isostatic effects of the last ice sheet in southern British Columbia. Quaternary Science Reviews, 21, 71-87.

Clague, J.J., Froese, D., Hutchinson, I., James, T.S. and Simon, K.M., 2005. Early growth of the last Cordilleran ice sheet deduced from glacio-isostatic depression in southwest British Columbia, Canada. Quaternary Research, 63, 53-59.

Cosma, T.N., Hendy, I.L., Chang, A.S., 2008. Chronological constraints on Cordilleran Ice Sheet glaciomarine sedimentation from core MD02-2496 off Vancouver Island (western Canada). Quaternary Science Reviews, 27, 941–955.

Dallimore, A., Enkin, R.J., Peinitz, R., Southon, J.R., Baker, J., Wright, C.A., Pedersen, T.F., Calvert, S.E. and Thomson, R.J., 2009. Post-glacial evolution of a Pacific coastal fjord in British Columbia, Canada: interactions of sea-level change, crustal response and environmental fluctuations; results from MONA Core MD02-2494. Canadian Journal of Earth Sciences, 45, 1345-1362.

Denton, G.H. and Hughes, T.J., 1981. The Last Great Ice Sheets. John Wiley and Sons, Inc., New York, 484 p.

Dethier, D.P., Pessl Jr., F., Keuler, R.F., Balzarini, M.A. and Pevear, D.R., 1995. Late Wisconsinian glaciomarine deposition and isostatic rebound, northern Puget Lowland, Washington. Geological Society of America Bulletin, 107, 1288-1303.

Dickin, A. P., 2004. Radiogenic Isotope Geology, Second Edition, Cambridge University Press, New York, 383-393.

Dziewonski, A.M. and Anderson, D.L., 1981. Preliminary reference Earth model. Physics of the Earth and Planetary Interiors, 25, 297-356.

Easterbrook, D.J., 1992. Advance and retreat of Cordilleran ice sheets in Washington, U.S.A. Géographie physique et Quaternaire, 46, 51-68.

Fairbanks, R.G., 1989. A 17,000-year glacio-eustatic sea level record: influence of glacial melting rates on the Younger Dryas even and deep-ocean circulation. Nature, 342, 637-642.

Farrell, W.E. and Clark, J.A., 1976. On postglacial sea level. Geophysical Journal of the Royal Astronomical Society, 46, 647-667.

Fedje, D.W. and Christensen, T., 1999. Modeling Paleoshorelines and Locating Early Holocene Coastal Sites in Haida Gwaii, American Antiquity, 64, 4, 635-652.

Fedje, D.W. and Josenhans, H.W., 2000. Drowned forest and archaeology on the continental shelf of British Columbia, Canada. Geology, 28, 99–102.

Flück, P., Hyndman, R.D. and Wang, K., 1997. Three-dimensional dislocation model for great earthquakes of the Cascadia subduction zone. Journal of Geophysical Research, 102, 20539-20550.

Flück, P., Hyndman, R.D. and Lowe, C., 2003. Effective elastic thickness T_e of the lithosphere in western Canada. Journal of Geophysical Research, 108, 2430, 13 p.

Friele, P.A. and Hutchinson, I., 1993. Holocene sea-level change on the central west coast of Vancouver Island, British Columbia. Canadian Journal of Earth Sciences, 30, 832-840.

Friele, P.A. and Clague, J.J., 2002. Readvance of glaciers in the British Columbia Coast Mountains at the end of the last glaciation. Quaternary International, 87, 45-58.

Fulton, R.J., 1967. Deglaciation studies in Kamloops region, an area of moderate relief, British Columbia. Geological Survey of Canada, Ottawa. Bulletin, 154, 36 p.

Gowan, E.J**.** and James, T.S., 2006. Glacio-isostatic adjustment modelling of improved postglacial sea-level constraints from Vancouver Island, British Columbia. EOS Transaction, AGU, 87, Fall Meeting Suplemental, Abstract G33B-0052.

Gowan, E.J., 2007. Glacio-isostatic Adjustment Modelling of Improved Relative Sea-level Observations in Southwestern British Columbia, Canada. M.Sc. thesis, University of Victoria, Victoria, BC, 148 pp.

Guilderson, T.P., Reimer, P.J. and Brown, T.A., 2005. The boon and bane of radiocarbon dating. Science, 307, 362-364.

Gutsell, J.E., Clague, J.J., Best, M.E., Bobrowsky, P.T. and Hutchinson, I. 2004. Architecture and evolution of a fjord-head delta, western Vancouver Island, British Columbia. Journal of Quaternary Science, 19, 497–511.

Hafsten, U., 1983, Biostratigraphic evidence for Late Weichselian and Holocene sea-level changes in southern Norway. Shorelines and Isostasy *Edited by* D.E. Smith and A.G. Dawson: Institute of British Geographers, Academic Press, London, 161-181.

Halstead, E.C., 1968. The Cowichan ice tongue, Vancouver Island. Canadian Journal of Earth Sciences, 5(6), 1409-1415.

Hebda, R.J., 1983. Late-glacial and postglacial vegetation history at Bear Cove Bog, northeast Island, British Columbia. Canadian Journal of Botany, 61, 3172-3192.

Hebda, R., 1988. Buffalo George update. The Midden, 20, 2.

Hebda, R.J., Howes, D. and Maxwell, B., 1997. Chapter 15, Brooks Peninsula as an ice age refugium. *In* Brooks Peninsula an ice age refugium on Vancouver Island, *Edited by* R.J. Hebda and J.C. Haggarty. BC Parks Ministry of Environment, Lands and Parks, Occasional Paper no. 5, 7 p.

Heiskanen, W.A., Vening Meinesz, F.A., 1958. The Earth and Its Gravity Field. Wiley, New York.

Hendy, I.L. 2009, A fresh perspective on the Cordilleran Ice Sheet, Geology, 37(1), 95–96; doi: 10.1130/focus012009.1.

Herzer, R.H. and Bornhold, B.D., 1982. Glaciation and post-glacial history of the continental shelf off southwestern Vancouver Island, British Columbia. Marine Geology, 48, 285-319.

Heusser, C.J., 1973. Environmental sequence following the Fraser advance of the Juan de Fuca Lobe, Washington. Quaternary Research, 3, 284-306.

Howes, D.E., 1981a. Terrain inventory and geological hazards: northern Vancouver Island. Province of British Columbia Ministry of Environment, Assessment and Planning Division, APD Bulletin 5, 105 p.

Howes, D.E., 1981b. Late Quaternary sediments and geomorphic history of north-central Vancouver Island. Canadian Journal of Earth Sciences, 18, 1-12.

Hughen, K.A., Baillie, M.G.L., Bard, E., Bayliss., A., Beck., J.W., Bertrand, C.J.H., Blackwell, P.G., Buck, C.E., Burr, G.S., Cutler, K.B., Damon, P.E., Edwards, R.L., Fairbanks, R.G., Friedrich, M., Guilderson, T.P., Kromer, B., McCormac, F.G., Manning, S.W., Bronk Ramsey, C., Reimer, P.J., Reimer, R.W., Remmele, S., Southon, J.R., Stuiver, M., Talamo, S., Taylor, F.W., van der Plicht, J. and Weyhenmeyer, C.E., 2004. Marine04 Marine radiocarbon age calibration, 26 - 0 ka BP. Radiocarbon, 46, 1059-1086.

Hutchinson, I., 1992. Holocene sea level change in the Pacific Northwest: a catalogue of radiocarbon dates and an atlas of regional sea-level curves. Occasional Paper No. 1, Institute of Quaternary Research, Simon Fraser University, Burnaby, B.C., 100 p.

Hutchinson, I. and Friele, P.A., 1993. Holocene sea-level change on the central west coast of Vancouver Island, British Columbia. Canadian Journal of Earth Sciences, 30, 832-840.

Hutchinson, I., James, T.S., Clague, J.J., Barrie, J.V. and Conway, K.W., 2004a. Reconstruction of late Quaternary sea-level change in southwestern British Columbia from sediments in isolation basins. Boreas, 33, 183-194.

Hutchinson, I., James, T.S., Reimer, P.J., Bornhold, B.D. and Clague, J.J., 2004b. Marine and limnic radiocarbon reservoir corrections for studies of late- and postglacial environments in Georgia Basin and Puget Lowland British Columbia, Canada and Washington, USA. Quaternary Research, 61, 193-203.

Hutchinson, I., James, T.S., Reimer, P.J., Bornhold, B.D. and Clague, J.J., 2005. Reply to letter to the editor from Easterbrook and Kovanen re *Quaternary Research* 61, 193-203, Washington, USA. Quaternary Research, 63, 226-227.

Hyndman, R.D., Yorath, C.J., Clowes, R.M., and Davis, E.E. 1990. The northern Cascadia subduction zone at Vancouver Island: seismic structure and tectonic history. Canadian Journal of Earth Sciences, 27, 313-329.

Hyndman, R.D., and Lewis, T.J., 1995, Review: The thermal regime along the southern Canadian Cordillera Lithoprobe corridor, Can. J. Earth Sci., 32, 1611 – 1617.

Hyndman, R.D., 2010. The consequences of Canadian Cordillera thermal regime in recent tectonics and elevation: a review. Canadian Journal of Earth Sciences, 47(5), 621-632.

James, T.S. and Ivins, E.R., 1998. Predictions of Antarctic crustal motions driven by present-day ice sheet evolution and by isostatic memory of the Last Glacial Maximum. Journal of Geophysical Research, 103, 4993–5017.

James, T.S., Clague, J.J., Wang, K. and Hutchinson, I., 2000. Postglacial rebound at the northern Cascadia subduction zone. Quaternary Science Reviews, 19, 1527-1541.

James, T.S., Hutchinson, I., Barrie, J.V., Conway, K.C. and Mathews, D., 2005. Relative sea-level change in the northern Strait of Georgia, British Columbia. Géographie physique et Quaternaire, 59, 113-127.

James, T.S., Gowan, E.J., Hutchinson, I., Clague, J.J., Barrie, J.V., Conway, K.C., 2009a. Sea-level change and paleogeographic reconstructions, southern Vancouver Island, British Columbia, Canada, Quaternary Science Reviews, doi:10.1016/j.quascirev.2008.12.022

James, T.S., Gowan, E.J., Wada I., Wang, K., 2009b. Viscosity of the asthenosphere from glacial isostatic adjustment and subduction dynamics at the northern Cascadia subduction zone, British Columbia, Canada, Journal of Geophysical Research, 114, B04405, doi:10.1029/2008JB006077.

Johnston, S.T., and Acton, S., 2003. The Eocene Southern Vancouver Island Orocline – a response to seamount accretion and the cause of basin and fold and thrust belt formation. Tectonophysics Special Issue – Modern and Ancient Orogenic belts, 365, 196-183.

Josenhans, H., Fedje, D., Pienitz, R. and Southon, J., 1997. Early humans and rapidly changing Holocene sea levels in Haida Gwaii-Hecate Strait, British Columbia, Canada. Science, 277: 71-74.

Karato, S.-i. and Wu, P., 1993. Rheology of the upper mantle: a synthesis. Science, 260, 771-778.

Kao, H., Shan, S.-J., Dragert, H., Rogers, G., Cassidy, J.F. and Ramachandran, K., 2005. A wide depth distribution of seismic tremors along the northern Cascadia margin. Nature, 436, 841-844.

Kovanen, D. J., and Easterbrook, D. J., 1997. Two advances of the Cordilleran Ice Sheet in the northern Puget Lowland, WA, during the Sumas Stade between 10,000 and 11,500 14 C-yrs. B.P. Geological Society of America Abstracts with Programs 29, 23.

Kovanen, D.J. and Easterbrook, D.J., 2002a. Paleodeviations of radiocarbon marine reservoir values for the northeast Pacific. Geology, 30, 243-246.

Kovanen, D.J. and Easterbrook, D.J., 2002b. Timing and extent of Allerød and Younger Dryas age (ca. 12,500-10,000 ^{14}C yr B.P.) oscillations of the Cordilleran Ice Sheet in the Fraser Lowland, western North America. Quaternary Research, 57, 208-224.

Lambeck, K., and Chappell, J., 2001. Sea level change through the last glacial cycle. Science 292, 679–686.

Lewis, T.J., Bentkowski, W.H., Davis, E.E. and Hyndman, R.D., 1988. Subduction of the Juan de Fuca plate: thermal consequences. Journal of Geophysical Research, 93, 15207-15225.

Libby, W.F., 1946. Atmospheric helium three and radiocarbon from cosmic radiation. Physical Review, 69, 671-672.

López, G.I., 2002. Paleoseismic Investigations on the central west coast of Vancouver Island, British Columbia, Canada: pre-historic Tsunami deposits in coastal lacustrine environments. University of Victoria, Victoria, BC, p 284.

López G.I. and Bobrowsky P.T., 2001. A 14,000 year-old-record from a coastal freshwater lake: Sedimentological evidence for tsunamigenic events on the west coast of Vancouver Island, British Columbia, Canada. In: International Tsunami Symposium, *Edited by*: Whitney R.L., Dunlap M., Ventenbergs K., IUGG Tsunami Commission, NOAA, USGS, Seattle, 491–500.

Mathews, W.H., Fyles, J.G. and Nasmith, H.W., 1970. Postglacial crustal movements in southwestern British Columbia and adjacent Washington state. Canadian Journal of Earth Sciences, 7, 690-702.

Mazzotti, S., Dragert, H., Henton, J., Schmidt, M., Hyndman, R., James, T., Lu, Y. and Craymer, M., 2003. Current tectonics of northern Cascadia from a decade of GPS measurements. Journal of Geophysical Research, 108, 2554.

McCammon, J.W., 1977. Surficial geology and sand and gravel deposits of Sunshine Coast, Powell River, and Campbell River areas. Province of British Columbia Ministry of Mines and Petroleum Resources, Victoria. Bulletin 65, 36 p.

Mitrovica, J.X. and Milne, G.A., 2003. On post-glacial sea level: I. general theory. Geophysics Journal International, 154, 253-267.

Mitrovica, J.X. and Peltier, W.R., 1991. On postglacial geoid subsidence over the equatorial oceans. Journal of Geophysical Research, 96, 20053-20071.

Muhs, D.R., Thorson, R.M., Clague, J.J., Mathews, W.H., McDowell, P.F., Kelsey, H.M., 1987. Pacific coast and mountain system. In: Graf, W.L. (Ed.), Geomorphic Systems of North America, Centennial Special Vol. 2. Geological Society of America, Boulder, CO, pp. 517–581.

Mosher, D.C. and Hewitt., 2004. Late Quaternary deglaciation and sea-level history of eastern Juan de Fuca Strait, Cascadia. Quaternary International, 121, 23-39.

Niskanen, E., 1943. On the deformation of the Earth's crust under the weight of a glacial ice-load and related phenomena. Annales Academiae Scientiarum Fennicae AIII. Geologica-Geographica, 7, 59 p.

NOAA, 1988. Data Announcement 88-MGG-02, Digital relief of the Surface of the Earth. NOAA, National Geophysical Data Center, Boulder, Colorado.

Osborn, G., Clapperton, Ch., Davis, P.T., Reasoner, M., Rodbell, D.T., Seltzer, G.O., Zielinski, G., 1995. Potential glacial evidence for the Younger Dryas event in the Cordillera of North and South America. Quaternary Science Reviews 14, 823e832.
Peltier, 1974. The impulse response of a Maxwell Earth. Reviews of Geophysics and Space Physics, 12, 649-669.

Peltier, 1985. The LAGEOS constraint on deep mantle viscosity: results from a new normal mode method for the inversion of viscoelastic relaxation spectra. Journal of Geophysical Research, 90, 9411-9421.

Peltier, W.R., 1994. Ice age paleotopography. Science, 265(5169):195--201,

Peltier, W.R., 1998. Postglacial variations in the level of the sea: implications for climate dynamics and solid-earth geophysics. Reviews of Geophysics, 36, 603-689.

Peltier, W.R., 2002. Global glacial isostatic adjustment: palaeogeodetic and space-geodetic tests of the ICE-4G (VM2) model. J. Quaternary Sci., Vol. 17 pp. 491–510. ISSN 0267-8179.

Porter, S.C. and Swanson, T.W., 1998. Radiocarbon age constraints on rates of advance and retreat of the Puget Lobe of the Cordilleran ice sheet during the last glaciation. Quaternary Research, 50, 205-213.

Ramachandran, K., Dosso, S.E., Spence, G.D., Hyndman, R.D., and Brocher, T.M., 2005. Forearc structure beneath southwestern British Columbia: A three-dimensional tomographic velocity model, J. Geophys. Res., 110, B02303, doi:10.1029/2004JB003258.

Ranalli, 1995. Rheology of the Earth, second edition. Chapman and Hall, London, UK, 413.

Ray G.E. and Kilby, C.E., 1996. Geology of the Mineral Hill - Wormy ake Area, Sechelt, British Columbia, BC Ministry of Energy, Mines, and Petroleum Resources, Open File 1996-06, NTS-92G/12W, http://www.empr.gov.bc.ca/Mining/Geoscience/PublicationsCatalogue/OpenFiles/1996/Documents/OF1996-06.pdf

Reimer, P.J., Baillie, M.G.L., Bard, E., Bayliss, A., Beck, J.W., Bertrand, C.J.H., Blackwell, P.G., Buck, C.E., Burr, G.S., Cutler, K.B., Damon, P.E., Edwards, R.L., Fairbanks, R.G., Friedrich, M., Guilderson, T.P., Hogg, A.G., Hughen, K.A., Kromer, B., McCormac, F.G., Manning, S.W., Ramsey, C.B., Reimer, R.W., Remmele, S., Southon, J.R., Stuiver, M., Talamo, S., Taylor, F.W., van der Plicht, J.and Weyhenmeyer, C.E., 2004. IntCal04 Terrestrial radiocarbon age calibration, 26 - 0 ka BP. Radiocarbon, 46, 1029-1058.

Roberts, M.C. and Rood, K. M., 1984. The role of the ice contributing area in the morphology of transverse fjords, British Columbia. Geografiska Annaler. Series A, Physical Geography, Vol. 66, 381-393.

Shaw, J. and Forbes, D.L., 1992. Barriers, barrier platforms, and spillover deposits in St. George's Bay, Newfoundland; paraglacial sedimentation on the flanks of a deep coastal basin. Marine Geology 105, 119–140.

Stein, C.A. and Stein S., 1992. A model for the global variation in oceanic depth and heat flow with lithospheric age. Nature, 359, 123-129.

Stuiver, M. and Reimer, P.J., 1993. Extended ^{14}C data base and revised Calib 3.0 ^{14}C age calibration program. Radiocarbon, 35, 215-230.

Stuiver, M. and Suess, H.E., 1966. On the relationship between radiocarbon dates and true sample ages. Radiocarbon, 8, 534-540.

Stumpf, A.J., Broster, B.E. and Levson, V.M., 2000. Multiphase flow of the late Wisconsinan Cordlleran ice sheet in western Canada. Geological Society of America Bulletin, 112, 1850-1863.

Swanson, T.W. and Caffee, M.L., 2001. Determination of ^{36}Cl production rates derived from the well-dated deglaciation surfaces of Whidbey and Fidalgo Islands, Washington. Quaternary Research, 56, 366-382.

Thackray, G.D., 2001. Extensive early and middle Wisconsin glaciation on the western Olympic Peninsula, Washington, and the variability of Pacific moisture delivery to the northwestern United States. Quaternary Research, 55, 257-270.

Turcotte, D.L. and Schubert, G., 2002. Geodynamics, Second Edition. Cambridge University Press, Cambridge, 456 p.

Ward, B.C., Wilson, M.C., Nagorsen, D.W., Nelson, D.E., Driver, J.C. and Wigen, R.J., 2003 Port Eliza cave: North American West Coast interstadial environment and implications for human migrations, Quaternary Science Reviews, 22, 14, 1383-1388.

Wilson, J.T., Falconer, G., Mathews, W.H. and Prest, V.K., 1958. Glacial map of Canada. Geological Association of Canada, Toronto, Ontario.

Yorath, C. J.; Nasmith, H. W., 1995, The Geology of Southern Vancouver Island : A Field Guide, Canada, Orca Book Publishers, 10-47.